Old Dominion University

ODU Digital Commons

Civil & Environmental Engineering Theses & Dissertations

Civil & Environmental Engineering

Summer 2009

3D Numerical Modeling of Hydrodynamic Flow, Sediment Deposition and Transport in Stormwater Ponds and Alluvial Channels

Leying Zhang
Old Dominion University

Follow this and additional works at: https://digitalcommons.odu.edu/cee_etds

Part of the Environmental Engineering Commons

Recommended Citation

Zhang, Leying. "3D Numerical Modeling of Hydrodynamic Flow, Sediment Deposition and Transport in Stormwater Ponds and Alluvial Channels" (2009). Doctor of Philosophy (PhD), Dissertation, Civil & Environmental Engineering, Old Dominion University, DOI: 10.25777/awrd-tp65
https://digitalcommons.odu.edu/cee_etds/95

This Dissertation is brought to you for free and open access by the Civil & Environmental Engineering at ODU Digital Commons. It has been accepted for inclusion in Civil & Environmental Engineering Theses & Dissertations by an authorized administrator of ODU Digital Commons. For more information, please contact digitalcommons@odu.edu.

3D NUMERICAL MODELING OF HYDRODYNAMIC FLOW, SEDIMENT DEPOSITION AND TRANSPORT IN STORMWATER PONDS AND ALLUVIAL CHANNELS

by

Leying Zhang
B.S. July 2001, Hefei University of Technology, China
M.S. May 2004, Hefei University of Technology, China

A Dissertation Submitted to the Faculty of
Old Dominion University in Partial Fulfillment of the
Requirement for the Degree of

DOCTOR OF PHILOSOPHY

ENVIRONMENTAL ENGINEERING

OLD DOMINION UNIVERSITY
August 2009

Approved by:

Laura J. Harrell (Director)

Jaewan Yoon (Member)

Gene J.-W. Hou (Member)

ABSTRACT

3D NUMERICAL MODELING OF HYDRODYNAMIC FLOW, SEDIMENT DEPOSITION AND TRANSPORT IN STORMWATER PONDS AND ALLUVIAL CHANNELS

Leying Zhang
Old Dominion University, 2009
Director : Dr. Laura J. Harrell

Prediction of flow and sediment transport is an important and challenging problem for stormwater management and river engineering applications. This thesis concerns primarily the computation of flow, sediment deposition and transport processes in stormwater ponds and alluvial channels based on a multiphase flow approach in modeling sediment transport. Starting from an existing hydrodynamic Reynolds Averaged Navier-Stokes flow solver, numerical models are developed to predict flow, sediment deposition and transport under the FLUENT software package. Two types of sediment transport models are formulated to consider quantities of present sediment phase volume fractions: a Discrete Phase Model in a Lagrangian frame where the sediment phase occupies a low volume fraction and particle-particle interactions are neglected; a Eulerian two-phase model where each phase is considered as an interpenetrating continuum and particle-particle interactions are not neglegible. The model is capable to model sediment transport with high volume fractions.

The solution methodologies are implemented numerically for different case studies. The Discrete Phase Model approach, together with a standard $k-\varepsilon$ turbulence model, is applied to stormwater pond modeling studies. The use of computational fluid dynamics to simulate flow fields and sediment depositions in stormwater tanks is beneficial because one may compare different factors that affect sedimentation efficiency. In particular, two

case studies with different inlet and outlet pipes arrangements are investigated under different steady inflow conditions and bed boundary conditions. A method is employed and hooked to FLUENT for accurate simulations of particle settling behavior in stormwater ponds. The method considers critical bed shear stress as a threshold and evaluates local bed shear stress with this value to determine the particle deposition behavior. It is demonstrated that this model is an efficient 3D hydrodynamic flow and sediment transport numeric model for low sediment-laden flows, thus providing engineers and scientists with a useful tool for studying sediment deposition with a variety of sediment sizes, inflow conditions, and geometry arrangements.

In order to gain more insight into the fundamental flow and sediment interaction mechanics of sediment transport, an Eulerian two-phase model embeded in FLUENT is implemented in an open channel with loose bed based on two-phase mass and momentum equations. These equations are used in conjunction with the constitutive relations that are obtained by applying kinetic theory. Different from traditional sediment transport models, this model uses the two-phase theory, and thus, has no need to invoke any empirical sediment transport formulas. In this application, predictions for turbulent fluctuations for the fluid phase are obtained using a modified $k-\varepsilon$ turbulence model with a supplement of extra terms which take into account the interphase turbulent momentum transfer. Predictions for turbulent quantities for the solid phase are obtained using Tchen-theory correlations for the discrete particles under homogeneous and steady turbulent flows. Besides simulation of sediment transport, the model also provides some ideas for simulating scour and bed deformation. The results presented in this study demonstrate that the model is efficient and quite accurate in dealing with sediment transport and scour simulation with loose bed.

Copyright, 2009, by Leying Zhang, All rights reserved

ACKNOWLEDGMENTS

I express my gratitude to my advisor Dr.Laura J. Harrell for her guidance, supervision and support throughout this entire work. Her kindness and patience enabled me to enjoy the process and conclusion of this work.

I thank Dr.Akan, Dr.Yoon and Dr.Hou, for their advice and time they gave on my research. The knowledge I learned from the courses taught by Dr.Akan and Dr.Yoon will benefit me for the rest of my life. I am also very grateful to Dr.Hou for his valuable suggestions and providing me necessary computer resources in his lab at the beginning. All of you kindly provided me help whenever I asked for it.

I acknowledge the help of my officemates, Kwisun Yu, Yanhong Zhao, Libin Zheng, Xin Wang, Kaixin Yang and Dr.Changqing Song, for their friendship and support.

I also thank the Civil and Environmental Engineering Department at the Old Dominion University for providing support in using FLUENT, Dr.Ayodeji Demuren and his graduate student Wayne Sexton for their help in sharing FLUENT license, and my friend Dr.Minwei Gong for sharing his valuable experinces in using FLUENT.

Special thanks goes to my husband Linfeng, my daughter Yueyang, as well as my parents and sisters for their love, patience, encouragement and everlasting support.

TABLE OF CONTENTS

Chapter Page

INTRODUCTION 1
1.1 Introduction 1
1.2 Background on numerical modeling of sediment transport 5
1.3 Literature review 7
1.3.1 Literature review on pond hydaulic performance investigation methods ..7
1.3.2 Literature review on sediment transport numerical modeling 14
1.4 Research contributions 19
1.5 Dissertation objectives 20
1.6 Outline of the dissertation 23

MATHEMATICAL FORMULATION OF STORMWATER POND MODELING 25
2.1 Introduction 25
2.2 Flow modeling and governing equations 26
2.3 Sediment phase modeling 29
2.3.1 Particle equations of motion 29
2.3.2 Simulation of fluctuating velocities 32
2.4 Numerical procedure 36
2.5 Calculation process 37

NUMERICAL SIMULATION OF POND FLOW AND SEDIMENT DEPOSITION USING A LAGRANGIAN DISCRETE PHASE MODEL 41
3.1 Introduction 41
3.2 Model set up 42
3.2.1 Mesh 44
3.2.2 Boundary conditions 45
3.2.3 Sediment transport 46
3.3 Results and discussion 50
3.3.1 Results of flow simulation 50
3.3.2 Sediment removal efficiency 57
3.3.3 Sediment spatial distribution 59
3.4 Diagonal arrangement of inlet and outlet pipes 63
3.4.1 Results of flow simulation 63
3.4.2 Sediment removal efficiency and spatial distribution 67
3.5 Conclusion 71

MATHEMATICAL FORMULATION OF AN EULERIAN TWO-PHASE MODEL 73

4.1 Introduction....73
4.2 Volume fractions....74
4.3 Governing equaitons....75
4.3.1 Continuity conservation equaitons....75
4.3.2 Momentum conservation equaitons....75
4.3.3 Interphase exchange coefficients....81
4.4 Turbulence models....81
4.4.1 Turbulence in the fluid phase....82
4.4.2 Turbulence in the solid phase....84

NUMERICAL SIMULATION OF SEDIMENT TRANSPORT AND SCOUR USING EULERIAN TWO-PHASE MODEL....88
5.1 Introduction....88
5.2 Experiment....88
5.3 Model set up....91
5.4 Solution method....94
5.5 Simulation results and discussion....96
5.5.1 Sediment concentration simulation....96
5.5.2 Sediment transport motion....100
5.5.3 Scour simulation....103
5.6 Conclusion....107

CONCLUSIONS AND RECOMMENDATIONS....109
6.1 Summary and conclusions....109
6.2 Recommendations for further study....111

REFERENCES....114

VITA....121

LIST OF TABLES

Table Page

1.1 Review of typical 2D and 3D numerical flow and sediment transport models.....17

2.1 Values of the constants in the $k-\varepsilon$ model.....28

2.2 Constants α_1, α_2, and α_3 values under different ranges of Re_p.....31

3.1 Cumulative size distribution of particles.....49

3.2 Setup parameters for particle tracking simulations.....58

5.1 Flow data.....89

5.2 Solution conditions and methods for simulation.....94

LIST OF FIGURES

Figure Page

1.1 Factors that influence the trap efficiency of ponds and reservoirs.....3

1.2 Schematic representation of sediment-laden flow over loose bed.....5

2.1 Comparison of drag coefficients from different literature equations..... .32

2.2 Uncoupled discrete phase calculations..... 37

2.3 Calculated procedures for the flow field..... 40

3.1 Sketch of two investigated ponds: (a) pond with pipes in central alignment; (b) pond with pipes in diagonal alignment..... 44

3.2 Gambit generated mesh for pond simulation.....45

3.3 Comparison between real and Rosin-Rammler modeled particle size..... 50

3.4 (a)-(e) Velocity contours at plane Z=0.1 m for different inflow conditions. 53

3.5 Velocity contours at plane Z=0.1 m for different inflow conditions (same color scale)..... . 54

3.6 Velocity vectors at plane Z=0.1 m for different inflow conditions. 55

3.7 Plot of pathlines in the pond..... 56

3.8 Comparison between measured and simulated sedimentation efficiencies based on *BSS* and *Trap* bed boundary conditions.....59

3.9 Simulated bed spatial deposits with *Trap* and *BSS* B.C. with V_{in}=0.15 m/s.....61

3.10 Simulated bed spatial deposits with *Trap* and *BSS* B.C. with V_{in}=0.2 m/s ... 61

3.11 Simulated bed spatial deposits with *Trap* and *BSS* B.C. with V_{in}=0.4 m/s 62

3.12 Simulated bed spatial deposits with *Trap* and *BSS* B.C. with V_{in}=0.6 m/s ... .62

3.13 Simulated bed spatial deposits with *Trap* and *BSS* B.C. with V_{in}=0.8 m/s ... .63

3.14 Velocity contours at plane Z=0.1 m for different inflow conditions (diagonal arrangement of inlet and outlet pipes) 65

3.15 Plot of pathlines in the pond with a diagonal alignment of inlet&outlet.....67

3.16 Simulated sedimentation efficiencies based on *BSS* and *Trap* bed boundary conditions with diagonal arrangement of inlet and outlet pipes..... 68

3.17 Comparison of sedimentation efficiencies based on *BSS* boundary condition between central and diagonal arrangement of inlet & outlet pipes. .69

3.18 (a)-(e) Simulated spatial deposits with *BSS* B.C. with diagonal pipes arrangement under different inflow conditions..... 71

4.1 Model components and equations in Eulerian two-phase model.....87

5.1 Schematic of experimental set up.....90

5.2 Numerical flow configuration of van Rijn's flume experiment.....91

5.3 Grids for two-phase model calculations..... 92

5.4 Contours of volume fraction of the sediment (at the beginning)..... 94

5.5 A typical bed profile with sediment phase volume fraction $\alpha_s \approx 0.5$.....96

5.6 Comparison of numerical results and van Rijn's measurements for sediment concentration profiles: (a) x/h=4; (b) x/h=10; (c) x/h=20; (d) x/h=40..... 99

5.7 Simulation results of bed load flux q_b and suspended load flux q_s 103

5.8 Contours of volume fraction during the development of scouring.....105

5.9 Comparison of bed profiles during the development of scouring.....107

CHAPTER I

INTRODUCTION

1.1 Introduction

Stormwater detention ponds and wetlands have been constructed for water quantity and water quality control purposes. Ponds have been used to protect against flooding by reducing the speed of runoffs entering our natural waterways and by reducing inflow peak discharge to an allowed outflow peak discharge. This process protects areas downstream from erosion as well. Most ponds also function to trap pollutants in runoffs such as nutrients, metals, and sediments from the surrounding land. For stormwater detention ponds, the main physical mechanism of pollutant removal is sedimentation.

The proportion of the incoming sediment that is deposited or trapped, i.e. trap efficiency (TE), is one of the most important properties of a pond or reservoir. This trap efficiency is dependent on the characteristics of the inflowing sediment and the retention time in the pond, which in turn is controlled by pond geometry and runoff characteristics. Figure 1.1 illustrates possible factors that will influence the trap efficiency of ponds and reservoirs.

Two types of models are available to predict trap efficiencies: empirical models to predict average TE on a mid-term basis and theoretical models to predict TE for a single event (Verstraeten and Poesen 2000)[1]. Heinemann (1984) gave an overview of the many

[1] The journal model used in this dissertation is based on ASCE (American Society of Civil Engineers) *Journal of Hydraulic Engineering*

empirical models that could be used for predicting TE. Brune's method and Churchill's method, which are two of the most widely used empirical models among them. Brune (1953) related trap efficiency to capacity/annual inflow ratio (C/I), while Churchill (1948) related TE to a sedimentation index (SI, period of retention divided by mean velocity), which included more hydraulic behavior information. However, empirical models were usually developed for large reservoirs, thus they are not suitable for smaller ponds. For the sake of this research, theoretical models have been developed to model the sediment behavior in ponds. Camp's model, DEPOSITS, CSTRS, and BASIN are four of the theoretically-based models to estimate trap efficiency. However, these models are based either on plug flow or on completely mixed systems which seldom occur in reality and only some aspects of sediment transport processes are considered in each model. Most of the time, the major mechanisms of water quality are closely related to the movement of water mixing processes. Actual retention time in a pond system is a function of the intermittent nature of inflows and flow patterns that develop in basins during flow events (Walker 1998). More knowledge is needed about hydrodynamics within pond systems in order to enhance the predictability of sediment transport, and thus, gain a much more realistic representation of the system's retention time (Benelmouffok and Yu 1989).

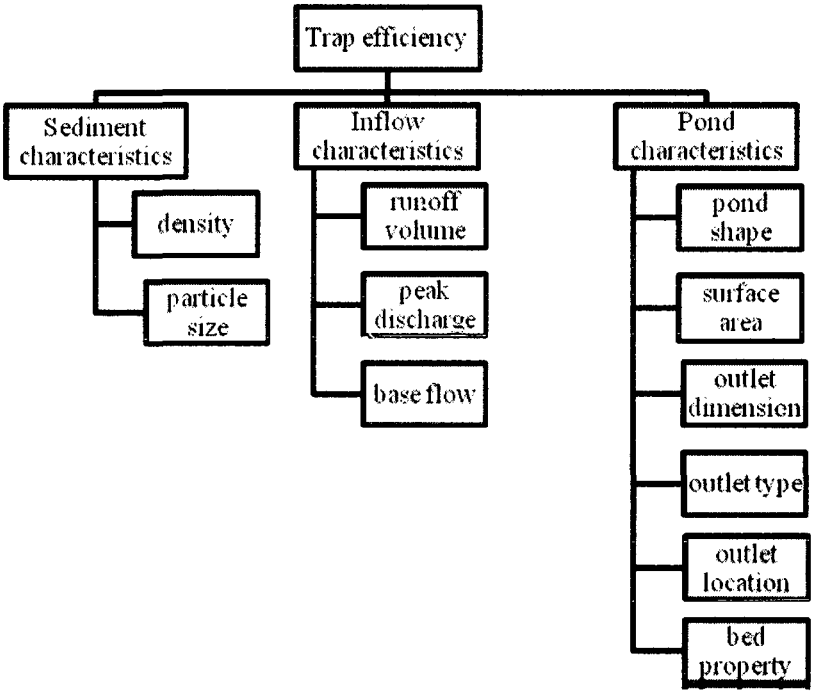

Figure 1.1 Factors that influence the trap efficiency of ponds and reservoirs

Given the many parameters that influence the sedimentation process (or TE) of reservoirs and ponds (see Figure 1.1), it is very difficult to predict TE in a simple manner. The most accurate predictions will be those based on theoretical relations that incorporate all of the influencing factors (Verstraeten and Poesen 2000). For example, factors such as pond shape, inlet/outlet configurations and physical environment can be included since they can significantly influence both hydraulic performances of these facilities and the sedimentation process. Such factors have led to different design recommendations for improving hydraulic performances and also ultimately for improving water quality. However, traditional design methods do not address hydrodynamic features of flow, and these methods cannot in advance evaluate sedimentation performances resulting from different measures such as baffles or different inlet/outlet positions.

Due to the limitations of traditional design methods and limitations of existing empirical/theoretical TE prediction models, the potential application of Computational Fluid Dynamics (CFD) in pond systems has been identified due to the following features:

(1) CFD modeling makes it possible to numerically solve flow, mass and energy balances in complicated flow geometries. The results show specific flow or heat transfer patterns that are hard to obtain experimentally or with conventional modeling methods.

(2) CFD offers an alternative way to study and evaluate the performance of existing detention ponds based upon their hydrodynamic features.

(3) CFD is a powerful tool to help in the design of new pond systems. Unlike traditional design methods, which do not address the hydrodynamic features or problems, the CFD tool can predict flow patterns and short-circuiting problems before the pond is built, and can also predict the effects of measures such as baffles or inlet/outlet reposition in advance to improve performance, thus greatly aiding engineers during the design process.

The above distinct features of CFD make it a useful and reliable tool both in the evaluation of current pond systems and in the design of new ones. In addition, reductions in the cost of computing power, combined with improved solution algorithms and turbulence models, and the development of versatile and user-friendly commercial CFD software have enabled CFD models to be applied to an ever increasing variety of fluid flow situations (Wood and Keller et al. 1998).

1.2 Background on numerical modeling of sediment transport

Flow and sediment transport calculations are one of the most important tasks in the fields of hydraulics, hydrology and water resources. Sediment transport in lakes, rivers or channels with mobile beds is a very complex two-phase phenomenon. In particular, the sediment concentration in the near bed region is generally much higher than that observed away from the bed, and the physical processes and interactions by which the particles are transported are somewhat different. Lots of attention has been paid to the transport process near this region. Figure 1.2 illustrates the nature of sediment motion including bed load and suspended load at a loose bed. Suspended load is comprised of fine sediment particles suspended and transported through the water body. Bed load is comprised of particles transported along the bed. The predominant mode of transport depends on size, shape, and density of particles in respect to velocity and turbulence field of water body (Celik and Rodi 1988).

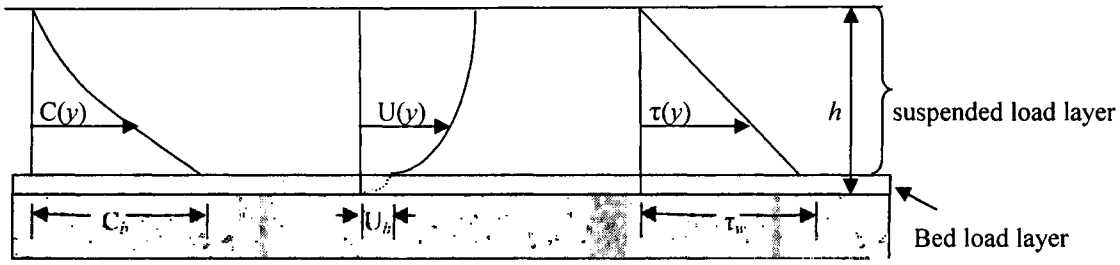

Figure 1.2 Schematic representation of sediment-laden flow over loose bed
C(y): concentration profile; U(y): velocity profile; $\tau(y)$: shear stress profile.

The estimation of flow and sediment transport is very difficult because flow in open waters is sometimes turbulent, the stream cross-section is irregular in geometry and may vary with time, and the sediment transport phenomenon itself is very complex (Wu

and Rodi et al. 2000). The sediment transport process of stormwater detention systems is similar to that of rivers or open channels. Successful simulation of flow and sediment transport in rivers, open channels, or stormwater detention systems requires the use of complex numerical models which will not only accurately predict mean flow but also the effect resulted from bed roughness, deformation of free surface and associated bed changes.

CFD is not only a promising tool for performance prediction and evaluating the flow field in detention ponds, but also is very helpful in modeling sediment transport inside them. Numerical models of flow and sediment transport have mostly been at the levels of 1-D and 2-D simulations, which neglect the influence of secondary flows (Wu and Rodi et al. 2000). When studies are to be carried out at the scale of a river reach with complex geometries, at least the 2-D or even a 3-D approach is required (Hodskinson and Ferguson 1998).

Many 1-D and 2-D flow and sediment transport models have been proposed for river engineering problems. In recent years, several 3D numerical models (Lin and Falconer 1996; Wu and Rodi et al. 2000) that incorporate modules to simulate the suspended sediment transport and/or the bed load transport have become available. Sediment transport in these numerical models is usually divided into the suspended load and the bed load. The suspended sediment transport is generally modeled by a convection-diffusion equation with a sediment settling velocity term included. For bed load transport, some mass balance equation is used for sediment transport within the bed load layer. Empirical relations to determine values such as the equilibrium bed load

transport are usually needed. Once the bed load and suspended load have been determined, some sediment mass balance equation integrated over the whole water depth will be used to calculate the resulting change of the bed level.

As sediment transport is a two-phase flow process, recent researchers have formulated general flow-sediment interaction models based on a two-phase flow approach. Such models predict sediment transport from more fundamental dynamical equations which employ granular kinetic theory, thereby avoiding the use of purely empirical sediment transport formulas, which are usually case-dependent. The two-phase formulations are developed based on more fundamental concepts, and thus are expected to have more general applicability to a range of problems (Zhao and Fernando 2007).

1.3 Literature review

1.3.1 Literature review on pond hydraulic performance investigation methods

The sediment removal efficiency (trap efficiency or sedimentation efficiency) of stormwater pond systems is often compromised by poor hydraulic design. Improved hydraulic design can reduce the concentration of sediments flowing out of outlet structures and thereby improve the water quality of the receiving environment. In pond design, it should be possible to determine quantitatively the improvement of removal efficiency due to changes in the layout designed to reduce short-circuiting and dead zones. A number of researchers have studied pond hydraulics via field measurements or laboratory scaled models. The work undertaken by Mangelson and Watters in the 1970s at the Utah Water Research Laboratory is one of the earliest and most extensive research

studies undertaken on pond hydraulics. Investigations were conducted on various factors such as the ponds' shape, baffling, length-to-width ratio and the positioning of inlets and outlets. Conclusions were made that the level of treatment effectiveness were greatly affected by these pond hydraulic characteristics (Mangelson and Watters 1972; Watters and Mangelson et al. 1973). Persson (2000) related hydraulic performance with pond shape and the location of inlets and outlets. Pettersson and German et al. (1998) investigated an open stormwater detention basin with respect to mass flows of pollutants and internal flow pattern. The conclusion drawn from this study was that simulations of internal flow patterns are essential in designing pond geometry, and inlet and outlet locations. Gharabaghi and Fata et al. (2006) used a hydrodynamic and sediment-transport model to examine the effect of pond geometry on sediment removal efficiency under varying storm events. The monitoring data and the modeling results clearly demonstrate the importance of proper pond size and geometry design. Other factors that influence hydraulic performance, including vegetation (Kadlec 1990; Moshiri 1993); wind (Kadlec and Knight 1996; Shaw and Watt et al. 1997); and temperature (Marecos de Monte and Mara 1987), were also studied.

During early 1970's, researchers did not consider that it is practically possible to model the hydraulics of the fluid flow throughout the pond mathematically. This led researchers to adopt the alternative approach of using tracer studies to measure the net results of the fluid movements and mixing within the pond as a distribution of retention time at the pond exit (Watters and Mangelson et al. 1973; Shilton 2000). By injecting a tracer instantaneously in the inlet and then measuring the outlet concentration, different systems will produce different residence time distribution functions (RTD). The RTD of

all storm events passing through the pond is necessary for a detailed analysis of a stormwater pond. Using the principles of similarity and dimensional analysis, a series of tracer studies could be undertaken on scale models in a laboratory. Direct application of tracers on real pond field observations is another choice. For example, Fisher (1990), Kadlec and Bastiaens et al. (1993), and Stairs (1993) have all reported studies where dye tracing experiments have been used to determine the residence time distribution for basins. Persson (2000) used tracers on a laboratory scaled model to compare hydraulic performance differences among different layouts.

However, both laboratory-scaled models and field observations have some limitations. Their major limitations include: their high costs, their difficulty to perform or use, and the inability to make them prior to the pond's creation, which imply the difficulty to influence the flow situation (Adamsson and Bergdahl et al. 2005). Meanwhile, tracer experiments are useful for studying existing ponds, but they cannot be used in a predictive manner. Secondly, small-scale laboratory tests will suffer from scale effects because most of the scale down models cannot satisfy complete mechanical similarities which require geometric, kinematic and dynamic similarities. There are several scale effects such as Reynolds number, Froude number, and so on. For example, the Froude number similarity based scale models may preclude the possibility of obtaining the Reynolds number similarity. Consequently, laboratory models will always over-emphasize viscous effects. The scale effects need to be considered when the experimental results are extrapolated to prototype situations.

Due to the limitations with experimental and observational investigations, numerical models seem to be an attractive alternative for studying pond hydraulic performances. Compared to conventional measurement methods, a significant advantage of computer-based numerical simulation is the reduction in both the time and high cost that are typically required to investigate design changes. It is also possible to study several pond layouts before the pond is built and the flow can be studied in detail without suffering from scale effects. In addition, it can be applied to different environmental conditions including those that could not be modeled under normal laboratory conditions. It has been widely accepted that a good numerical model can certainly be complementary to model tests and can assist design engineers in identifying the most crucial cases for which model tests may be conducted (Yang 2005). One goal of numerical models is to replace the costly physical model tests. Following are some examples using numerical models to study pond hydraulic performances.

Following are some examples using numerical models to study pond hydraulic performances. Kadlec (1994) explored three models that can explain the experimental tracer response curves. The system was treated as one-dimensional due to unavailability of analytical expressions for computation of pollutant removal, and difficulties with determining a two-dimensional flow pattern. He attempted to derive appropriate hydraulic parameters such as the Mannings number and dispersion coefficients for a wetland basin in the field so that a more detailed assessment of the flow type and mixing could be determined.

Hocking and Patterson (1994) used a quasi-two-dimensional, numerical, hydrodynamic model to evaluate the dispersal of tracers and residence time of local parcels of water in a reservoir. In this case, a previously developed one-dimensional model was modified so that variations in temperature, salinity and density in the vertical dimension could be modeled.

Despite the fact that two-dimensional modeling has been used extensively in modeling the behavior of pollutants in tidal flows (for example, Lin and Falconer (1997) and Falconer (1984) used such a model to predict the movement of pollutants and sediments in tidal estuaries in the UK) it has not been applied extensively to stormwater wetlands. The work of Anderssen and Dietrich et al. (1990) is one of the few to use this method. They used a steady state two-dimensional numerical model to assist in designing the layout of stormwater ponds. They used comparative assessments as the framework in which to do the development of the user-friendly system, where various pond configurations and designs could be assessed quickly. Based on this work, Andersson and Mooney et al. (1996) developed a linearized depth-averaged computer system NESSIE that interactively provided comparisons of the horizontal flow, streamline patterns and residence time patterns for different lake configurations. However, this steady state analysis is not suitable for ponds where transient events dominate.

Walker (1998) used a two-dimensional horizontal numerical model to determine the fate of incoming flows to a stormwater basin. Depth-averaged flow equations were solved using a computer model HYDRA written by the author, and transport equations were calculated using another finite-difference computer model TRANS, also written by

the author. The modeling technique can be applied to basins of any shape, and it is therefore possible to compare quantitatively different design configurations.

By the middle 1990s, the computer power and particularly the use of computational fluid dynamics software had grown significantly more powerful and user friendly. Thus it allows complex computer simulations of pond hydraulics to be undertaken. FIDAP, Mike21, PHOENICS, and FLUENT are some of the popular commercial CFD codes ever used by researchers to study pond hydraulics.

Wood and Greenfield et al. (1995) used commercial finite element method (FEM) software called FIDAP to qualitatively investigate the hydrodynamics of four pond systems. Pettersson and German et al. (1998) simulated flow patterns in an open stormwater detention pond with FIDAP as well. Conclusions drawn from this study was that simulations of internal flow pattern were essential in designing pond geometry, and inlet and outlet locations. However, FIDAP is limited to 2-dimensional and steady state simulation in a laminar flow regime.

Persson (2000) used the model Mike21 to analyze how the hydraulic performance differs between 13 ponds with hypothetically different layouts. Mike21 is a 2-D CFD package that was developed by the Danish Hydraulics Institute (DHI). It utilizes a depth-integrated approach assuming that the water mass is vertically homogeneous. It is a general numerical modeling system for the simulation of flows, waves and sediments in rivers, lakes, estuaries, bays and coastal areas and seas. By using Mike21, Persson (2000) also includes a discussion of short-circuiting, hydraulic efficiency and suitable

parameters for measuring hydraulic performance. Vega and Pena et al. (2003) used Mike21 to simulate hydrodynamic and advection-dispersion processes in a full-scale anaerobic pond located in southwest Colombia. A set of 12 configurations including inlet-outlet positioning, baffling and pond geometry were modeled.

Shilton (2000) applied PHOENICS CFD package, which is produced by Concentration, Heat and Momentum Limited (CHAM) of London, to explore the hydraulic performance for a wide range of design configurations and scenarios. To demonstrate the potential application of CFD to pond design, the paper presented a series of 3-dimensional and turbulent simulations of a small community pond. It showed how CFD can be applied for design by using the existing pond and the modified pond with a baffle added, thus it allowed direct comparison of the treatment efficiency both with and without the baffle. Shilton and Harrison (2003) provided some useful design information relating to factors such as inlet/outlet, baffles and wind. Pond hydraulic modeling was done with the help of PHOENICS CFD package as well.

Another competitive CFD package that has been applied in pond hydraulic performance simulation is FLUENT (FLUENT Incorporated 2007), which has been used extensively in flow modeling and solutions. FLUENT software package enables the flow domain to be discretised into a large number of cell volumes, for which the Navier-Stokes and mass conservation equations can be solved. Ta (1998) used FLUENT package to analyze the flow dynamics in a service reservoir with separate inlets/outlets and to study the reservoir mixing. Factors such as tank geometry, baffles and inlet arrangement which affect the flow pattern for both steady and unsteady flow conditions were

identified. Stovin and Saul (1996, 1998, 2000), and Stovin and Saul et al. (1999) used the FLUENT package to establish a numerical model of the flow field and to predict sediment retention efficiency for storage chambers. The influence of different length to breadth ratios on chamber performance was studied in detail. Adamsson and Bergdahl et al. (2005) investigated the use of FLUENT software as an engineering tool in stormwater pond design. This was done by comparing simulations in 3-dimensions with both flow pattern and tracer measurements in a large-scale model of a rectangular detention pond.

1.3.2 Literature review on sediment transport numerical modeling

(1) Single phase flow model approach

Most CFD sediment models currently applied to river problems are based on the governing equations for single-phase flows. The common procedure for modeling sedimentation involves splitting the problem into a flow model and into a sediment transport model (Olsen 1999; Wu and Rodi et al. 2000; Wanker and Gockler et al. 2001). The flow model provides the hydrodynamics (local velocities) for sediment movements. The sediment model affects the flow via the changes in the bed topography and in the local bed friction (Zeng 2006). These two models are coupled via more or less empirical formulas describing the mass exchange between suspended load, bed load and the deposited sediment itself.

Generally sediment transport modeling has spatial formulations varying from 1-D, 2-D depth averaged, to fully 3-D flow and sediment transport models. Popular 1-D sediment transport models include HEC6 (Thomas and Prashum, 1977), IALLUVIAL

(Karim and Kennedy 1982), MIKE11 (DHI 1999), CCHE1D (Wu and Vieira et al. 2004), GSTARS-1D, now called SRH-1D (Molinas and Yang 2004), MoSeTT (Smaoui and Boughanim et al. 2007) and so on. The governing equations in these models are the 1D St. Venant equations coupled with the continuity for the sediment. Typically the Manning or Chezy formula is used to close the governing equation systems.

In earlier studies, a depth-averaging technique was used to reduce the river flow to a 2-D problem. In the case when flow can be considered shallow and unstratified, a 2-D depth averaged sediment transport models can be used. The use of the models is applicable under large width-to-depth ratio conditions so that the magnitude of the vertical velocity is much smaller than that of the horizontal velocity and the pressure distribution is close to hydrostatic. In this model level, especially to our interest, (Benelmouffok and Yu 1989) used a vertically averaged 2-D hydrodynamic model to simulate pollutant transports and trappings in a wet detention pond, making it useful in analyzing wet pond modification for urban pollution control. Other popular models include SUTRENCH-2D (van Rijn 1987), USTARS (Lee and Hsieh et al. 1997), FLUVIAL 12 (Chang 1998), Mike21 (DHI 1999), CCHE2D (Jia and Wang 1999; Wu 2001; Wu 2004; Wu and Wang 2004), FAST2D (Minh Duc and Wenka et al. 2004), STREMR HySeD (Abad and Buscaglia et al. 2007) *etc.* In fact, the model proposed by van Rijn combined both 2-D and 3-D approaches. He used a 2-D depth-averaged approach for the flow hydrodynamics and a 3-D approach for the suspended sediment transport. A similar approach could also be found in Olsen (1999).

Complement to popular 2-D models listed above, SUTRENCH-3D, Mike 3, CCHE3D, FAST3D are corresponding 3-D models that are capable of simulating flow and sediment transport. In addition, some other 3-D models for water flow and sediment transport have been proposed in recent years. For example, Demuren (1991) reported his computational study for flow and sediment transport in the 180° laboratory channel bend studied experimentally by Odgaard and Bergs (1988). A finite volume method was used for solving the full Reynolds averaged Navier-Stokes (RANS) equations and the $k-\varepsilon$ turbulence model. A bed-load transport model was included to simulate the sediment transport. Wu and Rodi et al. (2000) presented a 3-D numerical model for calculating flow and sediment transport in open channels. It was proposed on the basis of the general-purpose FAST3D flow solver developed at the University of Karlsruhe (Zhu 1992). The flow is calculated from the full Reynolds-averaged Navier-Stokes equations with $k-\varepsilon$ turbulence model. Suspended-load transport is simulated through the general convection-diffusion equation with an empirical settling velocity term. Bed-load transport is obtained from an overall mass-balance equation. Olsen (2003) used a 3-D CFD model SSIIM to compute the formulation of the meandering pattern in an initially straight alluvial channel. The sediment transport was computed as bed load in addition to solving the convection-diffusion equation for suspended sediment transport. Refer to Table 1.1 for a review of typical 2D and 3D numerical flow and sediment transport models. In the purpose of evaluating the bed load transport, most of the available 3-D models were focusing on developing empirical expression for bed load transport. While the empirical models have been used extensively in engineering design, the details of processes that control the sediment transport are not fully understood. In addition, when it comes to

modeling high sediment concentrations in the fluid, the single phase flow model approach does not seem appropriate because it neglects momentum exchanges between fluid and particles.

Table 1.1 Review of typical 2D and 3D numerical flow and sediment transport models

Model and references	Flow	Sediment transport		Bed-elevation changes	Turbulence	Numerical method
		Bed load	Suspended load			
SUTRENCH-2D, van Rijn (1987)	Quasi Unsteady 2D	Yes	Yes (Quasi Unsteady 2D)	Total load concept	Yes	FEM with quadrangular grids
SUTRENCH-3D, van Rijn (1987)	Quasi Unsteady 2D, depth averaged	Yes	Yes (Unsteady 3D)	Bed load layer/ Total load approach	Yes	FVM with structured grids
MIKE21, DHI (1993)	Unsteady 2D depth averaged	Yes	Yes	Total load concept	Yes	FDM
MIKE3, DHI (1997)	Unsteady 3D hydrodynamic	Yes	Yes	Exner equation	Yes	Implicit ADI finite difference scheme
FAST2D, Minh Duc et al. (1998)	Unsteady 2D depth averaged	Yes	Yes	Total load concept	Yes	FVM with structured grids
FAST3D, Zhu (1992), Wu and Rodi et al. (2000)	Unsteady 3D hydrodynamic	Yes	Yes	Total load concept	Yes	FVM with structured grids
CCHE2D, Wu and Wang (2005)	Unsteady 2D depth averaged	Yes	Yes	Exner equation	Yes	FEM/FVM
CCHE3D, Wu and Wang (2005)	Unsteady 3D hydrodynamic	Yes	Yes	Exner equation/Total load concept	Yes	FVM
Benelmouffok and Yu (1989)	Unsteady 2D depth averaged	No	Yes	Not considered	No	FDM with rectangular grids
USTARS, Lee et al. (1997)	Quasi Unsteady 2D	Yes	Yes	Total load concept	No	FDM
FLUVIAL 12, Chang (1998)	Unsteady 2D	Yes	Yes	Allocation of scour and fill across a section	No	FDM
STREMR HySeD, Abad and Buscaglia et al. (2007)	Unsteady 2D, depth averaged	Yes	Yes	Exner equation	Yes	FVM
Demuren (1991)	Steady 3D	Yes	Yes	Algebraic equations and iterative procedure	Yes	FVM with structured grids
SSIIM, Olsen (2003)	Unsteady 3D hydrodynamic	Yes	Yes	Exner equation	Yes	FVM with structured grids
EFDC 3D, Hamrick (1992)	Unsteady 3D hydrodynamic	Yes	Yes	Total load concept	Yes	FDM with Cartesian or curvilinear-orthogonal grid

(2) Two-phase flow model approach

Clearly, sediment transport involves two phases: liquid phase and solid phase. Based on the two-phase concept, there are two different modeling approaches to simulate the transport of solid phases: Euler-Euler and Euler-Lagrange. In the Euler-Euler approach, different phases (fluid and sediment) are modeled as continuum using the Navier-Stokes equations. In the Euler-Lagrange approach, the sediment phase is represented by tracking discrete particles, taking momentum, heat and mass transfer between the two phases into account. Both consider the liquid phase as a continuum. Owing to the continuum description of the particulate suspension, Eulerian models require additional closure laws to describe particle-particle interactions. In most recent continuum models constitutive relations according to the kinetic theory of granular flow are incorporated. This theory is basically an extension of the classical kinetic theory of gases to dense particulate flows, which considers non-ideal particle-particle collisions and particle-particle drag. Discrete particle models on the other hand do not require additional closure equations for the suspended particulate phase since they compute the motion of every individual particle, with consideration of collisions and external forces acting on the particles.

In recent years, several papers have been reported to use Euler-Euler two-phase models that consider the dynamics of particle and fluid phases as well as interactions between them. It has been employed for sediment transport calculations in the framework of Navier-Stokes equations. Accordingly, suspended particles are treated as a continuous second phase that interacts with the fluid phase. Cao and Wei et al. (1995) presented an

analysis of velocity and sediment concentration profiles in open channel flows based on the fundamental equations for fluid-solid two-phase flows. Hsu and Jenkins et al. (2001) introduced a sediment transport model based on the two-phase mass and momentum equations, with appropriate closures for the fluid turbulence and near bed boundary conditions. Wanker and Gockler et al. (2001) used an Euler/Euler two-phase model to simulate the sedimentation effects and sediment transport. The model was validated to be applicable under dense flow regions. Zhao and Fernando (2007) successfully applied an Eulerian two-phase model, which implemented Euler-Euler coupled governing equations for flow and sediment phase, to simulate the scour around a long fixed pipeline placed just above a non-cohesive sandy bed.

In the same time, Stovin and Saul (1996, 1998, 2000), and Stovin and Saul et al. (1999) applied particle tracking under Lagrangian approach to combined sewer overflow efficiency prediction. Based on Lagrangian frame, Shams and Ahmadi et al. (2002) performed a computational modeling analysis of flow and sediment transport, and deposition in meandering rivers. Adamsson and Stovin et al. (2003) used Lagrangian particle tracking for modeling sediment transport.

By avoiding the use of purely empirical sediment transport formula which has been developed for specific applications, the two-phase formulations are developed based on more fundamental dynamic equations. Two-phase models are expected to have more general applicability to a range of problems.

1.4 Research contributions

In this thesis two noticeable features have been identified in modeling of flow and sediment transport processes:

(1) The use of computational fluid dynamics technique in stormwater pond modeling. It offers the way to solve flow and mass balances numerically for complicated flow geometries, which are hard to obtain with conventional modeling methods. In addition, CFD can predict pond performance for current pond systems, more importantly CFD makes it possible to evaluate pond performance in a predictive manner. The resulting cost saving and performance improvement are of great importance for engineers and planners especially in the design of new pond systems.

(2) The concept of multiphase flow approach in modeling sediment transport instead of using single phase flow model approach.

The main contributions of this thesis are to

(1) develop and implement sediment transport subroutines into FLUENT software, followed by application of the numerical model to predict flow, sediment deposition, and sediment spatial distribution in the bed with different arrangement of inlet and outlet pipes in stormwater ponds.

(2) model sediment transport in alluvial channels using an Eulerian two-phase model to simulate flow, bed load, suspended sediment transport, scour development and evolutions without invoking purely empirical sediment transport formula.

1.5 Dissertation objectives

The overall goal of this study is to develop and verify efficient and accurate 3D hydrodynamic numerical models, which are:

- capable to simulate flow hydrodynamics and sediment depositions, and to predict sedimentation efficiencies based on the Eularian-Lagrangian approach for low sediment-laden flows;
- capable to simulate flow, sediment transport, and bed deformation with loose bed based on Eulerian two-phase mass and momentum equations.

The main objectives of this study are as follows:

1. Numerical implementation of a Discrete Phase Model (DPM) in a Lagrangian frame to model flow and sediment transport in stormwater ponds. Specific tasks include:

   (1) construction of the model, including generation of the computational mesh and selection of appropriate boundary and initial conditions.

   (2) application of Rosin-Rammler expression to represent particle size distribution instead of using a mean diameter to represent all of the particle sizes.

(3) solving the fluid flow equations and using the model to investigate detail information on flow hydrodynamics under different inflow conditions.

(4) simulating the discrete particle trajectories using the solved fluid flow solutions to analyze sedimentation efficiencies based on different inflow conditions and geometry configurations.

(5) prediction of the effects of turbulence on the dispersion of particles using the stochastic tracking model, which includes the effect of instantaneous turbulent velocity fluctuations on the particle trajectories through the use of stochastic methods.

(6) application and comparison of the bed shear stress (*BSS*) boundary condition and *Trap* boundary condition to simulate particle deposition behavior on the pond bottom.

(7) analysis of sediment spatial distribution resulting from different bed boundary conditions and different inlet and outlet geometry arrangements.

2. Numerical implementation and validation of an Eulerian two-phase modeling approach for sediment transport in an open flume with a deformable bed. Specific tasks include:

(1) Develop a coupled model for a sediment-laden flow in an open flume, in which the flow-particle and particle-particle interactions are taken into account. Each of the two phases (fluid and sediment) is described using

appropriately modified Navier-Stokes equations, and coupling between the phases is achieved through the pressure and an interphasial exchange terms.

(2) Implement a modified $k-\varepsilon$ turbulence closure that take into account the interfacial turbulent momentum transfer between the fluid phase and the sediment phase.

(3) Verify the suspended sediment concentrations at different cross sections, which are predicted by the model, with experimental data available from literature.

(4) Apply and verify two-phase flow theory to simulate scour for the loose bed. Scour hole developing process is analyzed and simulated scour profiles are compared with measured profiles from the experiment.

1.6 Outline of the dissertation

Chapter II details the mathematical description of the flow model and the discrete phase model (DPM) in Lagrangian frame. Governing equations for both flow modeling and particle motion including their related parameters are described in detail. Numerical procedures to solve the equations and calculation process are presented in this chapter as well.

In Chapter III, numerical implementation of the discrete phase model in stormwater tanks is carried out, and is applied to two cases with different arrangements of

inlet and outlet pipes. To simulate sediment deposition in the bed, two different types of boundary conditions are used in both cases. Comparisons on flow hydrodynamics, sedimentation efficiency and sediment spatial distribution in the bed are investigated on both cases based on different inflow conditions, geometry configurations, and bed boundary conditions with non-uniform sediment size distributions.

Chapter IV presents the mathematical description of an Eulerian two-phase model. The continuity and momentum conservation equations for both fluid and sediment phases are introduced. A modified $k-\varepsilon$ turbulence model is used to predict turbulent quantities for the fluid phase. To obtain turbulent quantities for the solid phase, a simplified linear model based on Tchen's theory (Tchen 1947) is employed. In addition, transport equation for granular temperature as well as models to calculate interphase momentum exchange coefficients will be described in detail in this chapter.

In Chapter V, numerical implementation of the Eulerian two-phase model introduced in Chapter 4 is carried out in an open flume case study from literature. Simulation results of sediment concentrations in different cross sections are compared and verified with results from experimental data. The development of scour hole is investigated and is validated using experimental data from the literature as well.

Finally, summaries and conclusions are made and recommendations for future work are laid out in Chapter VI.

CHAPTER II

MATHEMATICAL FORMULATION OF STORMWATER POND MODELING

2.1 Introduction

This chapter introduces the mathematical details of stormwater pond modeling. Two main components are included: the flow model and the discrete phase model (DPM) in a Lagrangian frame. The flow model solves conservation equations for mass and momentum. The flow characteristics including velocity field are evaluated through the flow model. The $k-\varepsilon$ turbulence model is used for evaluation of the turbulence stress components. The Euler-Lagrange approach is one of the two numerical approaches to model multiphase flows. In this approach, the fluid phase is modeled as a continuum by solving the time-averaged Navier-Stokes equations. The sediment phase is represented by individual particles which are tracked through the calculated flow field and can exchange momentum and mass with the fluid phase when the coupled approach is used. Both phases will have volume fractions which represent the space occupied by each phase.

There are several assumptions made in this modeling application: (1) a basic assumption made in this modeling approach is that the sediment phase occupies a low volume fraction, which makes the model appropriate for low sediment-laden flows; (2) particles are spherical and particle-particle interactions are negligible; (3) the flow development is not influenced by the presence of sediments. In most cases this

assumption is valid since the sediment concentration is small with low sediment-laden flows.

2.2 Flow modeling and governing equations

The mathematical basis for a fluid flow model is developed from basic principles of mass and momentum conservation. The derivation of the system of Partial Differential Equations that govern flows in Cartesian coordinates is not presented here. Basically, the conservation law of physics is applied. The continuity equation is derived based on conservation of the fluid mass; and the derivation of momentum equation is based on Newton's second law which indicates the rate of change of momentum equals the sum of the forces on a fluid particle.

All flows encountered in engineering practices become unstable above a certain Reynolds number. Flows in the laminar regime can be completely described by solving the continuity and Navier-Stokes equations analytically, while turbulent flows give rise to additional stresses on the fluid, the so-called Reynolds stresses. Thus it is important to use an appropriate turbulence model for evaluating the flow field and turbulence stress components. The well established and the most widely used standard $k-\varepsilon$ turbulence model (Launder and Spalding 1974). is applied for this purpose.

With the assumptions in section 2.1, the flow field is determined by introducing the Reynolds-averaged Navier-Stokes equations. For an incompressible fluid flow, the equations of the continuity and balance of momentum in Cartesian coordinates are given as

$$\frac{\partial u_i}{\partial x_i} = 0 \tag{2.1}$$

Rate of change of mass in fluid element = Net rate of flow of mass into fluid element

$$\frac{\partial u_i}{\partial t} + u_j \frac{\partial u_i}{\partial x_j} = -\frac{1}{\rho}\frac{\partial p}{\partial x_i} + \frac{1}{\rho}\frac{\partial \tau_{ij}}{\partial x_j} + F_i \tag{2.2}$$

Rate of change of Momentum of fluid particle = Sum of forces on fluid particle

where u_i are the velocity components (u, v, and w accordingly); i, j indicates direction (x-, y-, z-direction accordingly); ρ is fluid density; p is pressure; and F_i is the gravitational body force per unit volume. The turbulent stress components τ_{ij} are calculated with the standard $k-\varepsilon$ turbulence model employing the following turbulent viscosity relation

$$\tau_{ij} = \rho \nu_t \left(\frac{\partial u_i}{\partial x_j} + \frac{\partial u_j}{\partial x_i}\right) - \frac{2}{3}\delta_{ij} k \tag{2.3}$$

$$\nu_t = C_\mu k^2 / \varepsilon \tag{2.4}$$

where ν_t is the turbulent kinematic viscosity; k is the turbulence kinetic energy and ε is its dissipation rate. k and ε can be obtained from the following transport equations:

$$\frac{\partial k}{\partial t} + \frac{\partial (u_j k)}{\partial x_j} = \frac{\partial}{\partial x_j}\left(\nu + \frac{\nu_t}{\sigma_k}\frac{\partial k}{\partial x_j}\right) + G - \varepsilon \tag{2.5}$$

$$\frac{\partial \varepsilon}{\partial t}+\frac{\partial (u_j \varepsilon)}{\partial x_j}=\frac{\partial}{\partial x_j}(\nu+\frac{\nu_t}{\sigma_\varepsilon}\frac{\partial \varepsilon}{\partial x_j})+C_{1\varepsilon}G\frac{\varepsilon}{k}-C_{2\varepsilon}\frac{\varepsilon^2}{k} \tag{2.6}$$

In words, the above two equations are indicating

Rate of change of k or ε + Transport of k or ε by convection = Transport of k or ε by diffusion + Rate of production of k or ε - Rate of destruction of k or ε

$$G=\nu_t(\frac{\partial u_i}{\partial x_j}+\frac{\partial u_j}{\partial x_i})\frac{\partial u_i}{\partial x_j} \tag{2.7}$$

The equations contain five constants C_μ, $C_{1\varepsilon}$, $C_{2\varepsilon}$, σ_k, σ_ε. Their values can be found in Table 2.1. The standard $k-\varepsilon$ model employs values for the constants that are determined from comprehensive data fitting for a wide range of experiments. They have been found to work fairly well for a wide range of wall-bounded and free shear flows (FLUENT Incorporated 2007).

Table 2.1 Values of the constants in the $k-\varepsilon$ model

C_μ	$C_{1\varepsilon}$	$C_{2\varepsilon}$	σ_k	σ_ε
0.09	1.44	1.92	1.0	1.3

2.3 Sediment phase modeling

In addition to solving transport equations for the continuous phase, a discrete second phase, which consists of spherical particles dispersed in the continuous phase, in a

Lagrangian frame of reference can be simulated by computing the trajectories of these discrete phase entities, as well as mass transfer to/from them. The coupling between the phases and its impact on both the discrete phase trajectories and the continuous phase flow can be included.

In this section, particle equations of motion which predict the trajectory of a discrete phase particle will be introduced. The simulation of associated instantaneous turbulent velocity fluctuations on the trajectories will be disclosed as well.

2.3.1 Particle equations of motion

The trajectory of a discrete phase particle is predicted by integrating the force balance on the particle, which is written in a Lagrangian reference frame. The force balance equates the particle inertia with the forces acting on the particle. For the x direction in Cartesian coordinates, it can be written as

$$\frac{du_p}{dt} = F_D(u - u_p) + \frac{g_x(\rho_p - \rho)}{\rho_p} + F_x \tag{2.8}$$

where u is the fluid phase velocity, u_p is the particle velocity, ρ is the fluid density, and ρ_p is the density of the particle. $F_D(u - u_p)$ is the drag force per unit particle mass due to the relative slip between the particle and the fluid, and the second term on the right-hand side is the gravitational force, which only appears in the vertical direction. F_x is an additional acceleration term that can be important under special circumstances. For example, "virtual mass" force is the force required to accelerate the fluid surrounding the

particle and is important when $\rho > \rho_p$. Other examples include the force due to pressure gradient in the fluid, thermophoretic force resulting from temperature gradient, and Saffman's lift force for submicron particles. Generally the drag force is the dominating force and F_D is defined as

$$F_D = \frac{18\mu}{\rho_p d_p^2} \frac{C_D \mathrm{Re}_p}{24} \tag{2.9}$$

here, μ is the dynamic viscosity of the fluid, d_p is the particle diameter, Re_p is the particle Reynolds number defined as

$$\mathrm{Re}_p = \frac{\rho d_p |u_p - u|}{\mu} \tag{2.10}$$

The drag coefficient, C_D, depends on various factors. At small particle Reynolds numbers ($\mathrm{Re}_p < 0.1$), the total drag coefficient is given by Stokes's law, and is as follows

$$\mathrm{C_D} = \frac{24}{\mathrm{Re}_p} \tag{2.11}$$

With an increasing particle Reynolds number, Stokes's law underestimates the drag. An often used expression for the drag coefficient is given by Schiller & Nauman (Clift and Grace et al. 1978)

$$C_D = \frac{24}{\mathrm{Re}_p}(1+0.15\mathrm{Re}_p^{0.687}) \qquad \mathrm{Re}_p < 1000$$

$$= 0.44 \qquad \mathrm{Re}_p \geq 1000 \qquad (2.11)$$

FLUENT uses equation by Morsi and Alexander (1972)

$$C_D = \alpha_1 + \frac{\alpha_2}{\mathrm{Re}_p} + \frac{\alpha_3}{\mathrm{Re}_p^2} \qquad (2.12)$$

where α_1, α_2, and α_3 are constants that apply to smooth spherical particles depends on the particle Reynolds number as indicated in Table 2.2 (Morsi and Alexander 1972). Figure 2.1 compares drag coefficients resulting from different drag coefficient equations. The Morsi and Alexander model is the most complete, adjusting the function definition frequently over a large range of Reynolds numbers, but calculations with this model may be less stable than with the other models.

Table 2.2 Constants α_1, α_2, and α_3 values under different ranges of Re_p

Re_p	α_1	α_2	α_3
$\mathrm{Re}_p < 0.1$	0	24.0	0
$0.1 < \mathrm{Re}_p < 1$	3.69	22.73	0.0903
$1 < \mathrm{Re}_p < 10$	1.222	29.1667	-3.8889
$10 < \mathrm{Re}_p < 100$	0.6167	46.5	-116.67
$100 < \mathrm{Re}_p < 1000$	0.3644	98.33	-2778
$1000 < \mathrm{Re}_p < 5000$	0.357	148.62	-4.75×10^4
$5000 < \mathrm{Re}_p < 10000$	0.46	-490.546	57.87×10^4
$\mathrm{Re}_p > 10000$	0.5191	-1662.5	5.4167×10^6

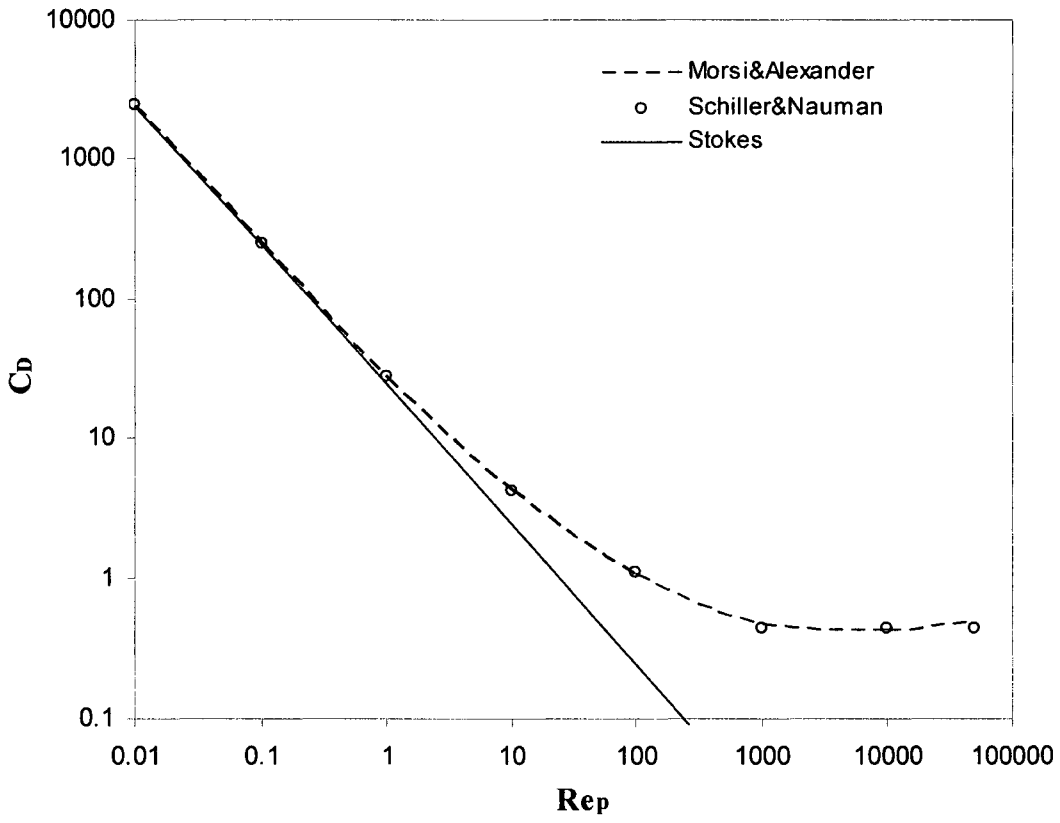

Figure 2.1 Comparison of drag coefficients from different literature equations

2.3.2 Simulation of fluctuating velocities

All the related forces can be included in Equation (2.8) which forms the basis for the discrete phase analysis that will be used in the computation. The particle equations of motion require knowledge of the instantaneous turbulent velocity fluctuations on the particle trajectories at each particle location and at every instance of time. Some researchers (Wilkinson and Waldie 1994; Pettersson 1997) assume that the particle trajectories may be calculated from the mean flow and neglect that the turbulence of the fluid affects the motion of particles. Others (Thomson 1987; Stovin and Saul 2000; Shams and Ahmadi et al. 2002; Adamsson and Stovin et al. 2003) insist that the

dispersion of small particles is strongly affected by the instantaneous fluctuating fluid velocity. Since most of the flow in nature is in a state of turbulent motion and turbulent flows are characterized by fluctuating velocity fields, it is more accurate to consider the effect of turbulent flow field on the dispersion of particles.

In this research, the Reynolds-averaged Navier-Stokes equations govern the transport of the averaged flow quantities, with the whole range of the scales of turbulence being modeled by the use of $k-\varepsilon$ turbulence model. The RANS-based modeling approach greatly reduces the required computational effort and resources, and is widely adopted for practical engineering applications.

The dispersion of particles due to turbulence in the fluid phase can be predicted using the stochastic tracking model, which is also called a discrete random walk model. In the stochastic tracking approach, the turbulent dispersion of particles is predicted by integrating the trajectory equations for individual particles, using the instantaneous fluid velocity, $\overline{u}+u'$, along the particle path during the integration. The random effects of turbulence on the particle dispersion are accounted for by computing the trajectory in this manner for a sufficient number of representative particles.

In the discrete random walk model, the fluctuating velocity component u', v', and w' are discrete piecewise constant functions of time and are sampled by assuming that they obey a Gaussian probability distribution. Their random value is kept constant over an interval of time given by the characteristic lifetime of the eddies, τ_e. The stochastic tracking model in FLUENT is based on eddy interaction model and the

discrete particle is assumed to interact with a succession of eddies. Each eddy is characterized by a Gaussian distributed random velocity fluctuation, u', v', and w', a time scale (life time of eddy) τ_e, and a length scale (size of eddy) L_e.

In more detail, the instantaneous velocities are given as

$$u' = \zeta\sqrt{\overline{u'^2}} \tag{2.13}$$

$$v' = \zeta\sqrt{\overline{v'^2}} \tag{2.14}$$

$$w' = \zeta\sqrt{\overline{w'^2}} \tag{2.15}$$

where ζ is a normally distributed random number; $\sqrt{\overline{u'^2}}$, $\sqrt{\overline{v'^2}}$, $\sqrt{\overline{w'^2}}$ are the local root-mean-square fluctuation velocities in the x, y, z directions respectively. Since the kinetic energy of turbulence is known at each point in the flow, these values of the RMS fluctuating components can be defined as

$$\sqrt{\overline{u'^2}} = \sqrt{\overline{v'^2}} = \sqrt{\overline{w'^2}} = \sqrt{2k/3} \tag{2.16}$$

for the $k-\varepsilon$ model.

The characteristic lifetime of the eddy is defined as a constant given by

$$\tau_e = 2T_L \tag{2.17}$$

where T_L is the time spent in turbulent motion along the particle path and it is given as

$$T_L = 0.15\frac{k}{\varepsilon} \tag{2.18}$$

for the $k-\varepsilon$ model.

The other option allows for a log-normal random variation of eddy lifetime that is given by

$$\tau_e = -T_L \log(r) \tag{2.19}$$

where r is a uniform random number between 0 and 1; T_L is given by Equation (2.18).

For the $k-\varepsilon$ model, the eddy length scale is given as

$$L_e = 0.15\frac{k^{3/2}}{\varepsilon} \tag{2.20}$$

The particle eddy crossing time is defined as

$$t_{cross} = -\tau \ln[1-(\frac{L_e}{\tau|u-u_p|})] \tag{2.21}$$

where $|u-u_p|$ is the magnitude of the relative velocity; τ is the particle relaxation time defined as

$$\tau = \frac{\rho_p d_p^2}{18\mu} \tag{2.22}$$

During interaction, the fluctuating velocity is kept constant. The interaction lasts until time exceeds the smaller of the eddy lifetime or the eddy crossing time. When this time is reached, a new value of the instantaneous velocity is obtained by applying a new value of ζ.

2.4 Numerical procedure

The partial differential equations for the mean flow Equation (2.1) and Equation (2.2), for the $k-\varepsilon$ turbulence model Equations (2.5) and (2.6) are solved using a control volume-based method (Launder and Spalding 1974; Patankar 1980) to convert the differential conservation equations to algebraic equations that can be solved numerically. In the present study, the first order upwind discretization scheme is used to calculate the derivatives of the flow and turbulence variables. The discretized equations are obtained by integrating over the control volumes formed by the non-staggered numerical grid. The resulted set of algebraic equations is solved by a semi-implicit iterative scheme which starts from an initial guess and converged solutions will be reached after a number of iterations. The iterative calculation is monitored during the whole process and it will be stopped when the maximum scaled residual decreases to 10^{-3} (the default convergence criterion in FLUENT) for all equations. The pressure-velocity coupling is achieved by using the Semi-Implicit Method for Pressure-Linked Equations (SIMPLE) pressure correction algorithm, which is essentially a guess-and-correct procedure for the pressure calculation (Versteeg and Malalasekera 1995).

To solve the equations of motion for the particles Equation (2.8), the Discrete Phase Model uses its own numerical mechanisms and discretization schemes. The underlying physics of the discrete phase model is described by ordinary differential equations as opposed to the continuous flow which is expressed in the form of partial differential equations (FLUENT Incorporated 2007). Implicit and trapezoidal are two numerical schemes, in combination with Automated Tracking Scheme Selection, considering most of the changes in the forces acting on the particles. The trapezoidal scheme uses a semi-implicit trapezoidal integration of Equation (2.8) while the implicit scheme uses an implicit Euler integration, which is unconditionally stable for all of the particle relaxation times. An automated tracking scheme selection is enabled to provide a mechanism to switch in an automated fashion between numerically stable lower order schemes (implicit) and higher order schemes (trapezoidal), which are stable only in a limited range.

2.5 Calculation process

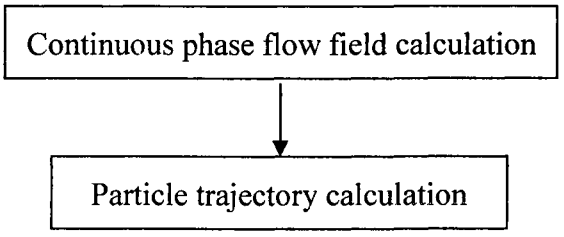

Figure 2.2 Uncoupled discrete phase calculations

Flow and sediment transports are calculated in a decoupled way, which is adequate when the discrete phase is present at a low mass loading. The two-step calculation procedure is illustrated in Figure 2.2. The continuous flow phase will not be

impacted by the presence of the sediment/discrete phase and the calculation will include the following two steps:

(1) Solve the continuous phase flow field. The flow chart for this step are shown in Figure 2.3, and the detailed calculation process is as follows

a) Start from an initial guess of flow field u^*, v^*, w^* including pressure field p^* and turbulence quantities.

b) Solve the discretised momentum equations using the guessed pressure quantities p^*.

c) Solve the pressure correction equation to obtain the corrected pressure p and velocities u, v, w.

d) Solve discretised turbulence transport equations, and update eddy viscosity μ .

e) Use the corrected pressure p as p^* and go back to (b) and repeat the calculations until a converged solution is obtained.

(2) Calculate the particle trajectories for sediment phase injections of interest.

a) Define the sediment properties including density with inert particle types.

b) Specify the initial conditions and particle size distributions.

c) Set boundary conditions for the discrete phase for all of the physical boundaries.

d) Start from the calculated flow field from step 1.

e) Compute the particle trajectories based on a fixed continuous-phase flow field.

f) Postprocessing for the discrete phase: based on repeated simulations, calculate sedimentation efficiencies, which is the proportion of the inflow sediment load that is settled, from summary reports of trajectory fates; Sampling trajectories on the bottom bed to get detailed information about positions of deposited particles which can be used to plot the spatial distribution of deposits in the bed.

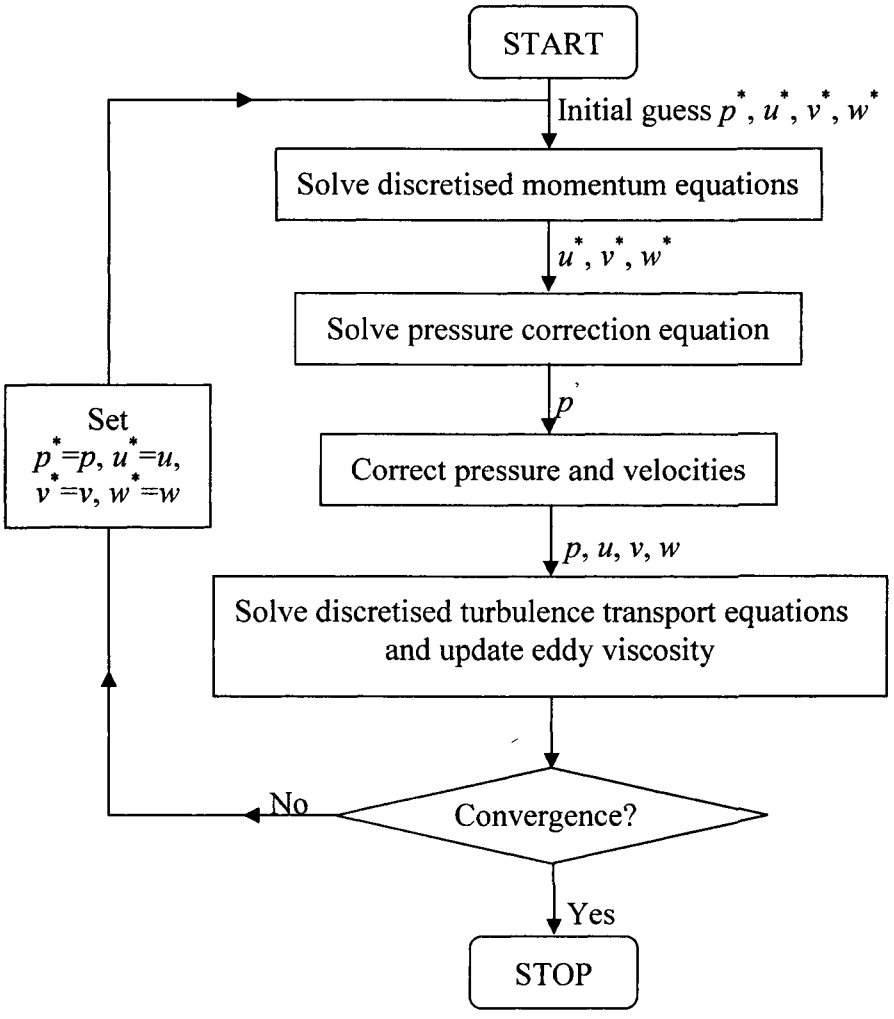

Figure 2.3 Calculation procedures for the flow field

CHAPTER III

NUMERICAL SIMULATION OF POND FLOW AND SEDIMENT DEPOSITION USING A LAGRANGIAN DISCRETE PHASE MODEL

3.1 Introduction

The ability of stormwater ponds to remove stormwater particles through sedimentation has been shown for many years. However, the lack of knowledge about flow and particle transport in stormwater ponds remains a significant problem for their design. Measurements and numerical simulations are two main ways to obtain information about flow and sediment behaviors inside the pond. However, measurements are costly, sometimes hard to perform and they are limited to existing ponds only (Adamsson and Bergdahl et al. 2005). Alternatively, numerical simulations offer a way to study the flow and sediment behavior in detail, even before the pond is built.

Advances in CFD have provided the basis for further insight into the dynamics of multiphase flows. Currently there are two different numerical approaches to model the multiphase flows: Euler-Euler and Euler-Lagrange (FLUENT Incorporated 2007). In this chapter, the Euler-Lagrange approach will be applied in case studies using the Lagrangian discrete phase model in FLUENT. The fluid phase is modeled as a continuum by solving the time-averaged Navier-Stokes equations. The sediment phase is represented by individual particles which are tracked through the calculated flow field and can exchange momentum and mass with the fluid phase. A fundamental assumption made in this model is that the sediment phase occupies a low volume fraction, which makes the model appropriate for low sediment-laden flows.

Given that many parameters can influence the sedimentation process of reservoirs and ponds, it is very difficult to predict trap efficiency, removal efficiency and sedimentation efficiency in a simple manner. As introduced in Chapter I, factors such as shape, inlet/outlet locations, vegetation and wind can influence the hydraulic performance greatly. In this Chapter, the focus will be on locations of inlets and outlets following the work of (Adamsson and Stovin et al. 2003), which investigated the impact of tank geometry. The flow pattern, sediment removal efficiency and spatial distribution of particles with respect to different inflow conditions will be studied.

3.2 Model set up

One of the most important goals in the present study is to see the potential applicability of CFD in the field of stormwater flow and sediment transport modeling. Thus simple geometries and steady state simulations are chosen. It could be extended to much more complex geometries and unsteady simulations as needed. There will be two pond case studies investigated in this chapter, each with a L×W×H of 2 m×0.972 m×0.45 m. Case 1 has aligned inlet and outlet positions along the longitudinal centerline, and Case 2 covers a diagonal arrangement of inlet and outlet, as shown in Figure 3.1. In each case, there are a 1 m length inlet pipe with a diameter of 0.19 m and a 1 m length outlet pipe with a diameter of 0.15 m. Both pipes have an invert elevation equal to the pond's bottom. A penstock was used on the outflow to regulate the flow depth to 0.196 m, according to the experimental setup in the literature (Stovin and Saul 1996; Adamsson and Stovin et al. 2003).

The sediment used is crushed olive stone with d_{50}=47 μm and a density of 1500 kg/m^3. Sediment particles are input at the upstream of the inlet pipe into the model tanks. Stovin and Saul (1996) defined the efficiency, η, as the proportion of the inflow sediment load that is settled.

$$\eta = \frac{settled\ sediment\ load}{settled\ sediment\ load + outflow\ sediment\ load}$$

Five steady inflow conditions will be simulated, with inlet velocities of 0.15 m/s, 0.2 m/s, 0.4 m/s, 0.6 m/s and 0.8 m/s respectively. Accordingly, the flow rate varies from 4.25 l/s to 22.67 l/s. For the two cases investigated, results are compared and verified with experimental data from (Stovin and Saul 1996) in Case 1. In Case 2, the same approach is extended to an application of a hypothetical stormwater pond with a diagonal inlet and outlet pipe arrangement.

(a)

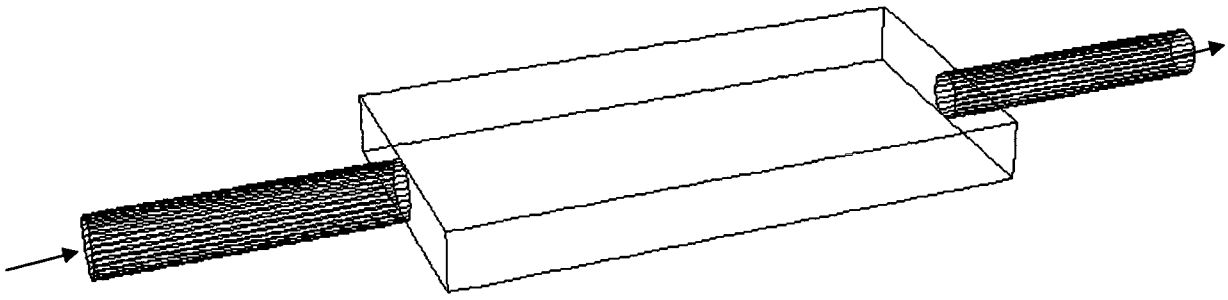

(b)

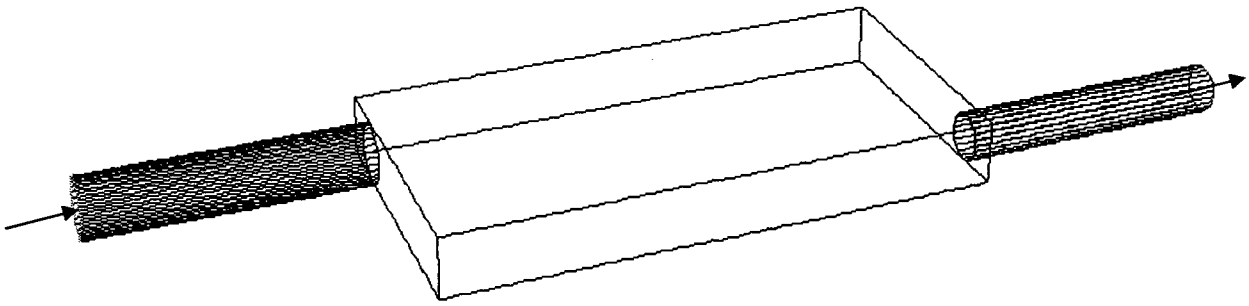

Figure 3.1 Sketch of two investigated ponds: (a) pond with pipes in central alignment; (b) pond with pipes in diagonal alignment

3.2.1 Mesh

The mesh for pond simulations was generated by GAMBIT, FLUENT's geometry and mesh generation software. Its single interface for geometry creation and meshing brings together most of FLUENT's preprocessing technologies in one environment. Advanced tools for journaling give users lots of freedom to edit and conveniently replay model building sessions for parametric studies (www.FLUENT.com). A three-dimensional grid system is built up in this study. For example, a 3-D grid system with 14193 nodes and 31398 cells is generated for Case 1. A Cooper meshing scheme is utilized for inlet pipe volume and outlet pipe volume, with primarily hexahedral elements. A TGrid meshing scheme composed of primarily tetrahedral, hexahedral and pyramidal elements is used for the pond volume. Figure 3.2 details the 3-D view of the GAMBIT generated system grid with a zoom-in look of inlet pipe-pond connection.

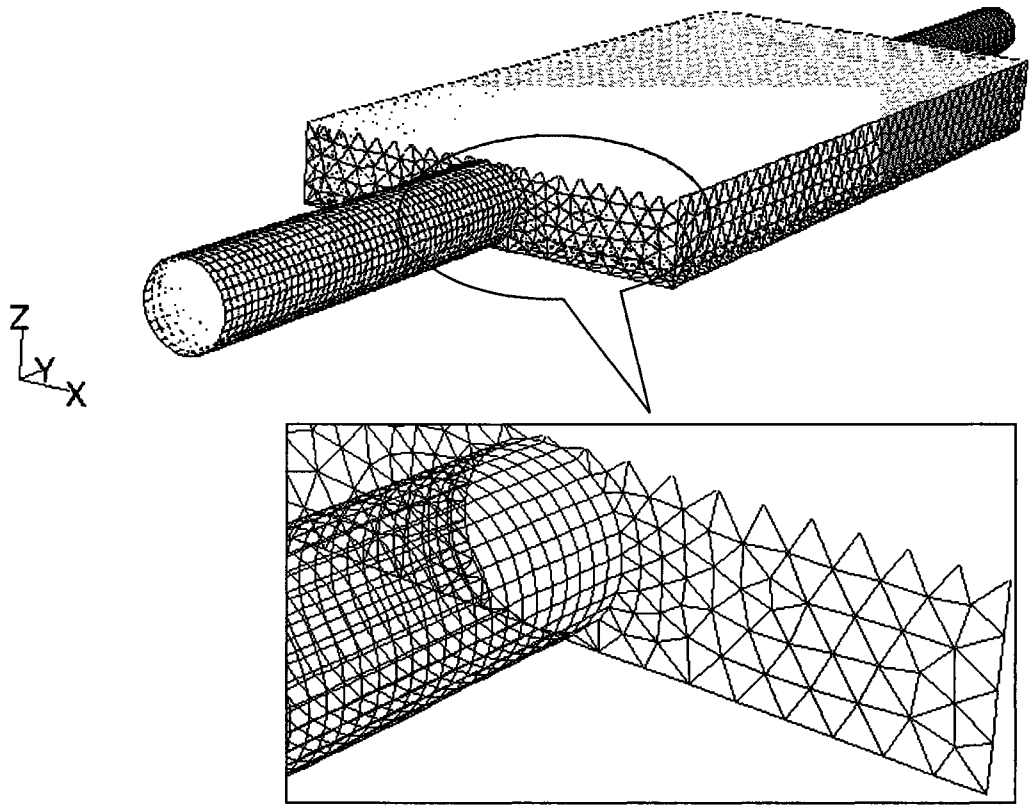

Figure 3.2 Gambit generated mesh for pond simulation

3.2.2 Boundary conditions

Flow simulations for ponds are performed using the FLUENT package, based on the mesh shown in Figure 3.2. The $k-\varepsilon$ turbulence model is used with standard wall functions. The boundary conditions at the walls, which include the walls for inlet and outlet pipes, the side and the bottom of the pond, were set to a wall boundary condition. The position of the water surface is set to 0.196 m as regulated using a penstock in the experiment. It is in reality a free surface, but is modeled as a symmetry plane where a zero-gradient condition is used for the velocity components parallel to the free surface,

while the gradients of k, ε and velocity components perpendicular to the free surface are set to zero. At the inlet, the velocity is set normal to the inlet surface with a uniform velocity varying from 0.15 m/s to 0.8 m/s for five simulations. The pressure outlet boundary condition, with gauge pressure at the outlet boundary, is specified for the flow exit.

The velocity components in the problem domain are set to zero as initial conditions. Initial turbulence parameter values for the turbulence kinetic energy, k, is set at $1 m^2/s^2$, and the turbulence dissipation rate, ε, is set at 1 m^2/s^3. The final solution is independent of these initial solution parameters.

3.2.3 Sediment transport

In addition to solving transport equations for the fluid phase, a discrete second phase (sediment particles) in a Lagrangian frame of reference can be simulated in FLUENT. The Lagrangian particle tracking approach assumes that sediment particles are spherical, and contain low concentrations, thus they do not interact with each other nor with the flow field. FLUENT can compute the trajectories of these particles as well as mass transfer to/from them. The coupling between the phases and its impact on both the discrete phase trajectories and the continuous phase flow can be included; however, for low sediment-laden flows it is more computationally efficient to calculate the flow field first and then the sediment transport. Specifically two FLUENT modeling capabilities are included:

(1) Calculation of the discrete phase trajectory using a Lagrangian formulation that includes the discrete phase inertia, hydrodynamic drag, and the force of gravity under steady state flow conditions;

(2) Prediction of the effects of turbulence on the dispersion of particles due to turbulent eddies present in the fluid phase. In this study, this effect is predicted using the stochastic tracking model, which includes the effect of instantaneous turbulent velocity fluctuations on the particle trajectories through the use of stochastic methods. For a sufficient number of representative particles, the random effects of turbulence on the particle dispersion can be obtained.

Particles are tracked through the flow field. When particles reach a physical boundary such as a wall or outlet boundary, discrete phase boundary conditions are applied to determine the fate of the trajectory at that boundary. Boundary conditions can be defined for each zone of the pond system. The selection of appropriate boundary conditions for the pond bed is vital for the accurate simulation of particle settling behavior (Adamsson and Stovin et al. 2003). Two bed boundary conditions are used and compared in this study:

(1) *Trap* boundary condition: The trajectory calculations are terminated under this boundary condition. In another word, particles settle while hitting the pond bed. This boundary condition excludes the possibility of particle resuspension after hitting the wall, thus it overestimates the sediment removal efficiency.

(2) Bed shear stress (*BSS*) boundary condition: A critical bed shear stress (τ_{cd}) for deposition is defined such that a particle hitting the bed is trapped if the local bed shear stress is below critical shear stress τ_{cd}; the particle is reflected if the local bed shear stress is larger than τ_{cd} (Stovin and Saul 1996; Stovin and Saul 2000; Adamsson and Stovin et al. 2003). The *BSS* boundary condition is a combination of *trap* and *reflect* boundary conditions. In *reflect* boundary condition, particles are reflected back into the flow until a certain number of times are reached. τ_{cd} is evaluated from measurements of the velocity distribution. For the d_{50}= 47 μm crushed olive stone used in the tests, τ_{cd} is found to lie between 0.03 and 0.05 N/m^2.

BSS boundary condition is not a standard component of FLUENT's particle tracking routine. Users need to write user defined functions (UDF) subroutine and hook it to FLUENT after its interpretation or compilation. In this case, a critical bed shear stress will be specified as a threshold. Whenever a particle hits a physical boundary for which the *BSS* boundary condition has been specified, the subroutine evaluates the local bed shear stress, which is the resultant from the *x*-, *y*-, and *z*-components of the wall shear stress for the corresponding cell. The particle hitting the boundary is trapped and the trajectory is terminated if the local bed shear stress is inferior to the threshold value; and the particle is reflected if the local shear stress is superior to the threshold.

Instead of using a mean diameter to represent all of the particle sizes, another novel feature of this study is the application of Rosin-Rammler expression to represent the particle size distribution. The complete range of sizes is divided into a number of

discrete intervals, each represented by a mean diameter for which trajectory calculations are performed. The Rosin-Rammler distribution function is based on the assumption that an exponential relationship exists between particle diameter d, and the mass fraction of particles with a diameter greater than d, Y_d (FLUENT Incorporated 2007):

$$Y_d = e^{-(d/\bar{d})^n} \tag{3.1}$$

where $\bar{d}$ is the diameter at which $Y_d = e^{-1} \approx 0.368$, and n is the spread parameter, which is given by:

$$n = \frac{\ln(-\ln Y_d)}{\ln(d/\bar{d})} \tag{3.2}$$

These parameters can be obtained after fitting the particle size data to the Rosin-Rammler exponential equation. A plot of Y_d vs. d is shown in Figure 3.3 based on data from cumulative size distribution of particles in Table 3.1. From Figure 3.3, we can estimate that $\bar{d} \approx 64$ μm corresponding to $Y_d \approx 0.368$. An average value of n=1.51 is obtained from the values in Table 3.1.

Table 3.1 Cumulative size distribution of particles

Diameter, d (μm)	Y_d	Y_d calculated	n
28	0.8	0.75	1.81
47	0.5	0.53	1.19
88	0.2	0.20	1.49
110	0.1	0.10	1.54

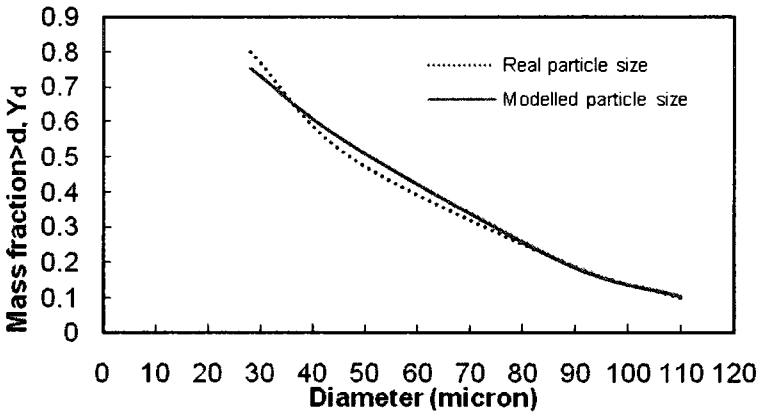

Figure 3.3 Comparison between real and Rosin-Rammler modeled particle size

3.3 Results and discussion

3.3.1 Results of flow simulation

Five different inflow conditions are simulated with V_{in}=0.15 m/s, 0.2 m/s, 0.4 m/s, 0.6 m/s and 0.8 m/s respectively. Particles are injected at the inlet surface after the flow simulations, and results related to this portion will be discussed in the following sections. The z=0.1 m plane, which sits between the tank bed and the top of the pipes, is chosen to show the simulated flow pattern of the pond. The velocity contours with different color scales for all five cases are shown in Figure 3.4 (a) through Figure 3.4 (e). These figures reveal similar flow patterns for all cases with a central jet going from inlet to outlet in the middle of the tank. Longitudinally the magnitude of velocities decreases along the jet until it reaches the vicinity of outlet pipes, where flow goes out and velocity magnitude increases. A lower velocity magnitude is observed in the upper sides of the pond close to the outflow pipe. In contrast, two distinct areas with relative high velocities are displayed in the lower sides of the pond close to the inlet pipe. As presented in Figure 3.6 (a) ~

Figure 3.6 (e), these two areas are two recirculating flow eddies developed at both sides of the jet. Figure 3.5 depicts velocity contours with the same color scale for all the cases, where the same color scale for V_{in}=0.8 m/s velocity contour is chosen. In this way, the velocity magnitude difference between cases can be clearly revealed: the higher inflow velocity, the higher velocity magnitude throughout the pond. With the same color scale, the central jet and side eddies are the strongest in case 5 under V_{in}=0.8 m/s inflow conditions. The outflow velocities are increasing correspondingly. More detail can be found in Figure 3.6 (a) ~ Figure 3.6 (e) with vector plot showing velocity directions and magnitudes simultaneously, and in Figure 3.7 where pathlines are used to visualize the flow of massless particles in the problem domain. In Figure 3.7, flow particles are released from the plane of the inlet pipe. A number of representative pathlines with different colors are used to picture the flow condition in the pond. It can be seen that most of the pathlines are follow the main flow string spanning from inlet pipe to outlet pipe. Only two separate pathlines are circulating along the main flow string in the lower portion of the tank close to the inlet pipe. The pattern of pathlines shown in Figure 3.7 corresponds to the flow condition of V_{in}=0.8 m/s, however the patterns of other inflow conditions are quite similar.

(a) V_{in}=0.15 m/s

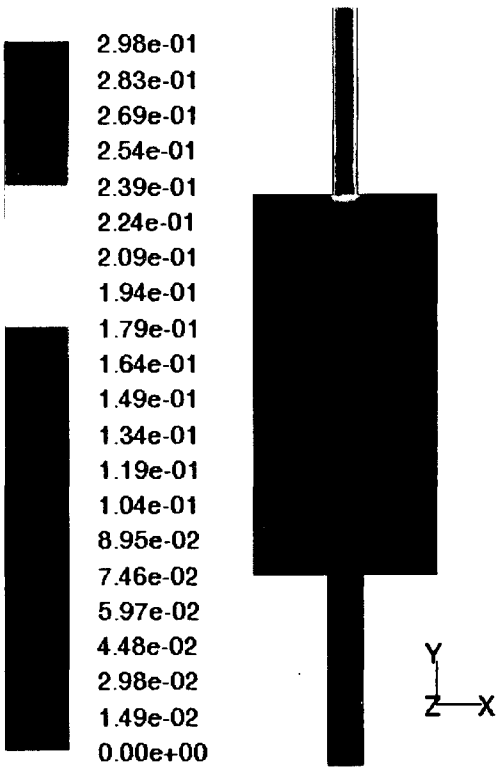

(b) V_{in}=0.2 m/s

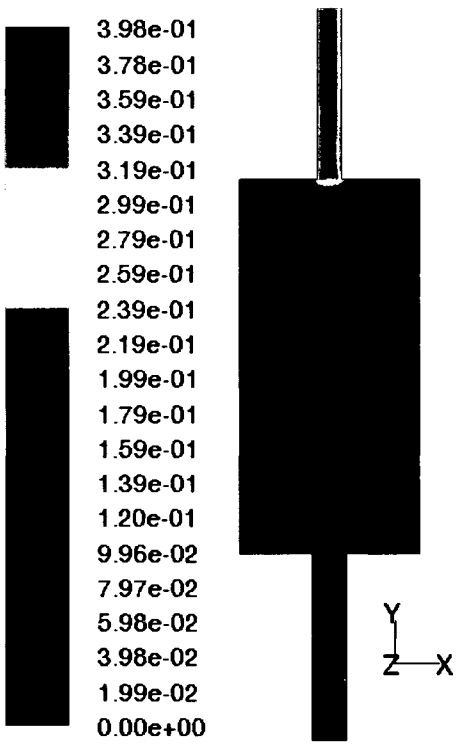

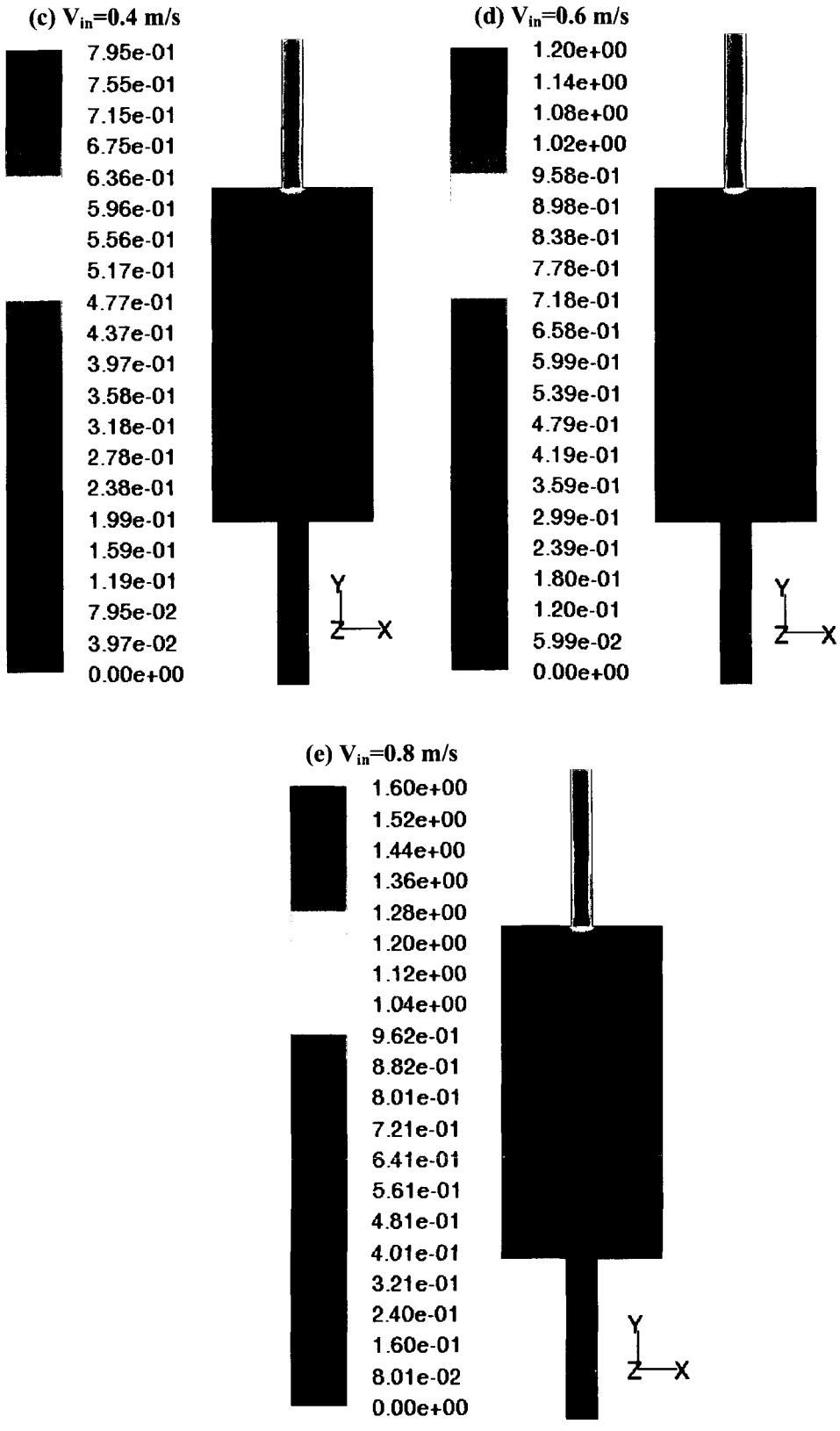

Figure 3.4(a)-(e) Velocity contours at plane Z=0.1 m for different inflow conditions

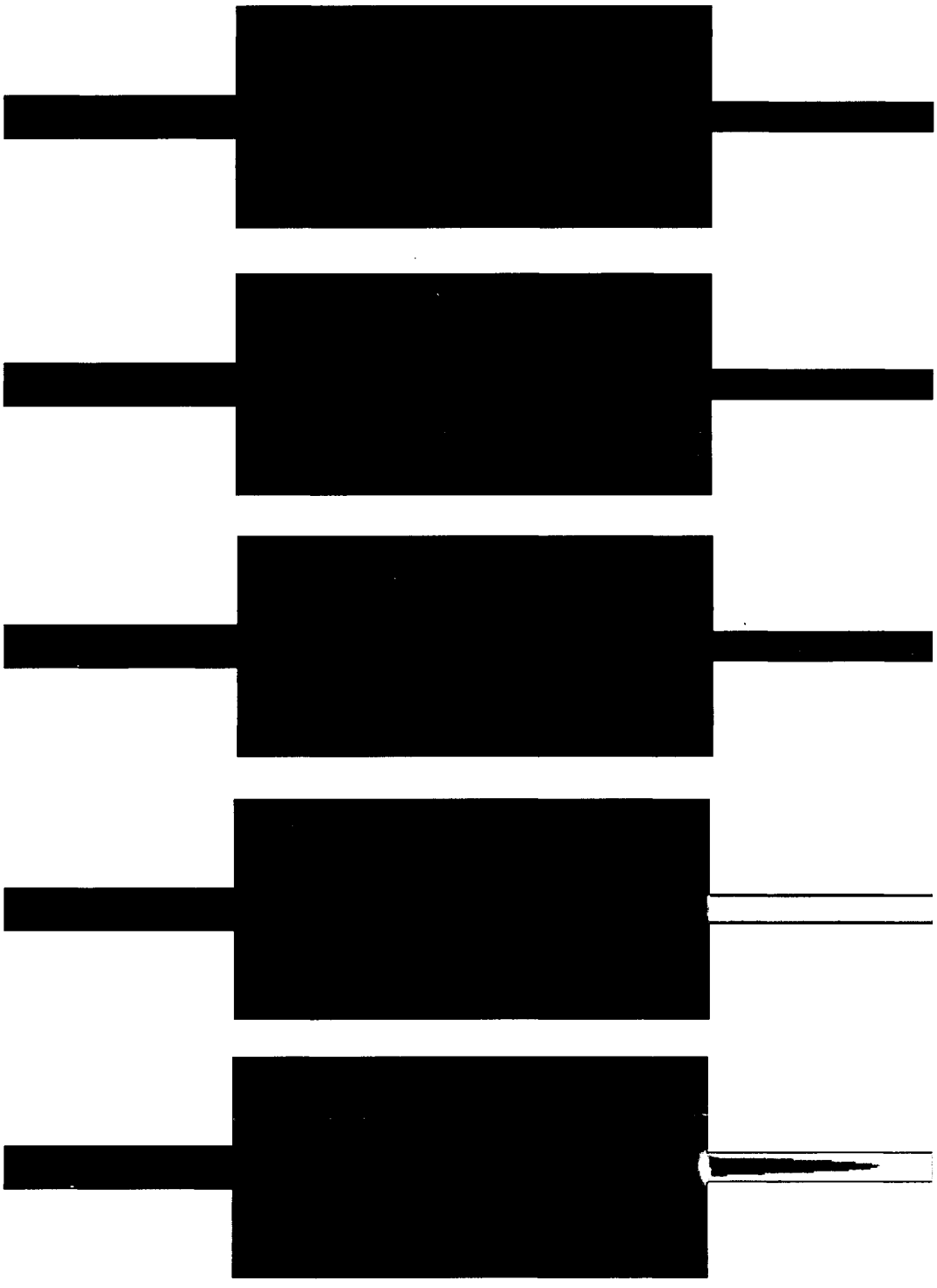

Figure 3.5 Velocity contours at plane Z=0.1 m for different inflow conditions (same color scale)

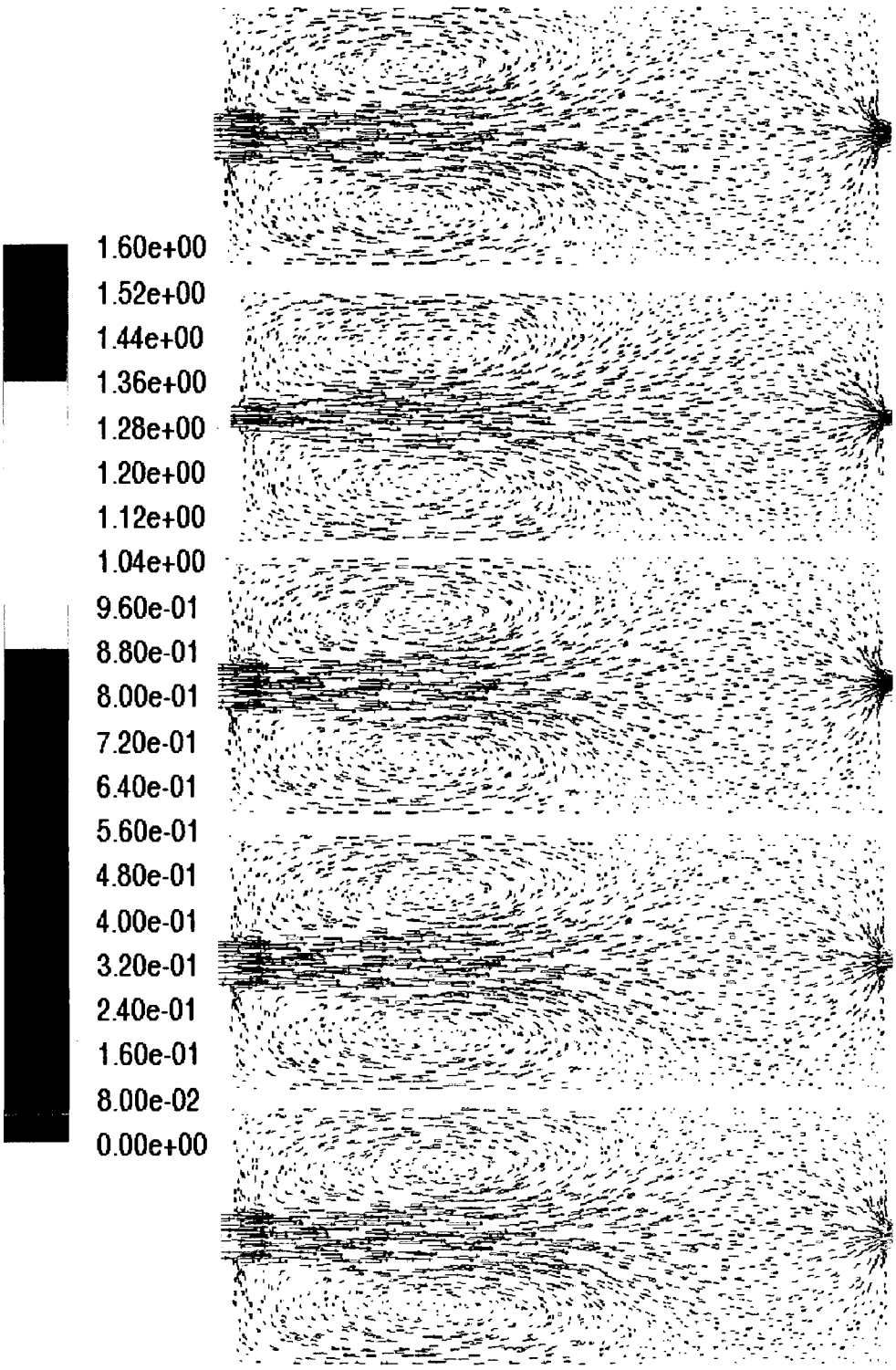

Figure 3.6 Velocity vectors at plane Z=0.1 m for different inflow conditions

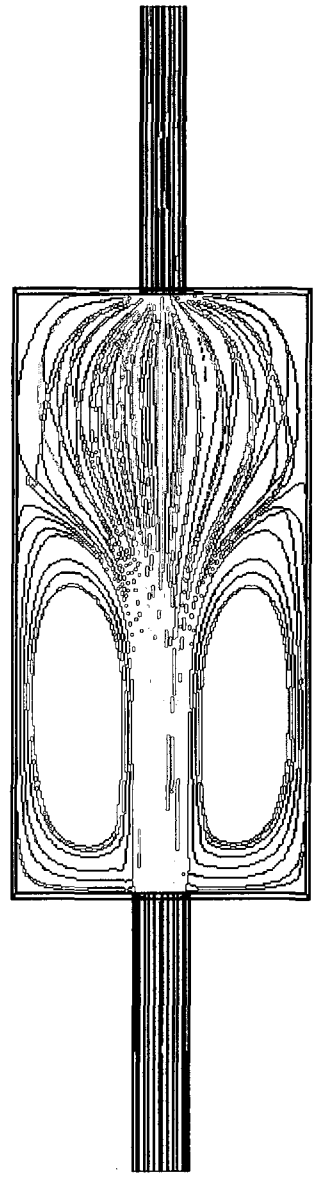

Figure 3.7 Plot of pathlines in the pond with central alignment of inlet and outlet pipes

3.3.2 Sediment removal efficiency

The discrete phase in a FLUENT model is set up by defining the initial position, velocity, size and total flow rate of individual particles. These initial conditions are used to initiate trajectory and mass transfer calculations, which are based on the force balance on particle and on the convective mass transfer from the particle using the local continuous phase conditions as the particles move through the flow.

The particle tracking setup values are detailed in Table 3.2. For each simulation, particles are injected from the inlet surface with 328 particles distributed evenly over the inlet surface. The particles used in simulations are representing olive stone with a density of 1,500 kg/m^3. Instead of using same particle sizes for each test, a Rosin-Rammler expression is used to represent the particle size distribution, with d_{20}=28 μm, d_{50}=47 μm, d_{80}=88 μm, d_{90}=110 μm. Particle tracking is a stochastic process, thus a number of repeat tests is necessary to ensure that the simulated efficiency is representative of the result obtained from an infinite number of simulations (Adamsson and Stovin et al. 2003). In this study, each reported efficiency result is made up of 10 repeat simulations, with 3,280 particles in total. A step length factor controls the time step size used to integrate the equations of motion for the particle. A value of 20 is used. A number of time steps (500,000) are selected to ensure particle tracks would not be aborted before reaching the bed or the outlet. However, the trajectory calculation will be aborted when the number of time steps exceeds 500,000. Two boundary conditions are applied for the bed for comparison: *BSS* and *Trap*.

Table 3.2 Setup parameters for particle tracking simulations

Parameter	Values
Inlet distribution	328 evenly distributed particles
Particle size d_{20}, d_{50}, d_{80}, d_{90}	28, 47, 88, and 110 μm
Particle density	1,500 kg/m^3
Number of simulations	10
Step length factor	20
Maximum number of time steps	500,000
Boundary condition for Walls	*reflect*
Boundary condition for Bed	*BSS, Trap*
Boundary condition for Inlet and Outlet	*Escape*

The results of the particle tracking simulations are used to calculate sedimentation efficiencies for each inflow conditions. These predictions are compared with the laboratory data from literature (Stovin and Saul 1996; Adamsson and Stovin et al. 2003). Figure 3.8 compares the sedimentation efficiencies resulted from measured data from laboratory, *BSS* boundary condition and *Trap* boundary condition for the tank bed, under different inflow conditions. Consistently for all three conditions: the higher the velocities, the lower the sedimentation efficiencies. With lower velocities, the pond can seem to remove sediments up to 80% or even higher, and with higher velocity approaching 0.8 m/s, the removal efficiency drops to as low as 8%. It shows that the *BSS* boundary condition predicts the results which fit the measured data well. Compared to *Trap* bed boundary condition, *BSS* boundary condition reproduces the measured sedimentation efficiencies much better. The *Trap* bed boundary condition overestimates the sedimentation efficiency for high velocities. This implies that in reality the particles are sometimes "bouncing" back while hitting the tank bed, rather than depositing out immediately as indicated in *Trap* boundary condition. For low velocities the *Trap* bed

boundary condition produces similar results with *BSS* bed boundary condition, closely reproducing the measured sedimentation efficiencies.

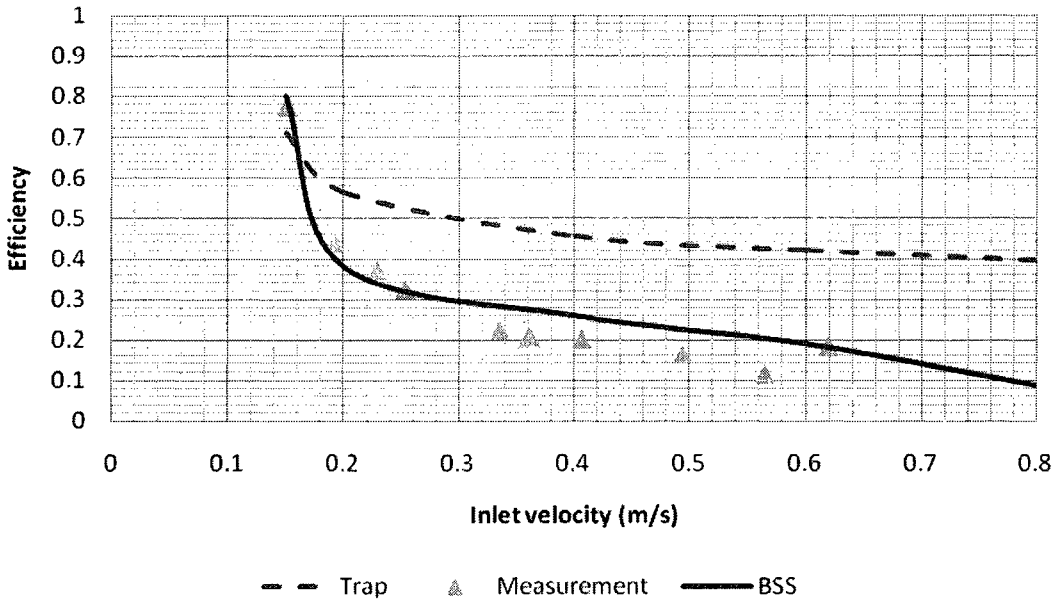

Figure 3.8 Comparison between measured and simulated sedimentation efficiencies based on *BSS* and *Trap* bed boundary conditions

3.3.3 Sediment spatial distribution

Sediment spatial distribution will provide detailed information about the position of the sediment deposits and it is especially important when the tank's maintenance is required. In this section, the sediment spatial distribution on the tank bottom is investigated for both *Trap* and *BSS* boundary conditions and their simulated spatial deposits on the bed are compared from Figure 3.9 to Figure 3.13 for five different inlet velocities: V_{in}=0.15 m/s, 0.2 m/s, 0.4 m/s, 0.6 m/s and 0.8 m/s respectively. In each figure, the rectangular frame is used to represent the bottom of the tank. Two upward arrows are

used to indicate inflow and outflow directions respectively, with inflow coming from the down center of the frame and outflow going out of the upper center of the frame.

For sediment spatial distribution under *Trap* boundary condition, sediment particles are settled down on the bed as soon as they hit the bottom. As observed from the figures, *Trap* boundary condition produced higher sedimentation efficiency than that of *BSS* boundary condition under high inflow velocities. And deposits under *Trap* boundary condition are mainly settled along the main flow path with relatively fewer deposits found on the bed area close to the side walls of the tank. On the contrary, deposits under *BSS* boundary condition rarely settle along the central jet, where much higher bed shear stresses are expected. This is true particularly under higher inlet velocities when the central jet almost extends directly from the inlet to the outlet. Most of the deposits are found apart from the main flow path. For example, with V_{in}=0.4 m/s or higher inflow conditions, the deposits are mostly settled on the two upper ends of the pond close to the side walls.

In addition, *BSS* bed boundary condition is more sensitive to the inflow conditions than that of *Trap* boundary condition. For both conditions, the higher inlet velocity is, the fewer deposits are found in the bed. However, BSS condition depicts a significant distinction between different inflow conditions not only in sediment spatial distribution but also in the total number of deposits, which are used to calculate the sedimentation efficiency and are found to agree with the measured results very well.

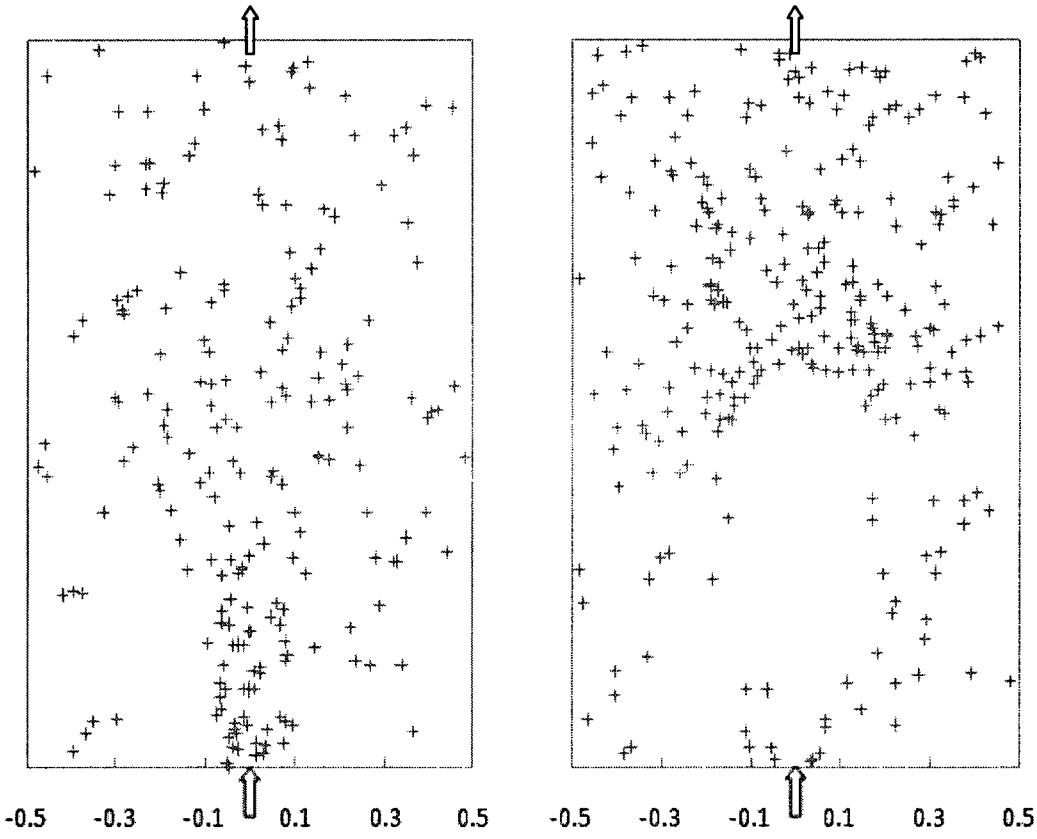

Figure 3.9 Simulated bed spatial deposits with *Trap* and *BSS* B.C. with V_{in}=0.15 m/s

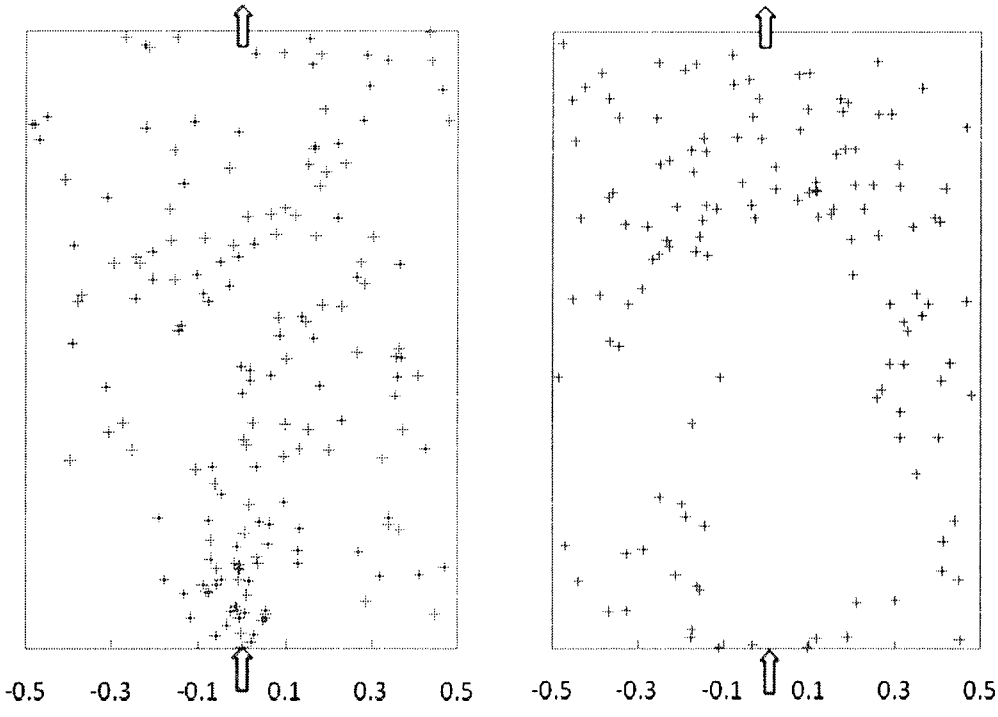

Figure 3.10 Simulated bed spatial deposits with *Trap* and *BSS* B.C. with V_{in}=0.2 m/s

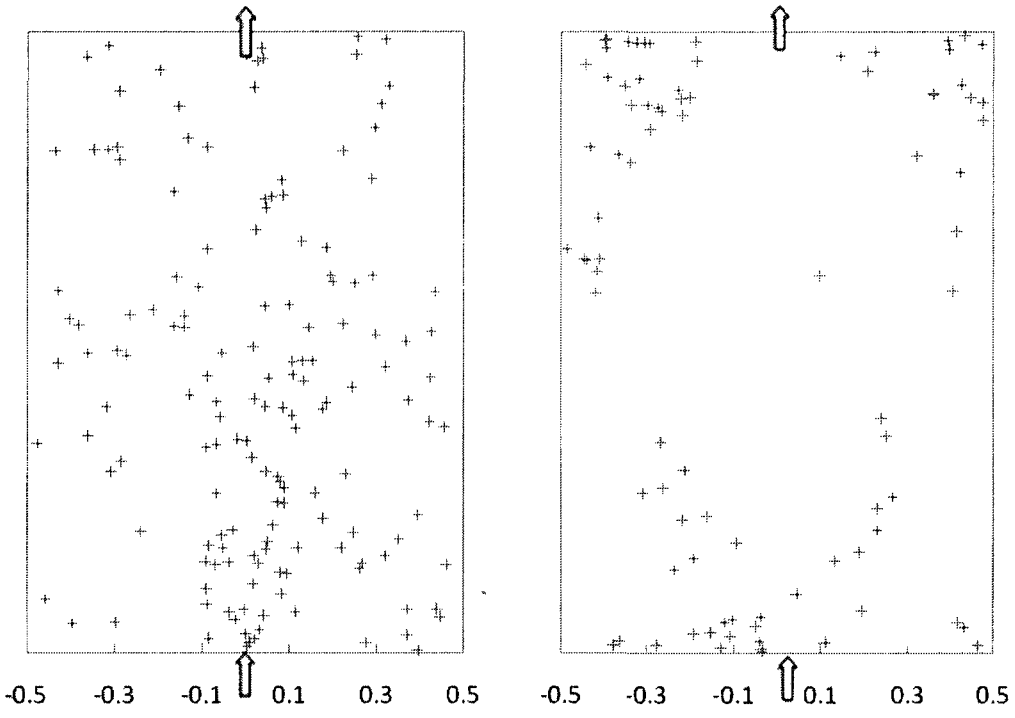

Figure 3.11 Simulated bed spatial deposits with *Trap* and *BSS* B.C. with V_{in}=0.4 m/s

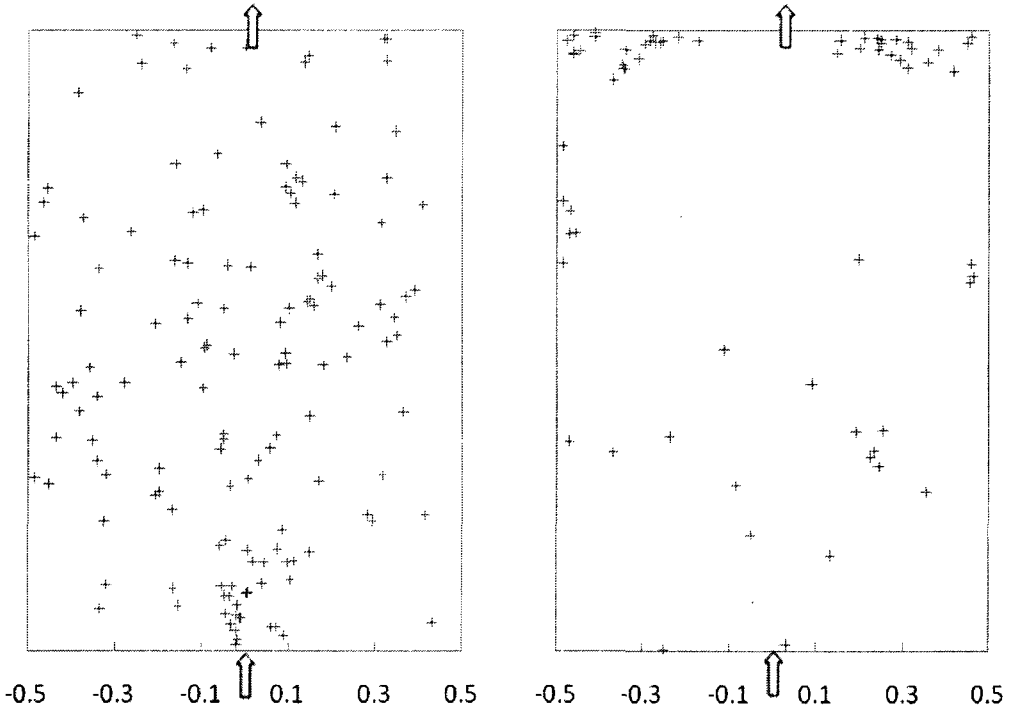

Figure 3.12 Simulated bed spatial deposits with *Trap* and *BSS* B.C. with V_{in}=0.6 m/s

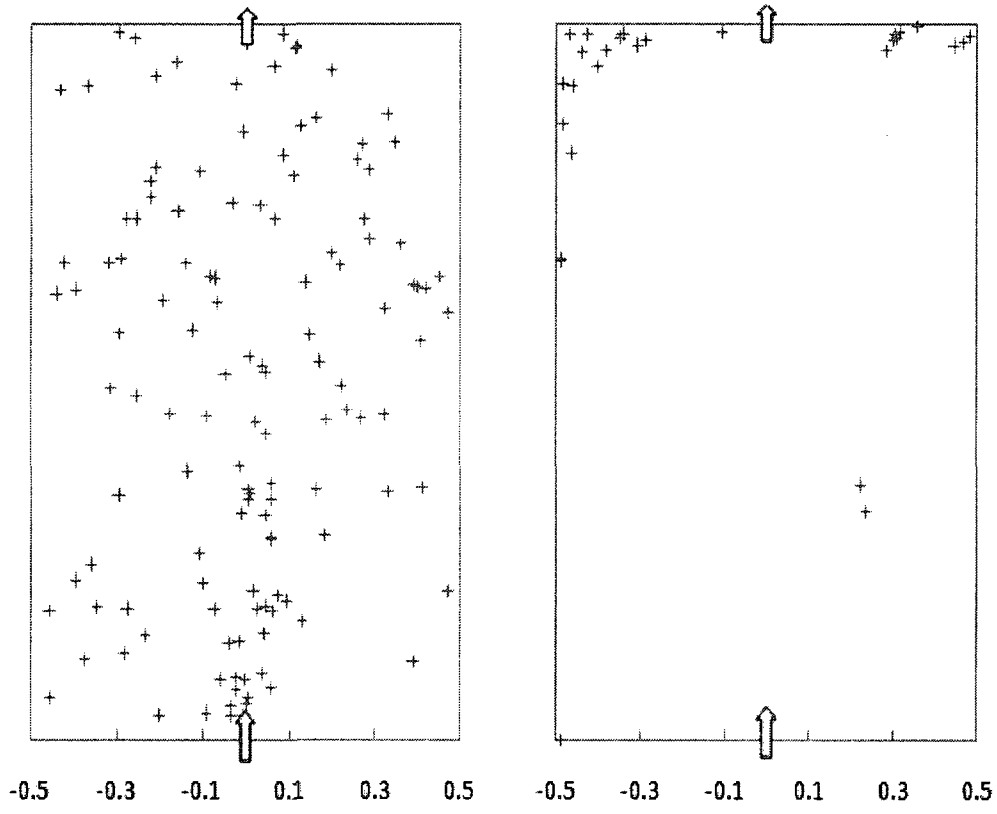

Figure 3.13 Simulated bed spatial deposits with *Trap* and *BSS* B.C. with V_{in}=0.8 m/s

3.4 Diagonal arrangement of inlet and outlet pipes

Another case study is applied in this section in the same pond but with diagonal arrangement of inlet and outlet pipes. The purpose of this study is trying to see the difference on the flow field, sedimentation efficiency and spatial distribution resulting from different inlet and outlet configurations.

3.4.1 Results of flow simulation

As in the previous case the flow conditions at plane Z=0.1 m under five different inflow conditions are shown in Figure 3.14. Different color scales are used for all

conditions. The velocity magnitude increases with the increasing inlet velocities. Similar flow patterns are observed in figure (a) V_{in}=0.15 m/s and (b) V_{in}=0.2 m/s with higher velocities occurring close to the pipes and lower velocities in upper left and lower right corners. The flow path goes through inlet to outlet in a diagonal direction and obviously the main flow path is longer with diagonal pipes arrangement than that of central arrangement. Starting from V_{in}=0.4 m/s, a small area with relatively higher velocities becomes apparent beside the downside of the right wall. It expands both in areas and magnitudes at high inlet velocities. This trend is clearly seen in Figure 3.15. At the same time, a small circulating area to the lower left of the inlet pipe is disappearing at higher velocities. Different from the pond with central alignment of inlet and outlet pipes, the flow patterns and pathlines under diagonal pipes arrangement for all five inflow conditions are not sharing similar shapes.

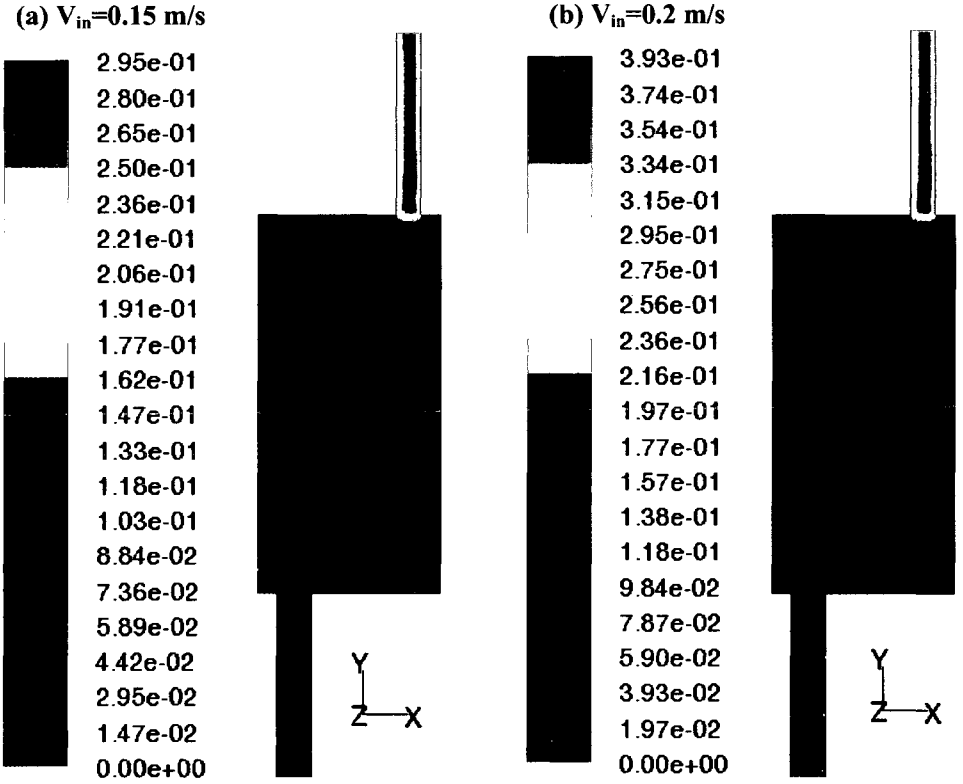

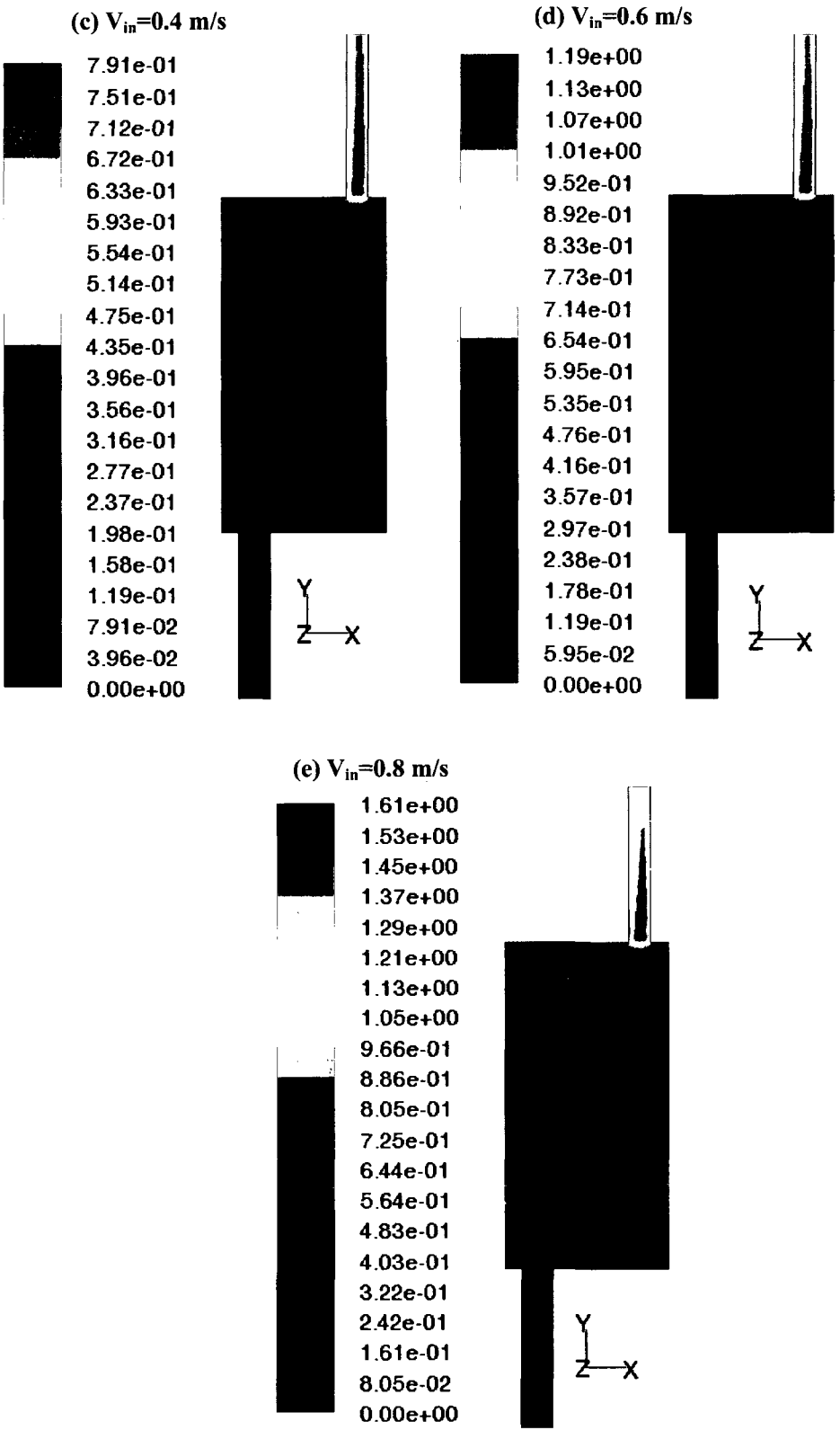

Figure 3.14 Velocity contours at plane Z=0.1 m for different inflow conditions (diagonal arrangement of inlet and outlet pipes)

(a) V_{in}=0.15 m/s **(b) V_{in}=0.2 m/s**

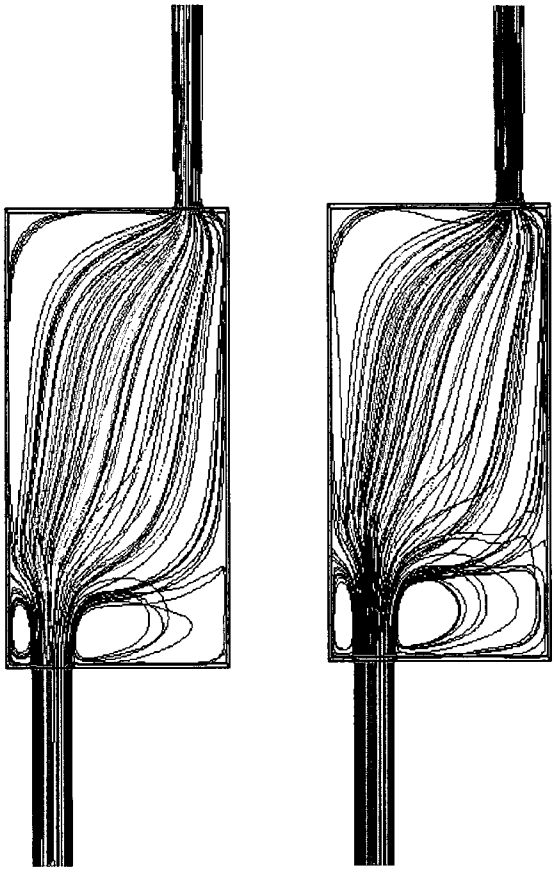

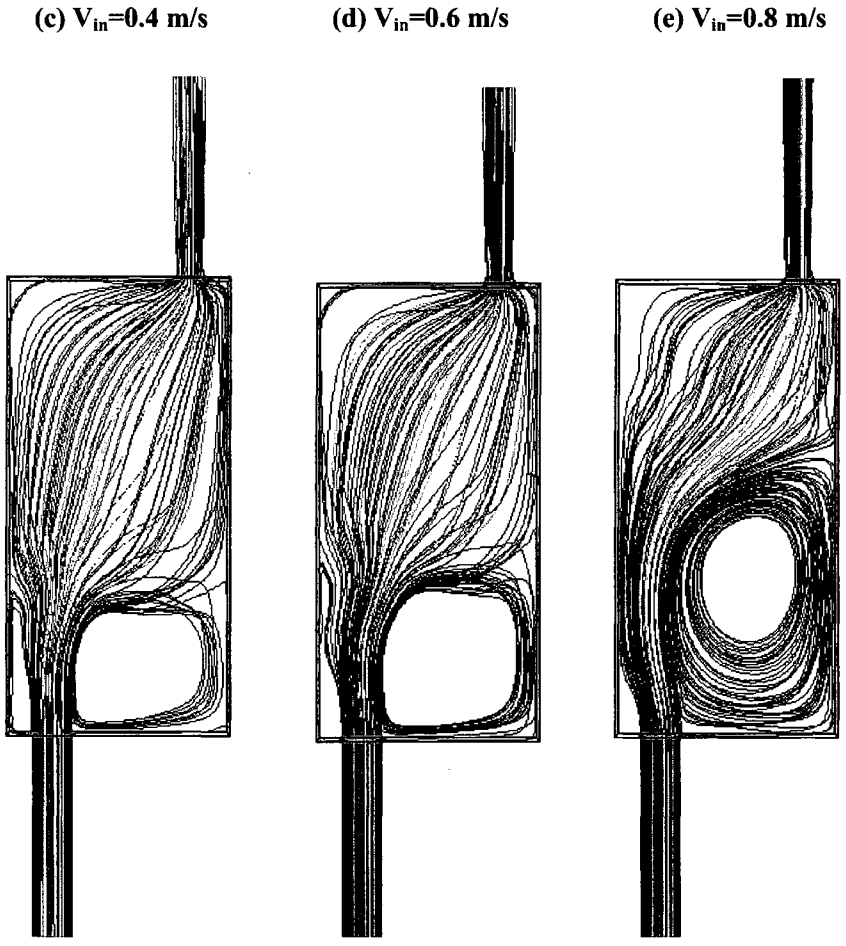

Figure 3.15 Plot of pathlines in the pond with a diagonal alignment of inlet & outlet

3.4.2 Sediment removal efficiency and spatial distribution

Both *Trap* and *BSS* boundary conditions are applied for this case study with diagonal pipes arrangement and sedimentation efficiencies calculated under these two boundary conditions are plotted and compared in Figure 3.16. At high inflow conditions, sedimentation efficiencies resulted from *Trap* boundary condition are consistently higher than that of *BSS* boundary condition with the biggest difference reaching as high as 79%.

Under low inlet velocities (≤ 0.15 m/s), both boundary conditions predict similar sedimentation efficiencies. This trend can be found in Figure 3.8 as well.

The simulated sedimentation efficiencies resulting from different inlet and outlet arrangements are shown in Figure 3.17. Both configurations estimate similar values for sedimentation efficiencies especially under inflow conditions with inlet velocities of 0.5 m/s or higher. For inlet velocities less than 0.5 m/s, diagonal pipe arrangement predicted higher sedimentation efficiencies than that of central arrangement. Basically diagonal arrangement of inlet and outlet pipes will provide a longer flow length, which will extend the time sediments will stay in the pond and will give more chance for sediments to settle in the bottom. However, eddies appearing under higher inflow conditions will impede the settling process and will at least partly reduce the sedimentation efficiencies.

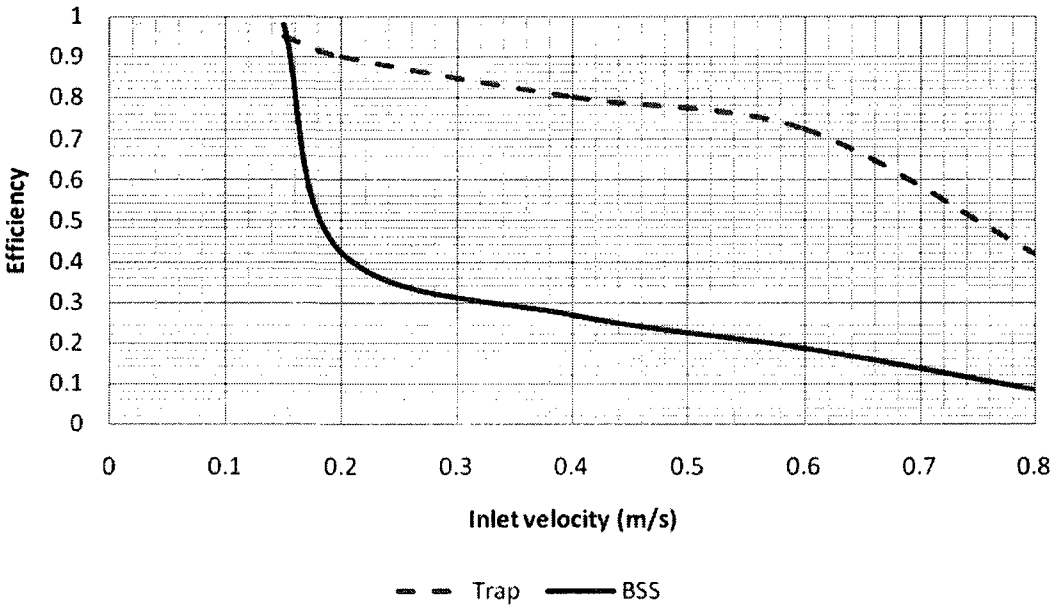

Figure 3.16 Simulated sedimentation efficiencies based on *BSS* and *Trap* bed boundary conditions with diagonal arrangement of inlet and outlet pipes

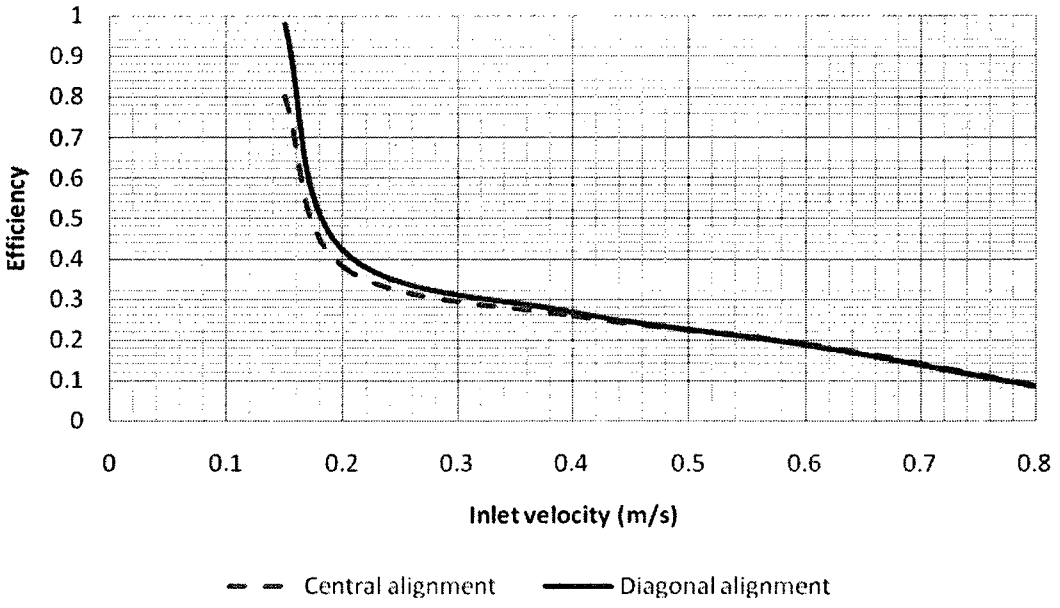

Figure 3.17 Comparison of sedimentation efficiencies based on *BSS* boundary condition between central and diagonal arrangement of inlet & outlet pipes

In this study, another focus has been put on the sediment spatial distribution on the bottom as well. Simulated spatial deposits under *BSS* boundary condition with diagonal pipes arrangement under different inflow conditions is displayed in Figure 3.18. It is clear that the number of deposits decreases with the increase of inlet velocities. At high inflow velocities, the main flow paths are almost clear of sediments. Most of the deposited sediments are gathered up on the upper left hand corner and lower right hand area. In Figure 3.18 (a) with V_{in}=0.15 m/s, deposited sediments are distributed over the bed except the front incoming flow jet area. In Figure 3.18 (b) deposited sediments tend to concentrate beside the main flow path and the two main deposition areas develop in the upper left and lower right hand corners. Starting from Figure 3.18 (c), the number of deposits in the lower right area reduces greatly, which is mainly due to the development of the flow eddy in that area. There is almost no deposition in that area under V_{in}=0.8 m/s, which produces the strongest eddy as can be seen in Figure 3.14 and Figure 3.15.

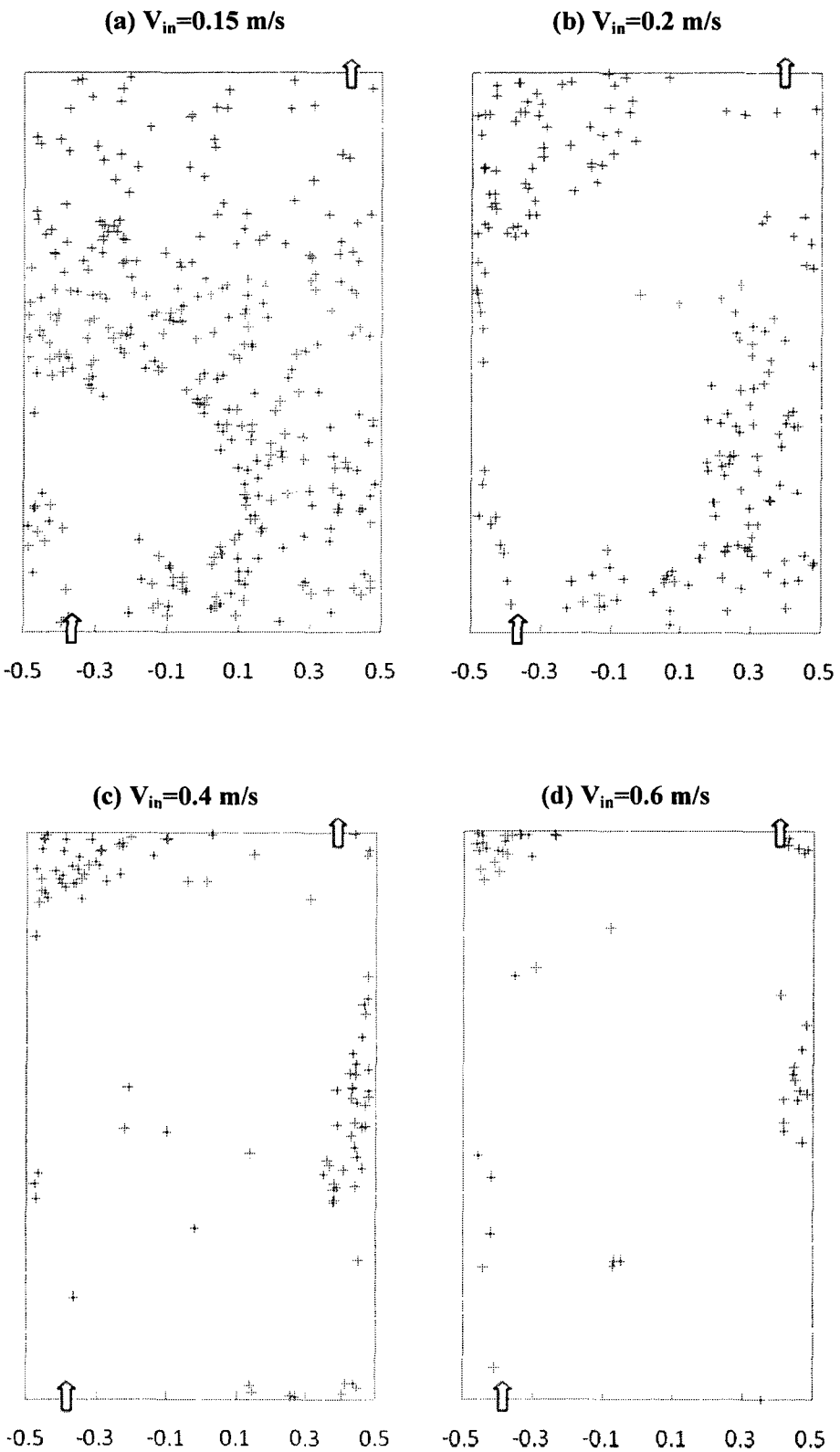
(a) V_{in}=0.15 m/s
(b) V_{in}=0.2 m/s
(c) V_{in}=0.4 m/s
(d) V_{in}=0.6 m/s
-0.5 -0.3 -0.1 0.1 0.3 0.5

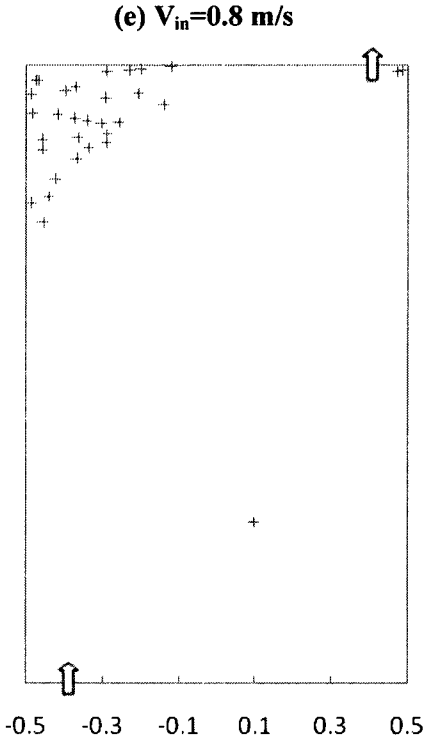

Figure 3.18 (a)-(e) Simulated spatial deposits with *BSS* B.C. with diagonal pipes arrangement under different inflow conditions

3.5 Conclusion

In this chapter the Lagrangian discrete phase model in FLUENT has been used to model particle trajectories in stormwater ponds, and to estimate sedimentation efficiencies of detention ponds. The main purpose of applying CFD in simulating flow fields and sediment depositions in stormwater ponds has been realized by investigating two case studies with different inlet and outlet pipes arrangement: Case 1 with central alignment of inlet and outlet pipes; Case 2 with diagonal arrangement of inlet and outlet pipes. In Case 1, the flow patterns resulting from five different inflow conditions are investigated; sedimentation efficiency and spatial distribution of deposited sediments in the bottom produced by five different inflow conditions and two different bed boundary conditions are studied in detail. In Case 2, a similar study has been carried out on

detention tanks with diagonal arrangement of inlet and outlet pipes. In addition, sedimentation efficiencies resulting from central and diagonal arrangement of inlet and outlet pipes have been compared and discussed in detail. It is demonstrated that this model is a quite efficient 3D hydrodynamic flow and sediment transport numeric model for low sediment-laden flows and for studies of sediment deposition with a variety of sediment sizes, inflow conditions, and geometric arrangements.

User-defined functions such as bed shear stress boundary conditions have been written and hooked to FLUENT to simulate the deposition behavior of the sediments. More UDFs are included to produce correct sediment spatial distribution on the bottom bed.

The results show the potential of CFD as an engineering tool in stormwater pond design and sediment deposition analysis. CFD modeling gives us a way to investigate different detailed designs of flow hydrodynamics and sedimentation behaviors before ponds are built as well as to investigate improvements of existing ponds.

CHAPTER IV

MATHEMATICAL FORMULATION OF AN EULERIAN TWO-PHASE MODEL

4.1 Introduction

In the Euler-Lagrange approach, the fluid phase is treated as a continuum by solving the time-averaged Navier-Stokes equations and the dispersed phase is solved by tracking a large number of particles through the calculated flow field. The dispersed phase can exchange momentum and mass with the fluid phase. More details can be found in Chapter II about mathematical formulation of this modeling approach and in Chapter III with modeling application in stormwater ponds. However, a fundamental assumption made in this model is that the dispersed second phase occupies a low volume fraction, even though high mass loading is acceptable. The particle trajectories are computed individually at specified intervals during the fluid phase calculation (FLUENT Incorporated 2007). This makes the model appropriate for the modeling conditions when the second phase is sufficiently diluted that the particle-particle interactions and the effects of the particle volume fraction on the fluid phase are negligible. In practice, these issues imply that the discrete phase must be present at a fairly low volume fraction, usually less than 10-12% (FLUENT Incorporated 2007). For any application where the volume fraction of the second phase is greater than this range or where particle-particle interactions cannot be neglected, it is more appropriate to turn to the Eulerian multiphase model, in our case, the Eulerian two-phase model.

The Eulerian multiphase model allows for the modeling of multiple, separate yet interacting phases. In this study there are two interacting phases: water and sediment, with each phase being treated mathematically as an interpenetrating continuum. Here an Eulerian treatment is used for each phase, in contrast to the Eulerian-Lagrangian treatment that is used for the discrete phase model.

In this chapter, focus will be put on the mathematical formulation of an Eulerian two-phase model embedded in the FLUENT software. Conservation equations for both continuity and momentum are specified. A modified $k-\varepsilon$ turbulence model will be introduced to model the turbulence in the fluid phase and that of the solid sediment phase will be modeled through a linear model based on Tchen's theory (Tchen 1947). Coupling between phases is achieved through the pressure and interphase exchange coefficients.

4.2 Volume fractions

In the Eulerian approach, each phase is treated mathematically as an interpenetrating continuum. The concept of phasic volume fraction, denoted here as α ($0 \le \alpha \le 1$), is introduced since the volume of a phase cannot be occupied by the other phases. These volume fractions are assumed to be continuous functions of space and time and their sum is equal to one. The laws for the conservation of mass and momentum are satisfied by each phase individually. The volume of phase q, V_q, is defined as

$$V_q = \int_V \alpha_q dV \tag{4.1}$$

with

$$\sum_{q=1}^{n} \alpha_q = 1 \tag{4.2}$$

4.3 Governing equations

Conservation equations for each phase are derived to obtain a set of equations, which have similar structures for all phases. These equations are closed by providing constitutive relations that are obtained by the application of kinetic theory in the case of granular flows.

4.3.1 Continuity conservation equations

The continuity equations for both the fluid phase *f* and solid phase *s* can be defined as

$$\frac{\partial}{\partial t}(\alpha_q \rho_q) + \nabla \cdot (\alpha_q \rho_q \vec{v}_q) = 0 \tag{4.3}$$

where $q=f$, s and $\alpha_f + \alpha_s = 1$. α_f is water volume fraction, and α_s is sediment volume fraction. ρ_f, ρ_s is mass density of water and sediment respectively.

4.3.2 Momentum conservation equations

The interphase momentum transfer between fluid and solid phases is one of the dominant forces in the fluid and solid phase momentum balances. This momentum

exchange is represented by a drag force. The drag force on a single sphere in a fluid has been well studied and empirically correlated for a wide range of particle Reynolds numbers as described in Chapter II. However, particle-particle interactions need to be considered when a single particle moves in a dispersed two-phase mixture, the drag is affected by the presence of other particles. The solid-phase momentum equation contains an additional term to account for momentum exchange due to particle-particle collisions. Syamlal and O Brien (1989), Gidaspow (1992), Wen and Yu (1966) are three of those who managed to calculate the momentum exchange coefficient of gas-solid systems.

Other important forces acting on a single particle include the static pressure gradient, solid pressure gradient (a normal force due to particle interactions), viscous and body forces (Zhao and Fernando 2007). Assuming the neglect of lift force which is more significant for larger particles, and virtual mass force which is appropriate when sediment density is much smaller than the water density, the momentum equations for the water phase *f* and solid phase *s* yield:

$$\frac{\partial}{\partial t}(\alpha_f \rho_f \vec{v}_f) + \nabla \cdot (\alpha_f \rho_f \vec{v}_f \vec{v}_f) = -\alpha_f \nabla P + \nabla \cdot \bar{\bar{\tau}}_f + \alpha_f \rho_f \vec{g} + K_{sf}(\vec{v}_s - \vec{v}_f) \tag{4.4}$$

$$\frac{\partial}{\partial t}(\alpha_s \rho_s \vec{v}_s) + \nabla \cdot (\alpha_s \rho_s \vec{v}_s \vec{v}_s) = -\alpha_s \nabla P - \nabla P_s + \nabla \cdot \bar{\bar{\tau}}_s + \alpha_s \rho_s \vec{g} + K_{fs}(\vec{v}_f - \vec{v}_s) \tag{4.5}$$

where $\vec{v}_f$ is the velocity for water phase *f* and $\vec{v}_s$ is the velocity for the sediment phase *s*; $K_{sf}(\vec{v}_s - \vec{v}_f)$ and $K_{fs}(\vec{v}_f - \vec{v}_s)$ are the interaction forces between two phases, $K_{sf} = K_{fs}$ are the interphase exchange coefficients, which will be discussed in detail in the

following section; P is pressure shared by both phases; $\overline{\overline{\tau}}_f$ is Reynolds stress tensor for the fluid phase. Closure of the solid phase momentum equation (Equation 4.5) requires a description of the solid phase stress and $\overline{\overline{\tau}}_s$ is stress tensor for the solid phase. It is given as

$$\overline{\overline{\tau}}_s = \alpha_s \mu_s (\nabla \vec{v}_s + \nabla \vec{v}_s^T) + \alpha_s (\lambda_s - \frac{2}{3}\mu_s) \nabla \cdot \vec{v}_s \overline{\overline{I}} \tag{4.6}$$

where μ_s is the shear viscosity of sediment phase. The solids stress tensor contains shear and bulk viscosities arising from particle momentum exchange due to translation and collision. λ_s is the bulk viscosity of the sediment, and accounts for the resistance of the granular particles to compression and expansion. The granular kinetic theory derived by Lun and Savage et al. (1984) was adopted to calculate λ_s as

$$\lambda_s = \frac{4}{3}\alpha_s \rho_s d_s g_{0,ss}(1+e_{ss})(\frac{\Theta_s}{\pi})^{1/2} \tag{4.7}$$

The calculation of shear viscosity includes collisional, kinetic parts, and an optional frictional part. In the dilute part of the flow, solids randomly fluctuate and have translation movement, and this form of viscous dissipation and stress is referred to as kinetic; at higher concentrations, solids can collide briefly giving rise to further dissipation and stress, referred to as collisional; at very high concentrations (more than 50% in volume), solids start to endure long, sliding and rubbing contacts, which give rise to a totally different form of dissipation and stress, referred to as frictional (Duarte and

Murata et al. 2008). This frictional component of viscosity can be included when particles of a solid phase reach the maximum solid volume fraction $\alpha_{s,\max}$, which is equal to 0.63 by default. Thus the solids shear viscosity can be given as

$$\mu_s = \mu_{s,col} + \mu_{s,kin} + \mu_{s,fr} \tag{4.8}$$

$$\mu_{s,col} = \frac{4}{5}\alpha_s \rho_s d_s g_{0,ss}(1+e_{ss})(\frac{\Theta_s}{\pi})^{1/2} \tag{4.9}$$

$$\mu_{s,kin} = \frac{\alpha_s d_s \rho_s \sqrt{\Theta_s \pi}}{6(3-e_{ss})}[1+\frac{2}{5}(1+e_{ss})(3e_{ss}-1)\alpha_s g_{0,ss}] \tag{4.10}$$

$$\mu_{s,fr} = \frac{p_s \sin\phi}{2\sqrt{I_{2D}}} \tag{4.11}$$

here d_s is sediment diameter; e_{ss} is the coefficient of restitution for particle collisions with a default value of 0.9; ϕ is the angle of internal friction, and I_{2D} is the second invariant of the deviatoric stress tensor; $g_{0,ss}$ is a radial distribution function that governs the transition from the "compressible" condition with $\alpha < \alpha_{s,\max}$, where the spacing between the solid particles can continue to decrease, to the "incompressible" condition with $\alpha = \alpha_{s,\max}$, where no further decrease in the spacing can occur. It is interpreted as the probability of collisions between particles when the solid phase becomes dense and is an important parameter in the description of the solids pressure resulting from granular kinetic theory. For one solid phase, it can be expressed as

$$g_{0,ss} = \left[1 - \left(\frac{\alpha_s}{\alpha_{s,\max}}\right)^{\frac{1}{3}}\right]^{-1} \tag{4.12}$$

The basic governing idea in the granular kinetic theory is that the solids are in continuous and chaotic motion within the fluid. This chaotic random motion is seen at very low concentrations (due to friction between fluid and particles, to fluid turbulence, to variation in pressure in the fluid and so forth) or at higher concentrations (due to solids collisions). A granular temperature Θ_s is introduced for the solid phase, which is proportional to the kinetic energy of the fluctuating particle motion. The calculation of Θ_s will be discussed in the following paragraphs.

p_s is a solid pressure used for granular flows in the compressible regime. The calculation of p_s is closely related to Θ_s. It is calculated independently and used for the pressure gradient term, ∇P_s, in the solid phase momentum Equation 4.5. It is composed of a kinetic term and a second term due to particle collisions:

$$p_s = \alpha_s \rho_s \Theta_s + 2\rho_s (1 + e_{ss}) \alpha_s^2 g_{0,ss} \Theta_s \tag{4.13}$$

The transport equation derived from kinetic theory takes the form

$$\frac{3}{2}\left[\frac{\partial}{\partial t}(\rho_s \alpha_s \Theta_s) + \nabla \cdot (\rho_s \alpha_s \vec{v}_s \Theta_s)\right] = (-p_s \bar{\bar{I}} + \bar{\bar{\tau}}_s) : \nabla \vec{v}_s + \nabla \cdot (k_{\Theta_s} \nabla \Theta_s) - \gamma \Theta_s + \phi_{fs} \tag{4.14}$$

where

$(-p_s\bar{\bar{I}}+\bar{\bar{\tau}}_s):\nabla\vec{v}_s$ = the generation of energy by the solid stress tensor;

$k_{\Theta_s}\nabla\Theta_s$ = the diffusive flux of granular energy, here k_{Θ_s} is the diffusion coefficient defined as

$$k_{\Theta_s}=\frac{15\mathrm{d}_s\rho_s\alpha_s\sqrt{\Theta_s\pi}}{4(41-33\eta)}\left[1+\frac{12}{5}\eta^2(4\eta-3)\alpha_s g_{0,ss}+\frac{16}{15\pi}(41-33\eta)\eta\alpha_s g_{0,ss}\right] \tag{4.15}$$

and

$$\eta=\frac{1}{2}(1+e_{ss})\,. \tag{4.16}$$

$\gamma\Theta_s$ = the collisional dissipation of energy, which represents the energy dissipation rate within the solid phase due to collisions between particles. It can be defined as

$$\gamma\Theta_s=\frac{12(1-e_{ss}^2)g_{0,ss}}{d_s\sqrt{\pi}}\rho_s\alpha_s^2\Theta_s^{\frac{3}{2}}; \tag{4.17}$$

ϕ_{fs} = the exchange of kinetic energy of random fluctuations in particle velocity from the solid phase to the fluid phase. It can be calculated from

$$\phi_{fs}=-3K_{fs}\Theta_s\,. \tag{4.18}$$

4.3.3 Interphase exchange coefficients

In Eulerian model, coupling between phases is achieved through the pressure and interphase exchange coefficients. The momentum exchange between phases is based on the value of interphase exchange coefficient K_{fs}. The Gidaspow's model (Gidaspow and Bezburuah et al. 1992) is used to determine the fluid-solid exchange coefficient described as following

$$K_{sf} = \frac{3}{4} C_D \frac{\alpha_s \alpha_f \rho_f \left|\vec{v}_s - \vec{v}_f\right|}{d_s} \alpha_f^{-2.65} \qquad \text{when } \alpha_f > 0.8 \tag{4.19}$$

where

$$C_D = \frac{24}{\alpha_f \operatorname{Re}_s}\left[1 + 0.15(\alpha_f \operatorname{Re}_s)^{0.687}\right]. \tag{4.20}$$

and

$$K_{sf} = 150 \frac{\alpha_s (1-\alpha_f)\mu_f}{\alpha_f d_s^2} + 1.75 \frac{\rho_f \alpha_s \left|\vec{v}_s - \vec{v}_f\right|}{d_s} \qquad \text{when } \alpha_f \le 0.8 \tag{4.21}$$

4.4 Turbulence models

In multiphase flows, the number of terms to be modeled in momentum equations is large, thus makes the modeling of turbulent fluctuations of velocities and scalar quantities extremely complex. In this study, predictions for turbulent fluctuations for the

fluid phase are obtained using a modified $k-\varepsilon$ turbulence model with supplement of extra terms which take into account the interphase turbulent momentum transfer; and predictions for turbulent quantities for the solid phase are obtained using Tchen-theory (Tchen 1947; Hinze 1975) correlations for the discrete particles in homogeneous and isotropic turbulent flows.

4.4.1 Turbulence in the fluid phase

The turbulent fluctuating quantities are calculated using the eddy viscosity model. The Reynolds stress tensor for the fluid phase f is described as

$$\overline{\overline{\tau}}_f = -\frac{2}{3}(\rho_f k_f + \rho_f \mu_{t,f} \nabla \cdot \vec{U}_f)\overline{\overline{I}} + \rho_f \mu_{t,f}(\nabla \vec{U}_f + \nabla \vec{U}_f^T) \tag{4.22}$$

$$\mu_{t,f} = \rho_f C_\mu \frac{k_f^2}{\varepsilon_f} \tag{4.23}$$

where $\vec{U}_f$ is the phase-weighted velocity; $\mu_{t,f}$ is the turbulent viscosity; $C_\mu = 0.09$.

Turbulent kinetic energy k_f and its dissipation rate ε_f are obtained from the modified $k-\varepsilon$ turbulence model:

$$\frac{\partial}{\partial t}(\alpha_f \rho_f k_f) + \nabla \cdot (\alpha_f \rho_f \vec{U}_f k_f) = \nabla \cdot (\alpha_f \frac{\mu_{t,f}}{\sigma_k} \nabla k_f) + \alpha_f G_{k,f} - \alpha_f \rho_f \varepsilon_f + \alpha_f \rho_f \Pi_{k_f} \tag{4.24}$$

$$\frac{\partial}{\partial t}(\alpha_f \rho_f \varepsilon_f) + \nabla \cdot (\alpha_f \rho_f \vec{U}_f \varepsilon_f) = \nabla \cdot (\alpha_f \frac{\mu_{t,f}}{\sigma_\varepsilon} \nabla \varepsilon_f) + \alpha_f \frac{\varepsilon_f}{k_f}(C_{1\varepsilon} G_{k,f} - C_{2\varepsilon} \rho_f \varepsilon_f) + \alpha_f \rho_f \Pi_{\varepsilon_f} \tag{4.25}$$

here $G_{k,f}$ is the production of turbulent kinetic energy as defined in Chapter II. Π_{k_f} and Π_{ε_f} represent the influence of the solid phase on the fluid phase. Π_{k_f} is derived from the instantaneous equation of the fluid phase which can be simplified to

$$\Pi_{k_f} = \frac{K_{fs}}{\alpha_f \rho_f}(k_{sf} - 2k_f + \vec{v}_{sf} \cdot \vec{v}_{dr}) \tag{4.26}$$

$$\Pi_{\varepsilon_f} = C_{3\varepsilon} \frac{\varepsilon_f}{k_f} \Pi_{k_f} \tag{4.27}$$

where k_{sf} is the covariance of the velocities of the fluid phase *f* and the solid phase *s*. It will be defined in Section 4.4.2; $\vec{v}_{sf}$ is the relative velocity between fluid phase and solid phase; $\vec{v}_{dr}$ is the drift velocity resulted from turbulent fluctuations in the volume fraction. It is equal to

$$\vec{v}_{dr} = -D_{t,sf}(\frac{1}{\sigma_{sf}\alpha_s} \nabla \alpha_s - \frac{1}{\sigma_{sf}\alpha_f} \nabla \alpha_f) \tag{4.28}$$

where $D_{t,sf}$ is the binary turbulent diffusion coefficient. See definition in Section 4.4.2; The default value for σ_{sf} is 0.75.

4.4.2 Turbulence in the solid phase

Based on Tchen's theory, the particle turbulent kinetic energy and the turbulent energy due to interphase interaction are expressed as algebraic functions of the continuous phase kinetic energy. The dispersion coefficients, correlation functions, and the turbulent kinetic energy of solid phase are evaluated by time and length scales that characterize the turbulence motion. Here, two time scales are used. The first time scale is the characteristic particle relaxation time which is related to inertial effects acting on the particle. It is defined as

$$\tau_{F,\ sf} = \alpha_s \rho_f K_{sf}^{-1} \left(\frac{\rho_s}{\rho_f} + C_V\right) \tag{4.29}$$

where C_V =0.5 is the added mass coefficient. The second time scale is the characteristic time of correlated turbulent motions or eddy-particle interaction time which is defined as

$$\tau_{t,sf} = \tau_{t,f}\left[1 + C_\beta \xi^2\right]^{-\frac{1}{2}} \tag{4.30}$$

where

$$\xi = \frac{\left|\vec{V}_r\right|}{\sqrt{\frac{2}{3}k_f}} \tag{4.31}$$

$$\tau_{t,f} = \frac{3}{2} C_\mu \frac{k_f}{\varepsilon_f} \tag{4.32}$$

$$C_B = 1.8 - 1.35\cos^2\theta \tag{4.33}$$

here $\vec{V}_r$ is the averaged value of the local relative velocity between a particle and the surrounding fluid; $\tau_{t,f}$ is a characteristic time of energetic turbulent eddies; θ is the angle between the mean particle velocity and the mean relative velocity.

A ratio between the two time scales is written as

$$\eta_{sf} = \frac{\tau_{t,sf}}{\tau_{F,sf}}. \tag{4.34}$$

The turbulent kinetic energy for the solid phase is written as follows:

$$k_s = k_f\left(\frac{b^2 + \eta_{sf}}{1 + \eta_{sf}}\right), \tag{4.35}$$

and the eddy viscosity for the solid phase is specified as

$$D_s = D_{t,sf} + \left(\frac{2}{3}k_s - b\cdot\frac{1}{3}k_{sf}\right)\tau_{F,sf}, \tag{4.36}$$

where

$$D_{t,sf} = \frac{1}{3}k_{sf}\tau_{t,sf} \tag{4.37}$$

$$k_{sf} = 2k_f\left(\frac{b+\eta_{sf}}{1+\eta_{sf}}\right) \tag{4.38}$$

$$b = (1+C_V)\left(\frac{\rho_s}{\rho_f}+C_V\right)^{-1} \tag{4.39}$$

Here $D_{t,sf}$ is the binary turbulent diffusion coefficient, and k_{sf} is the covariance of the velocities of the fluid phase f and the solid phase s as shown in Section 4.4.1.

In order to show the model components discussed in this chapter, a chart that includes most of equations in this model is presented in Figure 4.1 for better understanding of the model.

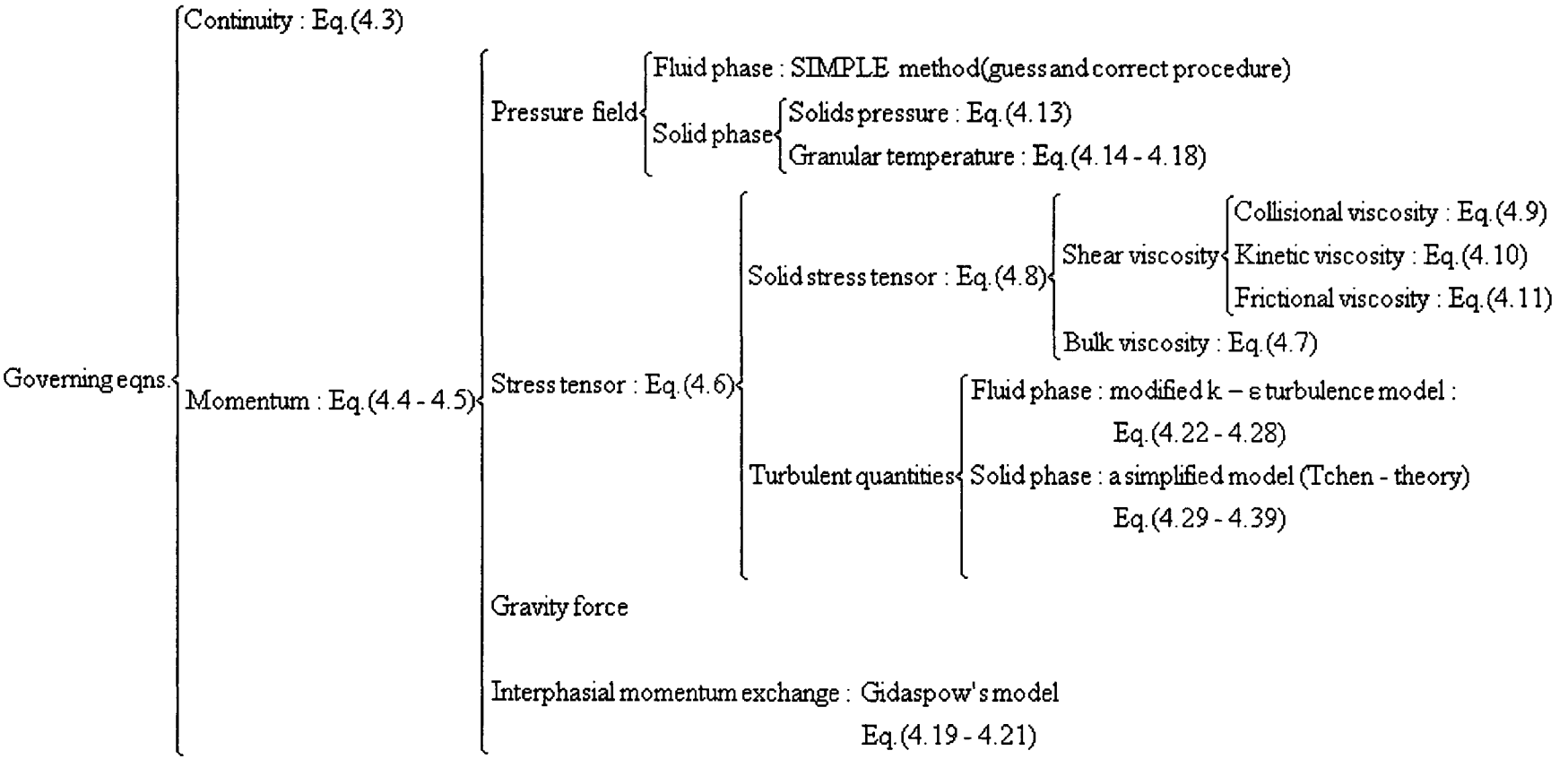

Figure 4.1 Model components and equations in Eulerian two-phase model

CHAPTER V

NUMERICAL SIMULATION OF SEDIMENT TRANSPORT AND SCOUR USING EULERIAN TWO-PHASE MODEL

5.1 Introduction

Chapter IV gives the mathematical formulation of Eulerian two-phase model. In Chapter IV, continuity and momentum equations for both solid and fluid phases are described. Closure of the solid phase momentum equation is achieved by applying kinetic theory for granular flows. A modified $k-\varepsilon$ turbulence model with supplement of extra terms which take into account the interphase turbulent momentum transfer is used to predict turbulent quantities for the fluid phase and method to predict turbulent quantities for the solid phase is also specified.

In this chapter we are trying to see the applicability of an Eulerian two-phase model embedded in FLUENT software in simulation of sediment transport processes and scouring with loose bed through a verification study which was done by van Rijn from Delft Hydraulic Laboratory (van Rijn 1981). The test case provided sediment concentration profiles at different cross sections and scour profile for verification purposes.

5.2 Experiment

A preliminary laboratory study was started in a flume of the Delft Hydraulic Laboratory to gain an insight into the entrainment of fine particles into the flow in the

case of erosion of sediment particles. This study was used in this dissertation as a case study and it will provide measured sediment concentration profiles and scour profile to validate the proposed Eulerian two-phase model.

A schematic of the experiment is shown in Figure 5.1. The experiment was carried out in a flume with a length of 30 m, a width of 0.5 m, a depth of 0.7 m and a maximum discharge of 0.25 m^3/s. The flume was divided into three sections: a 10m inflow section with a rigid bed, a 10m test section and a 10m outflow section with sediment beds. The water is pumped from a reservoir to the flume. The discharge is measured by a circular weir. The flow velocities in the section with the rigid bed were measured with a micro-propeller which had a diameter of 0.015 m. In the test section with the sediment bed flow velocities were measured by pitot-tubes. The sediment concentration measurement was taken by siphon-method. And the bed load transport was measured by a pit-type trap installed in the sediment bed at the end of the test section. In the chosen case study, a medium-fine sand with d_{50}=230μm was used. The flow depth was kept constant at a value of 0.25 m. The flow data is given in Table 5.1. The test considered an adjustment period in which equilibrium flow condition was established and a measuring period in which the water-sediment samples were taken.

Table 5.1 Flow data

Discharge (m^3/s)	Flow depth (m)	Mean flow velocity (m/s)	Particle diameter (μm)	Temperature (°C)	Flow period (s)
0.087	0.25	0.67	230	9	320

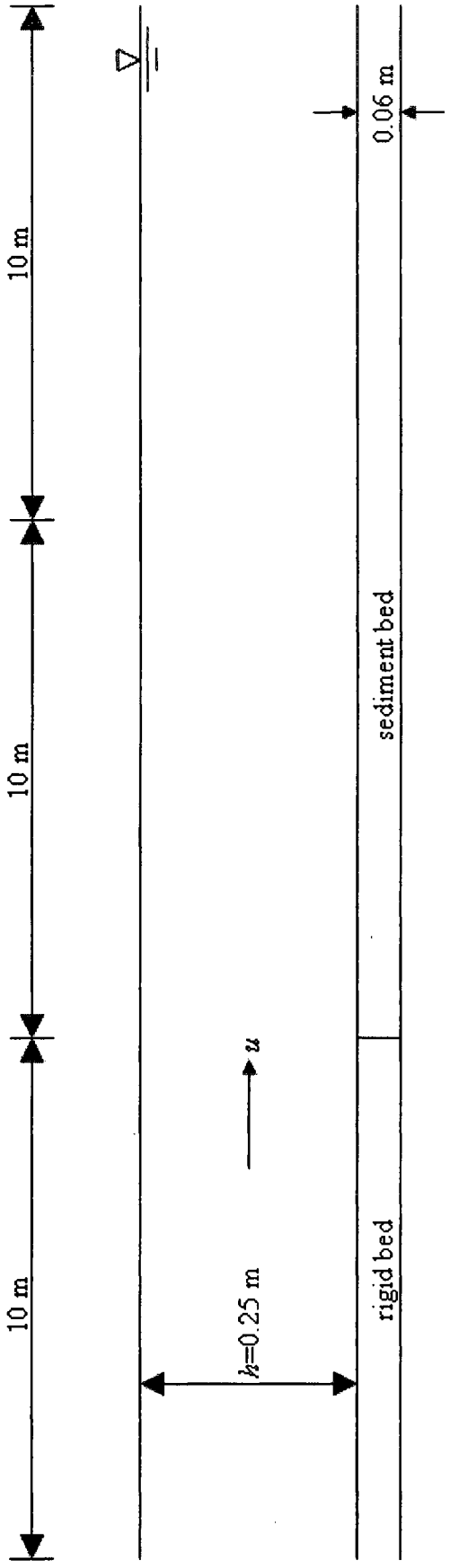

Figure 5.1 Schematic of experimental set up

5.3 Model set up

The numerical flow configuration used for the present study is shown in Figure 5.2. The channel is 0.5 m wide, 30 m long with a height of 0.25 m. The sand layer is 0.06 m depth with the sand particle diameter d_{50}=230μm. In the numerical computations, the two-phase model described in Chapter IV is set up to match the experimental configuration. Due to the simplicity of geometry and approaching uniform feature of the flow, and for the sake of saving computation time, a two-dimensional model is used in the simulation process and it turns out to reach good precision in this case.

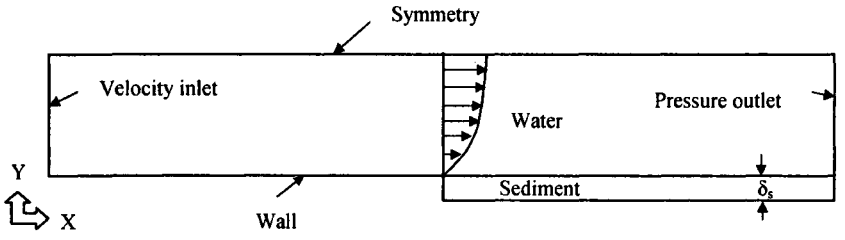

Figure 5.2 Numerical flow configuration of van Rijn's flume experiment. X is the streamwise direction, Y is the cross stream direction and δ_s is the thickness of the sand layer. Figure is not to scale.

In the simulations, a two-dimensional grid system with 96,571 nodes and 95,000 cells is generated with the grid generator GAMBIT of the FLUENT package. Two zones, the water and the sediment, are included in the grid. Figure 5.3 shows the complete view of the channel grid and an enlarged grid view for the portions between the inflow section and the test section.

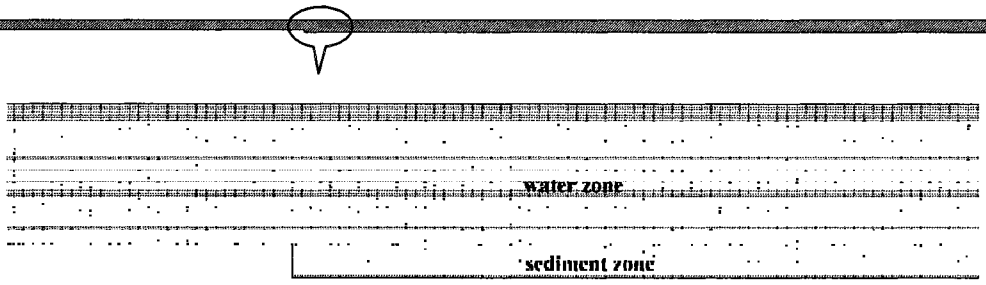

Figure 5.3 Grids for two-phase model calculations

The boundary conditions at the walls, which include the rigid bed for the inflow section, the bottom of the sand layer and the beginning plane of the sediment zone, were set to a wall boundary condition. It is assumed that the center of the grid cell close to a wall is within the logarithmic layer of the wall. The near-wall treatment of the $k-\varepsilon$ model avoids the need to integrate the model equations right through to the wall by making use of the wall functions. The water surface of the channel is in reality a free surface, but is modeled as a symmetry plane where a zero-gradient condition is used for the velocity components parallel to the free surface, while the gradients of k, ε and velocity components perpendicular to the free surface are set to zero. At the inlet, the velocity is set normal to the inlet surface with a uniform velocity of 0.67 m/s. At the end of the inflow section, a logarithmic velocity profile will be developed as the inlet condition to the test section. The pressure outlet boundary condition, with gauge pressure at the outlet boundary, is specified for the flow exit.

Various turbulence parameters are required. The turbulence intensity, I, is defined as the ratio of the root-mean-square of the velocity fluctuations, u', to the mean flow velocity, u_{avg}. An empirical formula is used to calculate the turbulence intensity:

$$I = \frac{u'}{u_{avg}} = 0.16(R)^{-1/8} \tag{5.1}$$

where R=Reynolds number (FLUENT Incorporated 2007). The inlet areas and wetted perimeters are used to estimate the turbulence length scale using

$$\lambda = 0.07 D_H \tag{5.2}$$

Where D_H =hydraulic diameter of the inlet. Then the value of k and ε can be computed using u, I and λ.

The velocity components in the problem domain are set to zero as initial conditions. Initial turbulence parameter values for the turbulence kinetic energy, k, is set at $1 m^2/s^2$, and the turbulence dissipation rate, ε, is set at 1 m^2/s^3. The final solution is independent of these initial solution parameters. The channel was filled at the beginning of the experiment with a 6 cm thick layer of sand with an initially flat surface. The volume fraction of sand is patched to the sediment zone before the calculation starts. Figure 5.4 shows the contours of volume fraction of the sediment at the beginning, with red color indicating sediment and blue indicating water.

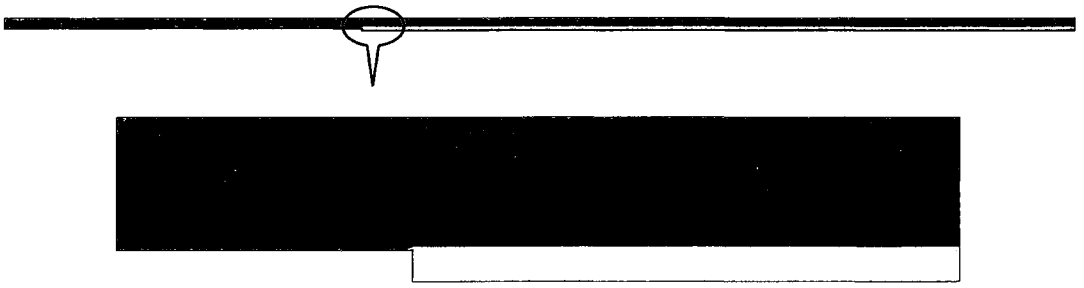

Figure 5.4 Contours of volume fraction of the sediment (at the beginning).

5.4 Solution method

Table 5.2 Solution conditions and methods for simulation

Model: Segregated	Space	Two dimension
	Time	Steady
	Turbulence	Modified k-ε model
Discretization methods	Pressure-velocity coupling	Phase Coupled SIMPLE
	Momentum	First order upwind
	Volume fraction	First order upwind
	Turbulence kinetic energy	First order upwind
	Turbulence dissipation rate	First order upwind

As for the Eulerian two-phase model, FLUENT uses the segregated solver to solve equations sequentially (i.e., segregated from one another). Table 5.2 summarizes the solution conditions and methods used. The phase coupled SIMPLE (PC-SIMPLE) algorithm is used for the pressure-velocity coupling. PC-SIMPLE is an extension of the

SIMPLE algorithm to multiphase flows. The velocities in each phase are solved in a segregated fashion. A vector equation formed by the velocity components of all phases is solved simultaneously. Then, a pressure correction equation is built based on total volume continuity rather than on mass continuity. Pressure and velocities are then corrected so as to satisfy the continuity constraint. Because the governing equations are non-linear and coupled, the solution loop must be carried out iteratively in order to obtain a converged numerical solution. For each iteration, the detail calculation procedure can be summarized with the following steps:

1. Update phase properties (e,g, density, viscosity) including turbulent viscosity (diffusivity) based on the current solution.

2. Solve the momentum equations for each phase using the recently updated values of pressure and face mass fluxes.

3. Solve the pressure correction equation using the recently obtained velocity field and the mass-flux.

4. Correct face mass fluxes, pressure, and the velocity field using the pressure correction obtained from Step 3.

5. Solve the equations for additional scalars such as turbulent quantities and granular temperature using the current values of the solution variables.

6. Check for the convergence of the equations.

These steps are continued until the convergence criteria are met.

5.5 Simulation results and discussion

5.5.1 Sediment concentration simulation

According to (Wang and Chien 1985; Zhao and Fernando 2007), the interface between water and sand in the physical experiment is taken as the profile which corresponds to the sediment volume fraction of $\alpha_s \approx 0.5$ calculated from the numerical simulation. Figure 5.5 shows a typical example of a bed profile corresponding to the contour level of $\alpha_s \approx 0.5$ obtained from the previous calculation step using the two-phase model. A developing scour hole can be seen in the beginning of the test section (right after the inflow section).

Figure 5.5 A typical bed profile with sediment phase volume fraction $\alpha_s \approx 0.5$

In order to validate sediment phase concentrations through the test section, the results of the present model for the typical case of net entrainment from loose bed are presented. Suitable outputs such as sediment volume fractions are extracted from the model for each interested cross section to calculate the sediment concentrations. Then the simulated results are compared with the measured results from van Rijn's experiment. In Figure 5.6, the two-phase model results of sediment concentration profiles at four

different locations/cross sections ((a) x/h=4; (b) x/h=10; (c) x/h=20; (d) x/h=40) along the channel are compared with measured data from van Rijn (1983). Here x=X-L, where X is the X-coordinate along the channel, and L indicates the length of inflow section. Here L=10 m.

It is clear that all of the predicted sediment concentration profiles follow a nearly logarithmic distribution as indicated from the literature, with almost zero sediment concentration approaching the water surface, increasing sediment concentration towards to the bed and remaining at an almost constant value as approaching the bed surface. There are some discrepancies though such as Figure 5.6 (a) at x/h=4 cross section and Figure 5.6 (b) at x/h=10 cross section show some degree of deviations from the simulated results. This may be attributed to the scour hole right in front of them, which contribute to the formation of the sand mound where these two positions are located. As claimed by (Wang and Chien 1985; Zhao and Fernando 2007), there exists a laminated-load layer beneath the water-sediment interface. Zhao and Fernando (2007) mentioned the sediment mound, which is formed right after the scour hole, is the place expected to cause enhanced laminated transport. The more complicated sediment motion in this place may lead to the discrepancy in these two sections. While their claim is speculative and future observational results and investigations need to be directed at such studies.

Generally the agreement can be seen to be good though they are not exactly fit to each other in some positions. The general trend of sediment concentration distribution is similar. The sediment concentration quantity difference is regarded as within the acceptable range. This gives confidence in the sediment concentration modeling using the

Eulerian two-phase model, given the complexity of the model and the novelty of this work in simulating sediment transport without invoking a purely empirical sediment transport formula.

(a)

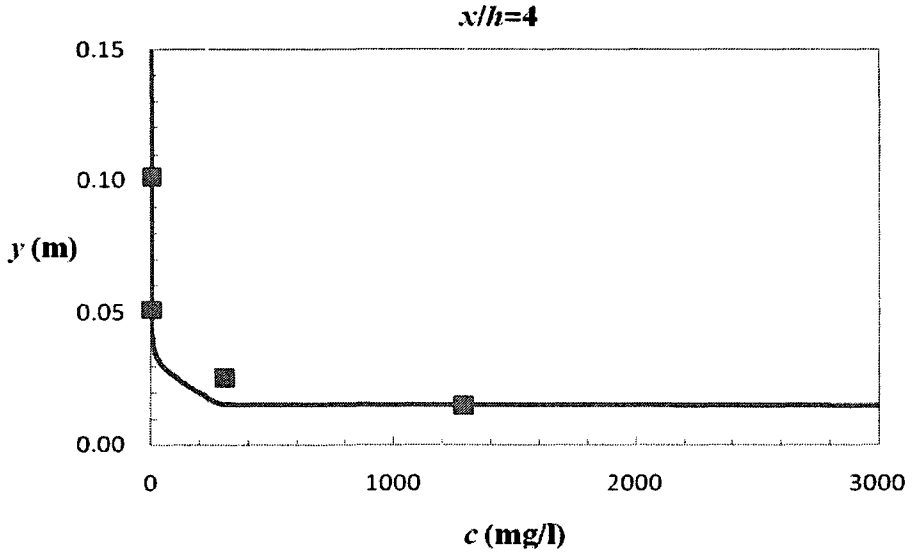

(b)

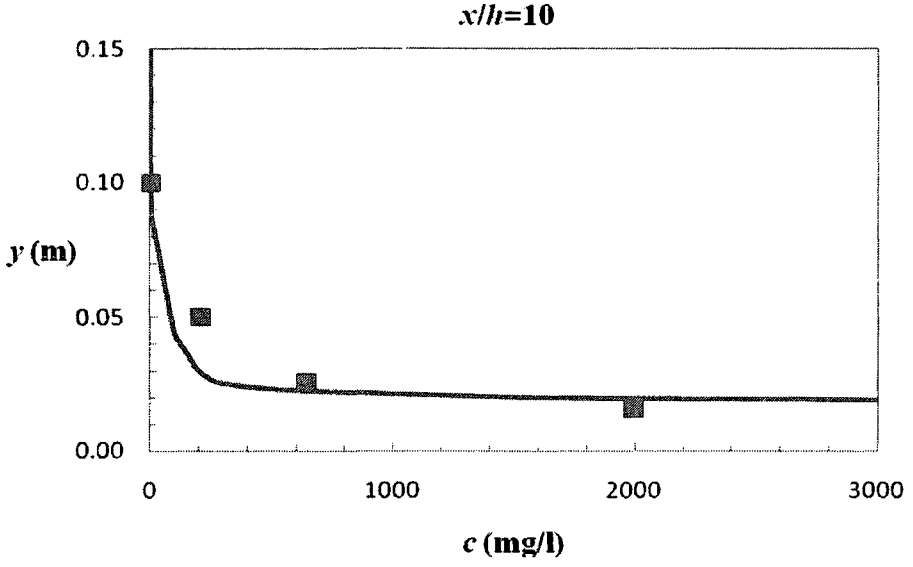

(c)

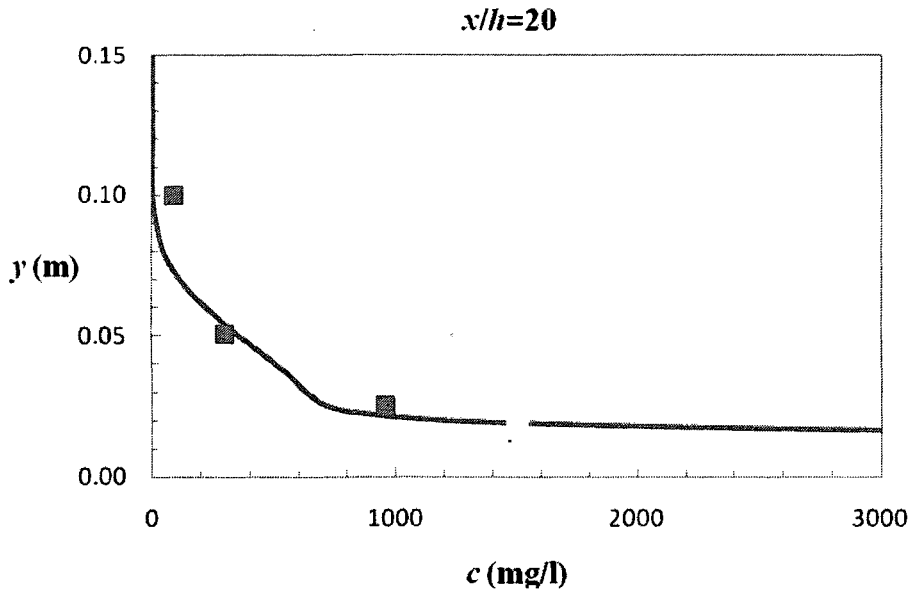

(d)

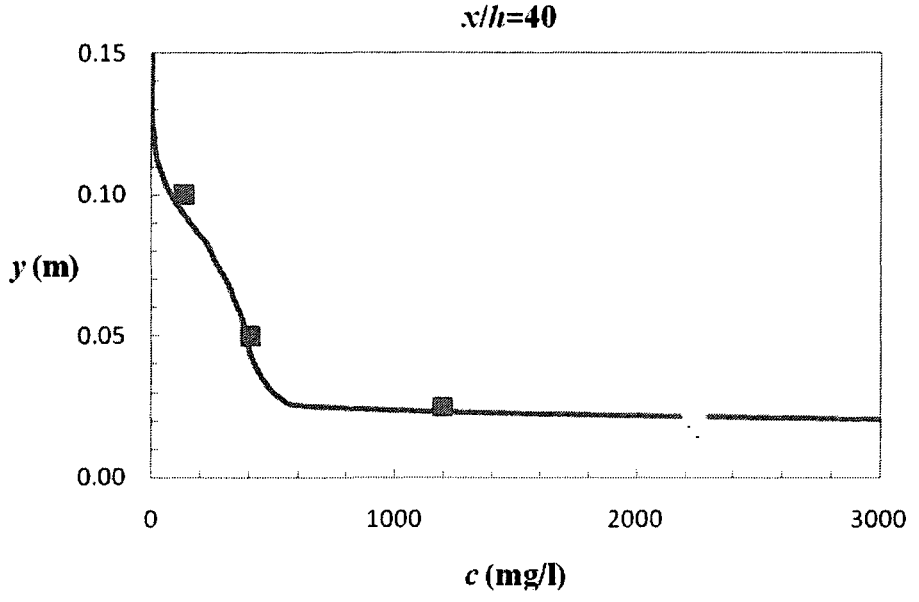

Figure 5.6 Comparison of numerical results and van Rijn's measurements for sediment concentration profiles: (a) x/h=4; (b) x/h=10; (c) x/h=20; (d) x/h=40.

———Calculation, ■ Measurements (van Rijn, 1983)

5.5.2 Sediment transport motion

Though discussions about a laminated load were lifted by Wang and Chien (1985), the sediment transport motion here only includes widely accepted suspended load and bed load. Bed load is the part of the total sediment load that is traveling along the bed and has more or less continuous contact with the bed, supported by inter-granular collisions rather than fluid turbulence. In contrast, the suspended load is the part of the total load which is moving without continuous contact with the bed as the result of the agitation of the fluid turbulence. The basic idea of splitting the total sediment load into bed load and suspended load is that two different mechanisms are effective during the sediment transport.

As to the boundary between the bed load and suspended load, arguments continue. Einstein (1950) suggested the boundary to be some grain diameters, within $(2\sim5)d_{50}$ above the bed. A layer of thickness of $\delta_b=3d_{50}$ above the water-sediment interface is used in this study. The sediment transport above this interface within a layer of thickness of $3d_{50}$ is considered as bed load. The bed load flux is calculated as

$$q_b = \alpha_s \delta_b U_s \tag{5.3}$$

where α_s is the sediment volume fraction and U_s is the sediment velocity.

The suspended load flux is calculated as

$$q_s = \int_{y_b+\delta_b}^{h} \alpha_s U_s dy \tag{5.4}$$

where y_b is the Y-coordinate corresponding to the surface where $\alpha_s \approx 0.5$ and h is the flow depth above the bed.

Simulation results of bed load flux and suspended load flux along the channel are shown in Figure 5.7. Figures of intermediate sediment loads-1 and intermediate sediment loads-2 show the intermediate results during the process of establishing steady state condition. The steady state condition sediment load flux is illustrated in the Figure sediment load-3. In all three figures, suspended load flux is consistently higher in magnitude than bed load flux. At the beginning, the bed load transport is somewhat non-uniform, but at later stages it becomes more spatially uniform. For suspended load transport, the load flux right after the inflow section immediately surges to a value of around 0.0007 m^2/s in the beginning, as shown in Immediate sediment loads-1. Then the peak of the suspended transport moves downstream as the sediment mound moves away from the inflow section. The distribution of suspended load tends to be more uniform in the later stages as well. The magnitude of suspended transport in the final steady state condition is a little suppressed as depicted in the third figure compared to the previous two figures.

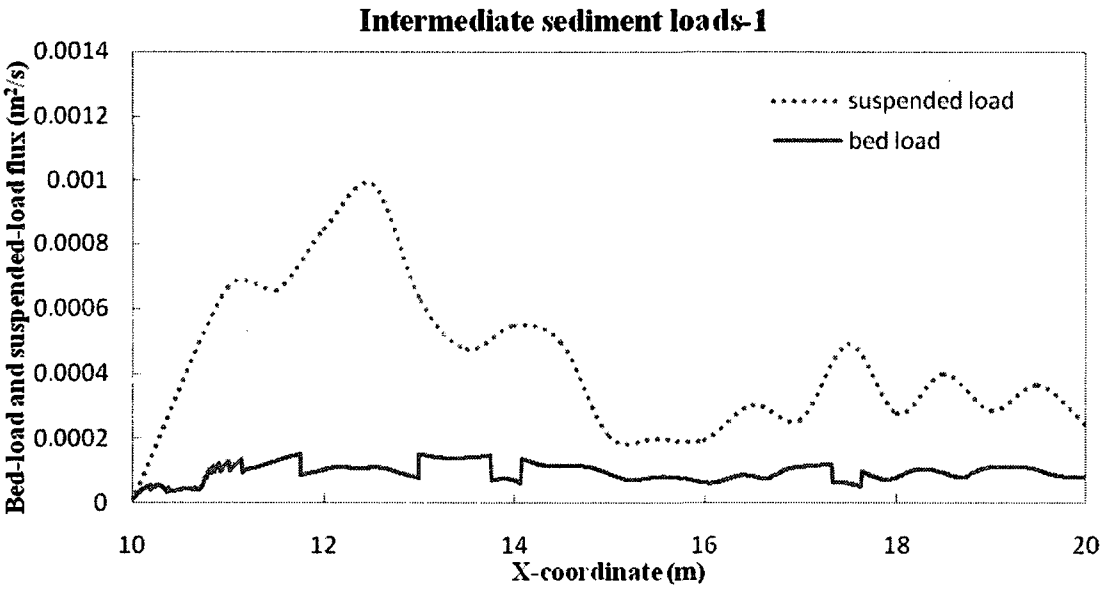
Intermediate sediment loads-1
Bed-load and suspended-load flux (m²/s)
0.0014
0.0012
0.001
0.0008
0.0006
0.0004
0.0002
0
suspended load
bed load
10
12
14
16
18
20
X-coordinate (m)

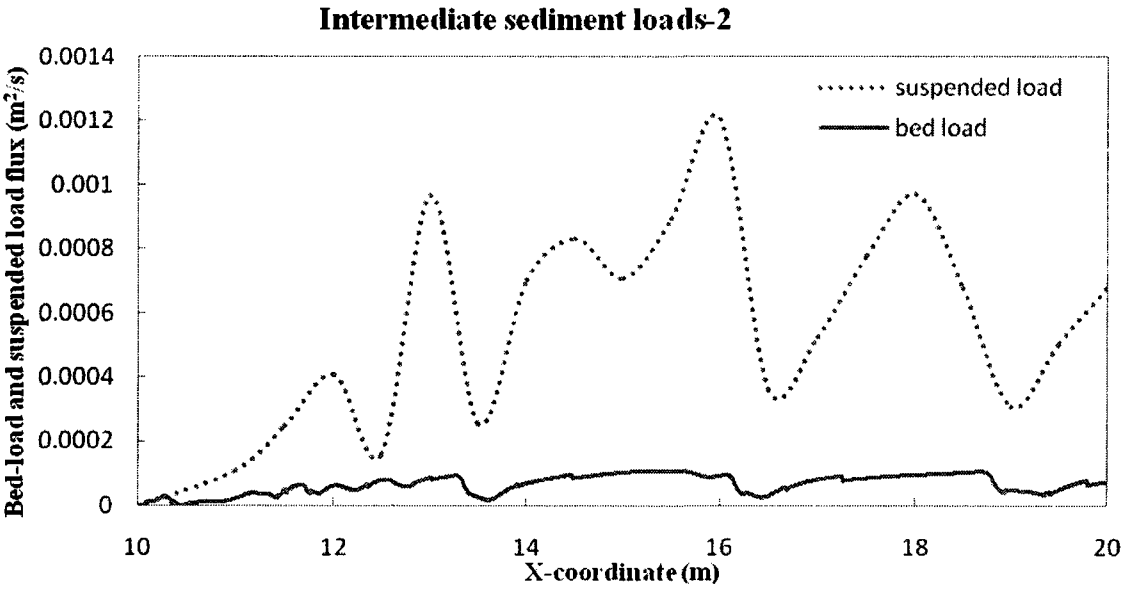
Intermediate sediment loads-2
Bed-load and suspended load flux (m²/s)
0.0014
0.0012
0.001
0.0008
0.0006
0.0004
0.0002
0
suspended load
bed load
10
12
14
16
18
20
X-coordinate (m)

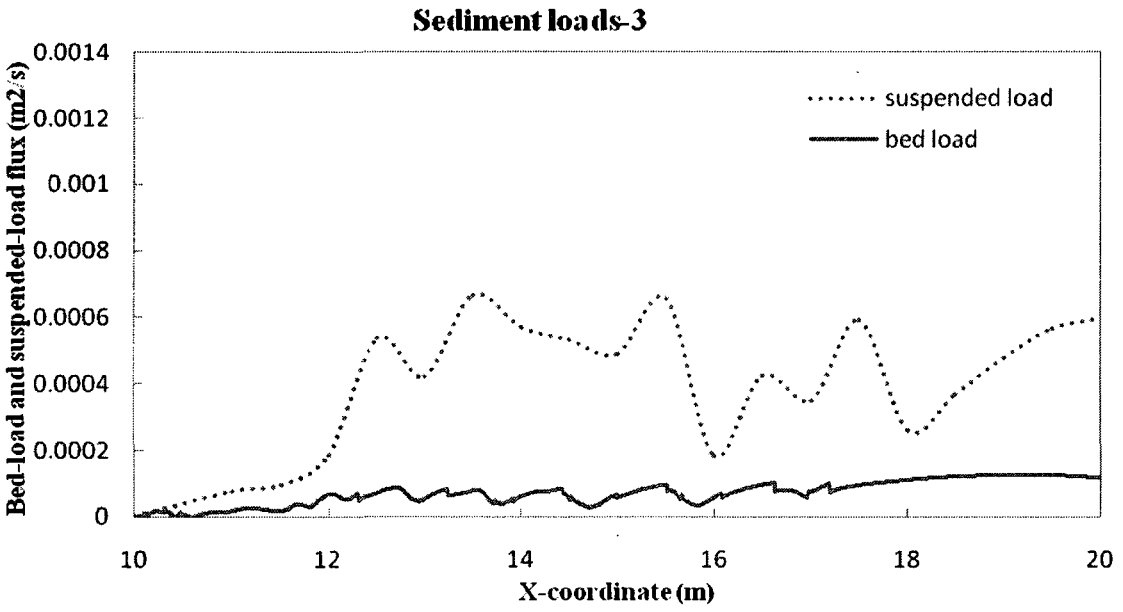

Figure 5.7 Simulation results of bed load flux q_b and suspended load flux q_s

5.5.3 Scour simulation

Figure 5.8 shows the results of bed profiles in the Eulerain two-phase model during simulation processes. As mentioned, the volume fraction of sediment (phase-2) with $\alpha_s \approx 0.5$ was chosen as the water-sediment interface corresponding to the laboratory experiments in van Rijn's report. As illustrated in all three contour plots, a scour hole appears in the test section right after the inflow section. From plots (a) through (c), the sour hole expands in magnitude both longitudinally and vertically, as approaching to the steady state condition for both flow and sediment simulation. Accordingly, the sediment mound right after the scour hole slowly moves downstream. In addition, the color transition shown in the interfaces between the water and the sediment indicates the changing volume fractions for the sediment phase, thus the sediment concentration changes accordingly. As investigating the output files for sediment volume fractions,

very tiny values of sediment volume fractions can be observed in the upper water phase though it is barely seen in the plots.

In Figure 5.9, the bed profiles that are determined computationally are compared with experimental scour profile data from van Rijn's report. The red line represents the scour profile from experimental data and the black dots stands for the simulation results from the two-phase model. Initially the sediment particles in the scour hole tend to be ejected fast. The ejected particles are supported by the strong turbulence fluctuations. With a decay of turbulence further down, the particles are deposited to form a mound. As the scour depths continue to increase slowly at later stages, the mound moves away slowly as a result of downstream sediment transport from the sediment mound. Finally an approximate dynamic equilibrium situation is achieved with the particles flown into and carried out from the scour hole are in a balanced state. The development of scouring can be seen from Figure 5.9 (a) - (c) as well. As depicted in the final stage in Figure 5.9 (c), the agreement between the predicted and measured scour profiles are highly encouraging. The small deviation between the predicted and measured profiles maybe partly attributed to the time delay of flow adjustment following scour as pointed out by (Zhao and Fernando, 2007). Time scales for flow adjustment and particle-turbulence interaction are different. When the bed profile varies, the flow needs time to adjust to the bed profile variation.

(a)

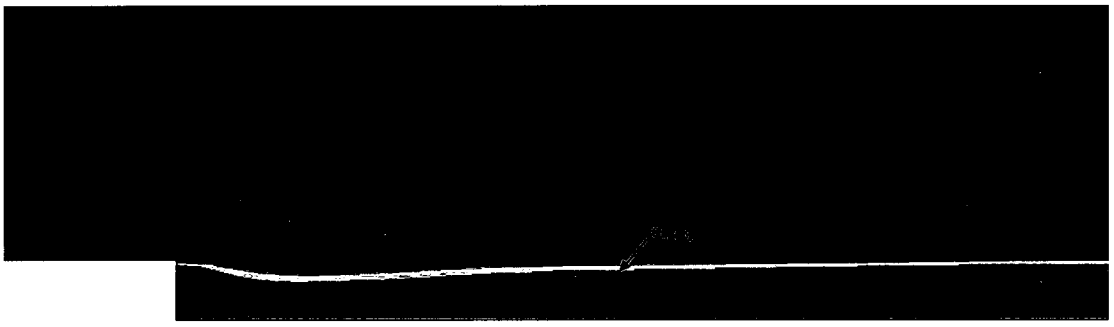

(b)

(c)

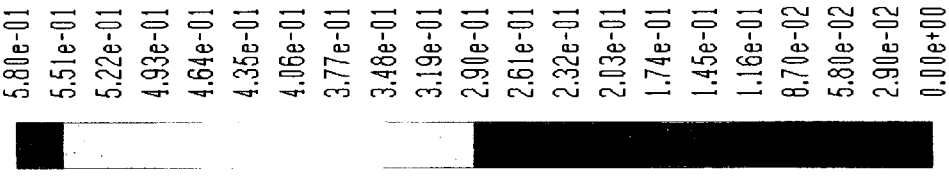
5.80e-01
5.51e-01
5.22e-01
4.93e-01
4.64e-01
4.35e-01
4.06e-01
3.77e-01
3.48e-01
3.19e-01
2.90e-01
2.61e-01
2.32e-01
2.03e-01
1.74e-01
1.45e-01
1.16e-01
8.70e-02
5.80e-02
2.90e-02
0.00e+00

Figure 5.8 Contours of volume fraction during the development of scouring

(a)

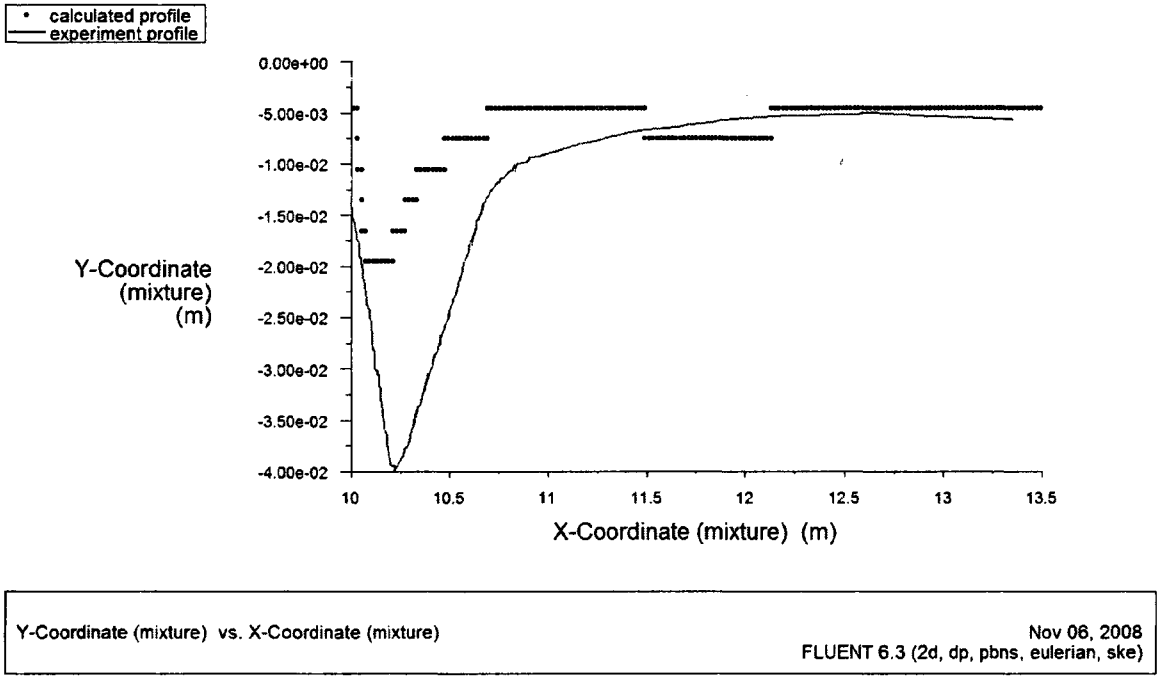

(b)

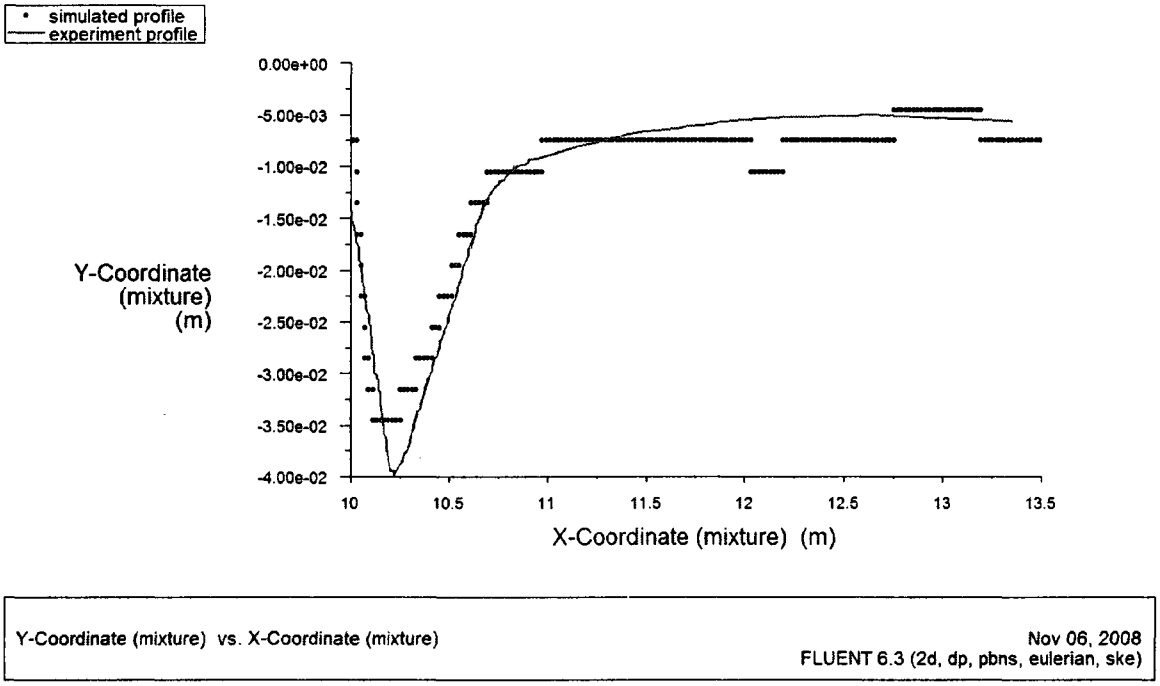

(c)

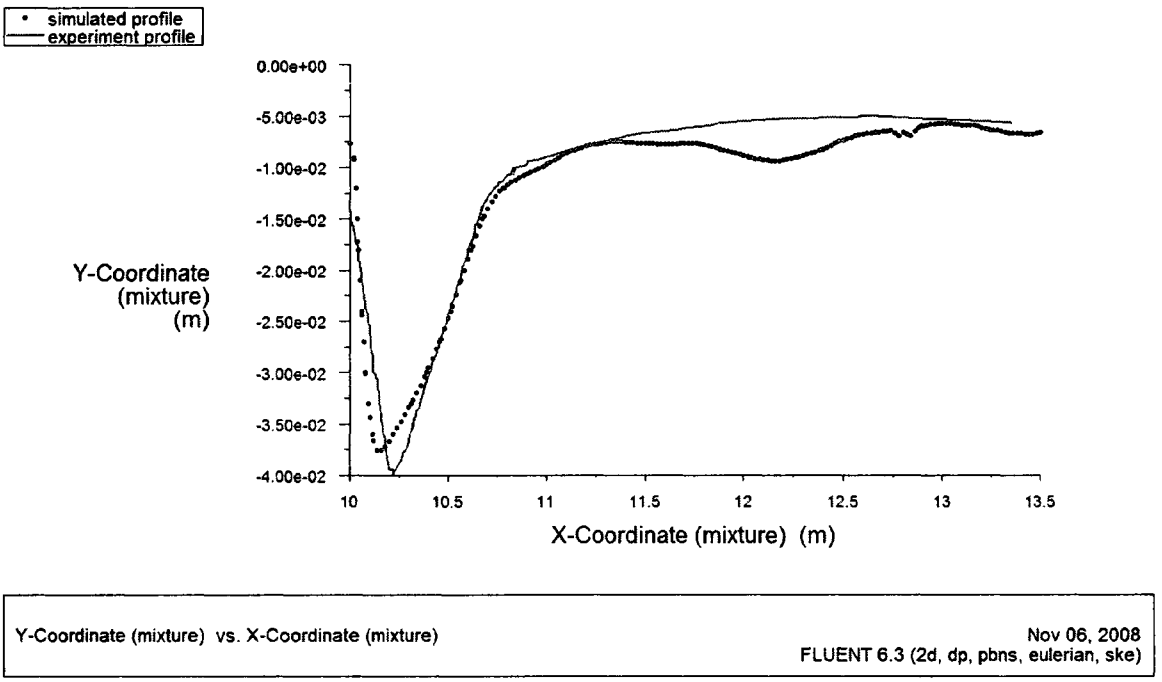

Figure 5.9 Comparison of bed profiles during the development of scouring

5.6 Conclusion

The use of computational fluid dynamics modeling for simulation of sediment transport and scour processing has been demonstrated by employing an experiment channel study from van Rijn's report. The simulation is conducted by using CFD software FLUENT package. An Eulerian two-phase model, using structured computational mesh, has been constructed. The momentum equations for both water and sediment phases are implemented with Euler-Euler coupling between them and a modified $k-\varepsilon$ turbulence closure scheme is used for the water phase. Both flow-particle

and particle-particle interactions are considered with their effects parameterized in the two-phase system.

The model is tested to be effective by verifying sediment concentration profiles along the channel for net entrainment from a loose bed. The validation is carried out in four different cross sections positioned along the test section. In addition, the scour hole developing process is analyzed and simulated scour profiles are compared with measured profiles from the experiment. The results are highly encouraging considering the complexity of the model and the fact that it does not need any empirical sediment transport formulas.

Two-phase model approaches provide an alternative way to traditional sediment transport modeling. Due to the capability to include flow-particle and particle-particle interactions, a two-phase model is applicable to highly intensity flows as well, which proves to be difficult for traditional sediment transport models.

In this Chapter, a relatively simple 2D steady case study is chosen due to the availability of validation data and consideration of reducing the computation time. However, it succeeds to provide decent simulation results for this case study. For future modeling purposes, it can be easily integrated to a 3D or unsteady simulation by applying to more complex problems.

CHAPTER VI

CONCLUSIONS AND RECOMMENDATIONS

6.1 Summary and conclusions

In Chapter II and Chapter III, the discrete phase model, which is capable of simulating flow hydrodynamics and predicting sedimentation efficiencies for low sediment-laden flows, was presented as one of the multiphase flow approaches. In this approach, the fluid phase is modeled as a continuum by solving the time-averaged Navier-Stokes equations. The sediment phase is represented by individual particles which are tracked through the calculated flow field by integrating the force balance on the particle. The mathematical formulation of the model was shown in Chapter II. Governing equations for both flow modeling, including equations of the continuity and balance of momentum, and for particle motions with a balance of all forces acting on the particle, were described. The stochastic tracking model and its mathematical formulation were introduced to predict dispersion of particles due to turbulence in the fluid phase.

The developed solution methodology in Chapter II was implemented numerically in Chapter III. First of all, the model was set up with a three-dimensional grid system with the help of geometry and mesh generation software GAMBIT. Then, initial and boundary conditions for the model were specified for both flow and sediment phase. Particularly *Trap* and *BSS* boundary conditions were explained and applied in the sediment transport simulation. Flow pattern and hydrodynamics were investigated in detail under different inflow conditions after the flow model was solved. Motions of

individual particles and their deposition patterns in the bed were analyzed using a Lagrangian particle trajectory analysis procedure based on solved fluid flow solutions. In particular, the sedimentation patterns of particles of different sizes under different flow conditions are analyzed with different inlet and outlet pipes arrangement. It was demonstrated that this model is a quite efficient 3D hydrodynamic flow and sediment transport numeric model for low sediment-laden flows, thus providing engineers and scientists with a useful tool for studying sediment depositions with a variety of sediment sizes, inflow conditions, and geometric arrangements.

The other multiphase flow approach, the Eulerian two-phase model, was described in Chapter IV and Chapter V. The Eulerian two-phase model is an alternate option, while the assumption that a dispersed sediment phase occupies a low volume fraction in the discrete phase model is not valid. This two-phase model is capable to simulate flow, sediment transport, and bed deformation with loose bed based on two-phase mass and momentum equations. In this approach, the two interacting phases, water and sediment, are treated mathematically as interpenetrating continua and an Eulerian treatment is used for each phase. Chapter IV addresses mathematical formulation of the model. Conservation equations including continuity and momentum equations for each phase are derived. In the case of granular flows, these equations are closed by providing constitutive relations that are obtained by applying kinetic theory. In this application, modeling of turbulent fluctuations of velocities and scalar quantities are different for each phase. Predictions for turbulent fluctuations for the fluid phase are obtained using a modified $k-\varepsilon$ turbulence model with supplement of extra terms which take into account the interphase turbulent momentum transfer; predictions for turbulent quantities for the

solid phase are obtained using Tchen-theory correlations for the discrete particles under homogeneous and steady turbulent flows.

In Chapter V the numerical implementation of the Eulerian two-phase model was subsequently carried out in an open channel flume study. The model was set up with a two-dimensional grid system built in GAMBIT. Boundary conditions (including determination of turbulence parameters) and initial conditions were specified. The results indicated that, in general, simulated sediment concentrations at different cross sections were well predicted as compared with experimental results from the literature. The shapes of bed profiles during scour development converged to corresponding shapes obtained from the experiment. The present solution was also employed to study the sediment transport motion involving suspended load and bed load. All the results presented in this study demonstrate that the model is efficient and quite accurate in dealing with sediment transport and scour simulation with loose bed, and without invoking any empirical sediment transport formula.

6.2 Recommendations for further study

In applying these two multiphase models to practical problems, attention should be paid to the following points:

First, these models were developed based on several assumptions. For each models, sediment is considered spherical, thus it is not applicable for practical problems associated with sediments with nonspherical shapes. The discrete phase model assumes that the sediment phase occupies a low-volume fraction and particle-particle interactions

are negligible, thus it is not recommended for use in high sediment-laden problems. In the Eulerian two-phase model, the use of Tchen's theory in predicting turbulent quantities came with a simplified assumption that the turbulence was homogeneous and isotropic in order to gain a great deal of understanding about turbulent flows.

Second, different models can be selected to calculate water-sediment momentum interaction term in the Eulerian two-phase model. In our study the Gidaspow's model (Gidaspow and Bezburuah et al. 1992) was used to determine the fluid-solid exchange coefficient. This model is recommended for fluidized beds where a bed of solid particles will behave as a fluid, like a liquid or gas. The model of Wen and Yu (Wen and Yu 1966) and Syamlal-O'Brien model (Syamlal and O'Brien 1989) are other available models that can be used in calculate fluid-solid exchange coefficient. Or one can develop his own to model this interaction term by adding new modules through user-defined functions.

Based on the summaries and conclusions of this research work, recommendations for potential future work are proposed in the following directions:

(1) Implement and validate a time dependent application for both discrete model and a Eulerian two-phase model in order to adequately determine the development of sediment transport process and bed deformation under unsteady flow conditions. The current flow hydrodynamics model and sediment transport model can be already used for time accurate simulations. Steady state solutions were enough in the applications in this thesis. However, attention should be paid to meshes with movable beds while performing time accurate simulations.

(2) Extend sediment transport models in the Eulerian two-phase model to be able to account for the presence and transport of non-uniform sediment particles, which is most of the case in natural channels and rivers. One possible direction is to regard different sediment sizes as distinct phases with each phase being treated mathematically as interpenetrating continua. Additional sets of conservation equations should be added as well and solid-solid momentum interaction terms need to be developed between sediment phases with different sizes.

(3) Verify the bed load and suspended load data in the Eulerian two-phase model application by experiment data, which is not available in the referenced literature. More work must be done to ensure that the model is suitable for practical purposes.

(4) In the discrete phase model approach, try other pond related configurations such as different length to width ratio, different inlet and outlet types such as weir, or different vertical positions of inlet/outlet structures to derive practical sedimentation curves with respect to the chosen configurations, aiming to provide a practical reference for engineers and planners in the field of stormwater management and water resources engineering.

REFERENCES

Abad, J. D., Buscaglia, G. C., and Garcia, M. H. (2007). "2D stream hydrodynamic, sediment transport and bed morphology model for engineering applications." *Hydrological Processes*, 22(10), 1443-1459.

Adamsson, A., Stovin, V., and Bergdahl, L. (2003). "Bed shear stress boundary condition for storage tank sedimentation." *Journal of Environmental Engineering*. 129(7). 651-658.

Adamsson, A., Bergdahl, L., and Lyngfelt, S. (2005). "Measurement and three-dimensional simulation of flow in a rectangular detention tank." *Urban Water Journal*, 2(4), 277-287.

Andersson, B., Mooney, J., and Stricker, J. (1996). "Decision support for the design of constructed wetlands." *Applied Mathematical Modelling*, 20(1), 93-100.

Anderssen, R.S., Dietrich, C.R., and Green, P.A. (1990). "Designing Artificial Lakes as Pollution Control Devices." *Mathematics and Computers in Simulation*, 32, 77-82.

Benelmouffok, D. E., and Yu, S. L. (1989). "Two-dimensional numerical modeling of hydrodynamics and pollutant transport in a wet detention pond." *Water Science and Technology,* 21, 727-738.

Brune, G. M. (1953). "Trap efficiency of reservoirs." *Transactions of the American Geophysical Union*, 34, 407-418.

Cao, Z., Wei, L., and Xie, J. (1995). "Sediment-laden flow in open channels from two-phase flow viewpoint." *ASCE Journal of Hydraulic Engineering*, 121(10), 725-735.

Celik, I., and Rodi, W. (1988). "Modeling suspended sediment transport in nonequilibrium situations." *ASCE Journal of Hydraulic Engineering*, 114(10): 1157-1190.

Chang, H. H. (1998). *Generalized computer program: Users' manual for FLUVIAL-12: Mathematical model for erodible channels*, San Diego, CA.

Churchill, M.A. (1948). "Discussion of Analyses and use of reservoir sedimentation data by L.C. Gottschalk." *Proceedings of the federal interagency sedimentation conference,* Denver, Colorado, 139-40.

Clift, R., Grace, J. R., and Weber, M. E. (1978). *Bubbles, drops, and particles*, Academic Press, London.

Danish Hydraulic Institute (1999). MIKE21 user guide book for window 95/98/2000/NT.

Demuren, A. O. (1991). "Development of a mathematical model for sediment transport in meandering rivers." *Rep. No. 693*, Inst. for Hydromechanics, University of Karlsruhe, Karlsruhe, Germany.

Duarte, C. R., Murata, V. V., and Barrozo, M. A. S. (2008). "Experimental and numerical study of spouted bed fluid dynamics." *Brazilian Journal of Chemical Engineering*, 25(1), 95-107.

Einstein, H.A. (1950) "The bed-load function for sediment transportation in open channel flows." *Techn Bulletin No. 1026*, US Dept of Agriculture.

Falconer, R. A. (1984). "A mathematical model study of the flushing characteristics of a shallow tidal bay." *Proc. Inst. Civil Eng.*, 77, 311-332.

Fisher, P.J., (1990). "Hydraulic characteristics of constructed wetlands at Richmond NSW, Australia." *Constructed Wetlands in Water Pollution Control*, Cooper, P.F., Findlater, B.C., ed., Permagon Press, Oxford, 21-31.

FLUENT Incorporated. (2007). *FLUENT 6.3 user's guide*. Lebanon, New Hampshire, USA.

Gharabaghi, B., Fata, A., Seters, T. V., Rudra, R. P., MacMillan, G., Smith, D., Li, J. Y., Bradford, A., Tesa, G. (2006). "Evaluation of sediment control pond performance at construction sites in the Greater Toronto Area." *Canadian Journal of Civil Engineering*, 33(11), 1335-1344.

Gidaspow, D., Bezburuah, R., and Ding, J.(1992). "Hydrodynamics of Circulating Fluidized Beds, Kinetic Theory Approach." *Proceedings of the 7th Engineering Foundation Conference on Fluidization*, New York, 75-82.

Hamrick, J. H. (1992). "A three-dimensional environmental fluid dynamics computer code: Theoretical and computational aspects." *Special Rep. No. 317, Applied Marine Science and Ocean Engineering*, Virginia Institute of Marine Science, Gloucester Point, VA.

Heinemann, H. G. (1984). "Reservoir trap efficiency." *Erosion and sediment yield: some methods of measurement and modelling*, Hadley, R.F. and Walling, D.E., ed., 201-218.

Hinze, J. O. (1975). *Turbulence*. McGaw-Hill Publishing Company, New York

Hocking, G.C. and Patterson, J.C. (1994). "Modelling tracer dispersal and residence time in a reservoir." *Ecological Modell*ing, 74, 63-75.

Hodskinson, A., and Ferguson, R. I. (1998). "Numerical modelling of separated flow in river bends: model testing and experimental investigation of geometric controls on the extent of flow separation at the concave bank." *Hydrological Processes*, 12(8), 1323-1338.

Hsu, T. J., Jenkins, J. T., and Liu, P. L. F. (2001). "Modeling of sediment transport-a two-phase flow approach." *Coastal Dynamics'01*, Lund, Sweden.

Jia, Y., and Wang, S. S. (1999). "Numerical model for channel flow and morphological change studies." *ASCE Journal of Hydraulic Engineering,* 125(9), 924-933.

Kadlec, R. H. (1990). "Overland flow in wetlands: vegetation resistance." *ASCE Journal of Hydraulic Engineering*, 116(5), 691-705.

Kadlec, R. H. (1994). "Detention and mixing in free water wetlands." *Ecological Eng*ineering, 3, 345-380.

Kadlec, R. H., Bastiaens, W., and Urban, D. T. (1993). "Hydrological Design of Free Water Surface Treatment Wetlands." *Constructed Wetlands for Water Quality Improvement*. Moshiri, G.A., ed., CRC Press, Boca Raton, FL, 77-86.

Kadlec, R. H., and Knight, R. L. (1996). *Treatment Wetlands*. Lewis Publishers, Chelsea, Michigan.

Karim, M. F., and Kennedy, J. F. (1982). "IALLUVIAL:A computer-based flow and sediment-routing model for alluvial streams and its application to the Missouri river." *Iowa Institute of Hydraulic Research Technical Report No. 250*, University of Iowa, Iowa city, Iowa.

Launder, B. E. and Spalding, D. B.(1974). "The Numerical Computation of Turbulent Flows." *Computer Methods in Applied Mechanics and Engineering*, 3, 269-289.

Lee, H. Y., Hsieh, H. M., Yang, J. C., and Yang, C. T. (1997). "Quasi two-dimensional simulation of scour and deposition in alluvial channels." *ASCE Journal of Hydraulic Engineering*, 123(7), 600-609.

Lin, B. L., and Falconer, R. A. (1996). ''Numerical modelling of three dimensional suspended sediment for estuarine and coastal waters.'' *Journal of Hydraulic Research*, Delft, The Netherlands, 34(4), 435-456.

Lin, B. L., and Falconer R.A. (1997). "Tidal flow and transport modeling using ULTIMATE QUICKEST scheme." *ASCE Journal of Hydraulic Engineering,* 123 (4), 303-314.

Lun, C. K. K., Savage, S. B., Jeffrey, D. J. and Chepurniy, N. (1984). "Kinetic Theories for Granular Flow: Inelastic Particles in Couette Flow and Slightly Inelastic Particles in a General Flow Field." *Journal of Fluid Mechanics*, 140, 223-256.

Mangelson, K. and Watters, G. (1972). "Treatment efficiency of waste stabilization ponds." *Journal of the Sanitary Engineering Division,* SA2, 407-425.

Marecos de Monte, M. H. F., and Mara, D. D. (1987). "The hydraulic performance of waste stabilization ponds in Portugal." *Water Science and Technology*, 19(12), 219-227.

Minh Duc, B., Wenka, T., and Rodi, W. (2004). "Numerical modeling of bed deformation in laboratory channels." *ASCE Journal of Hydraulic Engineering*, 130(9), 894-904.

Molinas, A., and Yang, J. C. (1986). *Computer program user's manual for GSTARS*, U.S. Department of Interior, Bureau of Reclamation, Engineering Research Center, Washington, D.C.

Morsi, S. A., and Alexander, A. J. (1972). "An Investigation of Particle Trajectories in Two-Phase Flow Systems." *Journal of Fluid Mechanics*, 55(2), 193-208.

Moshiri, G. A. (1993). *Constructed wetlands for water quality improvement.* Lewis Publishers, Chelsea, Michigan.

Odgaard, A. J., and Bergs, M. A. (1988). ''Flow processes in a curved alluvial channel.'' *Water Resources Research*, 24(1), 45-56.

Olsen, N. R. B. (1999). ''Two-dimensional numerical modelling of flushing processes in water reservoirs.'' *Journal of Hydraulic Research,* 37(1), 3-16.

Olsen, N. R. B. (2003). "Three-Dimensional CFD Modeling of Self-Forming Meandering Channel." *ASCE Journal of Hydraulic Engineering*, 129(5), 366-372.

Patankar, S. V. (1980). *Numerical Heat Transfer and Fluid Flow.* Hemisphere, Washington, DC.

Persson, J. (2000). "The hydraulic performance of ponds of various layouts." *Urban Water*, 2, 243-250.

Pettersson, T. J. R. (1997). ''FEM-modeling of open stormwater detention ponds.'' *Nordic Hydrology,* 28(4/5), 339-350.

Pettersson, T. J. R., German, J., and Svensson, G. (1998). "Modelling of flow pattern and particle removal in an open stormwater detention pond." *HydraStorm'98*, Adelaide, Australia, 64-68.

Shams, M., Ahmadi, G., and Smith, D. H. (2002). "Computational modeling of flow and sediment transport and deposition in meandering rivers." *Advances in Water Resources*, 25, 689-699.

Shaw, J. K. E., Watt, W. E., Marsalek, J., and Anderson, B. C. (1997). "Flow pattern characterization in an urban stormwater detention pond and implications for water quality." *Journal of Water Quality Research*, Canada 32(1), 53-71.

Shilton, A. (2000). "Potential application of computational fluid dynamics to pond design." *Water Science and Technology*, 42(10–11), 327-334.

Shilton, A., and Harrison, J. (2003). "Development of guidelines for improved hydraulic design of waste stabilization ponds." *Water Science and Technology*, 48(2), 173-180.

Smaoui, H., Boughanim, G., and Chapalain, G. (2007). "1D vertical model for suspended sediment transport in turbulent tidal flow: Application to the English Channel." *Computers & Geosciences*, 33(9), 1111-1129.

Stairs, D.B. (1993). "Flow characteristics of constructed wetlands: tracer studies of the hydraulic regime." M.S. Thesis, Oregon State University.

Stovin, V. R., and Saul, A. J. (1996). "Efficiency prediction for storage chambers using computational fluid dynamics." *Water Science and Technology*. 33(9), 163-170.

Stovin, V. R., and Saul, A. J. (1998). "A computational fluid dynamics(CFD) particle tracking approach to efficiency prediction ." *J.CIWEM.* 14, 103-110.

Stovin, V. R., and Saul, A. J. (2000). "Computational fluid dynamics and the design of sewage storage chambers." *Water Science and Technology*. 33(9), 163-170.

Stovin, V. R., Saul, A. J., Drinkwater, A., and Clifforde, I. (1999). "Field testing CFD-based predictions of storage chamber gross solids separation efficiency." *Water Science and Technology*. 39(9), 161-168.

Syamlal, M., and O'Brien, T. J. (1989). "Computer Simulation of Bubbles in a Fluidized Bed. " *AIChE Symposium Series*, 85, 22-31.

Ta, C. T., (1998). "Computational fluid dynamic tools for treated water reservoir mixing studies." *Proceedings 1998 water quality technology conference*, San Diego, CA.

Tchen, C. M. (1947). "Mean value and correlation problems connected with the motion of small particles suspended in a turbulent fluid." Ph.D. Thesis, University of Delft, The Netherlands.

Thomas, W. A., and Prashum, A. I. (1977). "Mathematical model of scour and deposition." *Journal of Hydraulic Division*, 110(11), 1613-1641.

Thomson, D. J. (1987). "Criteria for the selection of stochastic models of particle trajectories in turbulent flows." *Journalof Fluid Mechanics,* 180, 529-556.

Van Rijn, L. C. (1987). "Mathematical modeling of morphological processes in the case of suspended sediment transport." *Delft Hydraulics Communication No. 382*, Delft, the Netherlands.

Vega, G. P., Pena, M. R., Ramirez, C., and Mara, D. D. (2003). "Application of CFD modeling to study the hydrodynamics of various anaerobic pond configurations." *Water Science and Technology*, 48(2), 163-171.

Versteeg, H. K., and Malalasekera, W. (1995). *An introduction to computational fluid dynamics: The finite volume method*, Prentice Hall, UK.

Verstraeten, G., and Poesen, J. (2000). "Estimating trap efficiency of small reservoirs and ponds: methods and implications for the assessment of sediment yield." *Progress in Physical Geography*, 24 (2), 219-251.

Wang, Z., Chien, N. (1985) "Experimental study of motion of laminated load." *Sci Sin* 28, 102–112.

Walker, D. (1998). "Modeling residence time in stormwater ponds." *Ecological Engineering*, 10, 247-262.

Wanker R, Gockler G, and Knoblauch, H. (2001). "Numerical modeling of sedimentation utilizing a Euler/Euler approach." *Computational Methods in Multiphase Flow*, 30, 327-336.

Watters, G. Z., Mangelson, K. A. and George, R. L. (1973). *The Hydraulics of Waste Stabilization Ponds*. Utah Water Research Laboratory – College of Engineering, Utah State University.

Wen, C.-Y., and Yu, Y. H. (1966). Mechanics of Fluidization. *Chemical Engineering Progress Symposium Series*, 62, 100-111.

Wilkinson, D., and Waldie, B. (1994). ''CFD and experimental studies of fluid and particle flow in horizontal primary separators.'' *Transactions of the Institution of Chemical Engineers, Part A,* 72(A), 189-196.

Wood, M., Greenfield, P., Howes, T., Johns, M. and Keller, J. (1995). "Computational fluid dynamic modelling of wastewater ponds to improve design." *Water Science and Technology*, 31(12), 111-118.

Wood, M.G., Howes, T., Keller, J., and Johns, M. R. (1998). "Two dimensional computational fluid dynamic models for waste stabilisation ponds." *Water Research*, 32(3), 958-963.

Wu, W. (2001). "CCHE2D sediment transport model," *Technical Report No. NCCHE-TR-2001-3*, National Center for Computational Hydroscience and Engineering, The University of Mississippi.

Wu, W. (2004). "Depth-averaged 2-D numerical modeling of unsteady flow and nonuniform sediment transport in open channels", *ASCE Journal of Hydraulic Engineering*, 130(10), 1013-1024.

Wu, W., Rodi, W., and Wenka, T. (2000). "3D numerical modeling of flow and sediment transport in open channels." *ASCE Journal of Hydraulic Engineering*, 126(1), 4-15.

Wu, W., Shields, F. D., Bennett, S. J., and Wang, S. S. (2005). "A depth averaged 2-D model for flow, sediment transport and bed topography in curved channels with riparian vegetation." *Water Resources Research*, 41, 1-15.

Wu, W., Vieira, D. A., and Wang S. S. Y. (2004). "A 1-D numerical model for nonuniform sediment transport under unsteady flows in channel networks." *ASCE J. Hydraulic Engineering*, 130(9), 914-923.

Wu, W. and Wang, S. S. Y. (2004). "Depth-averaged 2-D calculation of flow and sediment transport in curved channels." *International Journal of Sediment Research*, 19(4), 241-257.

Yang, Q. (2005). "Numerical investigations of scale effects on local scour around a bridge pier." M.S. Thesis, The Florida State University.

Zeng, J. (2006). "Fully 3D non-hydrostatic model to compute flow, sediment transport and bed morphology changes for an alluvial open channel bend." Ph.D. thesis, Dept. of Civil and Environmental Engineering, University of Iowa, Iowa city, Iowa.

Zhao, Z. and Fernando, H. J .S. (2007). "Numerical simulation of scour around pipelines using an Euler-Euler coupled two-phase model." *Environmental Fluid Mech*anics, 7, 121-142.

Zhu, J. (1992). ''An introduction and guide to the computer program FAST3D.'' *Res. Rep. of Inst. for Hydromech. in Karlsruhe Univ.*, Karlsruhe, Germany.

VITA

for

Leying Zhang

Leying Zhang was born in Dongyang, China on September 9th, 1979. She entered the Department of Civil and Environmental Engineering, Hefei University of Technology, China in 1997, where she earned a B.S. degree in 2001 and a M.S. degree in 2004. In August 2004, she entered the Department of Civil and Environmental Engineering at Old Dominion University for Ph.D. study in Environmental Engineering program. Her research interests include surface water resources management, watershed level water quality management using Genetic Algorithms, flow and sediment transport modeling using CFD.